doi.org/10.26434/chemrxiv.12756023.v2

Using Visible Light to Tune Boronic Acid–ester Equilibria

Joseph Accardo, Emily McClure, Martin Mosquera, Julia Kalow

Submitted date: 11/08/2020 • Posted date: 12/08/2020

Citation information: Accardo, Joseph; McClure, Emily; Mosquera, Martin; Kalow, Julia (2020): Using Visible Light to Tune Boronic Acid–ester Equilibria. ChemRxiv. Preprint.
https://doi.org/10.26434/chemrxiv.12756023.v2

We report a series of azobenzene boronic acids that reversibly control the extent of diol binding via photochemical isomerization. When the boronic acid is ortho to the azo group, the thermodynamically-favored E isomer binds weakly with diols to form boronic esters. Isomerization of the E azobenzene to its Z isomer enhances diol binding, and the magnitude of this enhancement is affected by the azobenzene structure. 2,6-Dimethoxy azobenzene boronic acids show over 20-fold enhancement in binding upon E–Z isomerization, which can be triggered with red light. Competition experiments and computational studies suggest that the changes in binding affinity originate from stabilization of the E boronic acids and destabilization of the E boronic esters. We demonstrate a correlation between diol binding and photostationary state: different wavelengths of irradiation yield different quantities of bound diol. Higher binding constants for the Z isomer relative to the E isomer was observed with all diols investigated, including cyclic diols, nitrocatechol, biologically relevant compounds, and polyols. This photoswitch was employed to “catch and release” a fluorescently tagged diol in buffered water. By tethering this photoswitch to a poly(ethylene glycol) star polymer, we can tune the stiffness of covalent adaptable hydrogels using different wavelengths of visible light. This work establishes photoswitchable equilibria as a tool for the reversible ligation of molecular and macromolecular species.

File list (3)

Using visible light to tune boronic acid–ester equilibria

Joseph V. Accardo, Emily R. McClure, Martín A. Mosquera[†] and Julia A. Kalow*

Department of Chemistry, Northwestern University, Evanston, Illinois, 60208, United States

Supporting Information Placeholder

ABSTRACT: We report a series of azobenzene boronic acids that reversibly control the extent of diol binding via photochemical isomerization. When the boronic acid is *ortho* to the azo group, the thermodynamically-favored *E* isomer binds weakly with diols to form boronic esters. Isomerization of the *E* azobenzene to its *Z* isomer enhances diol binding, and the magnitude of this enhancement is affected by the azobenzene structure. 2,6-Dimethoxy azobenzene boronic acids show over 20-fold enhancement in binding upon *E*–*Z* isomerization, which can be triggered with red light. Competition experiments and computational studies suggest that the changes in binding affinity originate from stabilization of the *E* boronic acids and destabilization of the *E* boronic esters. We demonstrate a correlation between diol binding and photostationary state: different wavelengths of irradiation yield different quantities of bound diol. Higher binding constants for the *Z* isomer relative to the *E* isomer was observed with all diols investigated, including cyclic diols, nitrocatechol, biologically relevant compounds, and polyols. This photoswitch was employed to "catch and release" a fluorescently tagged diol in buffered water. By tethering this photoswitch to a poly(ethylene glycol) star polymer, we can tune the stiffness of covalent adaptable hydrogels using different wavelengths of visible light. This work establishes photoswitchable equilibria as a tool for the reversible ligation of molecular and macromolecular species.

INTRODUCTION

Dynamic covalent chemistry (DCC) enables thermodynamically-driven reorganization of molecular and macromolecular systems.[1] In the last 20 years, dynamic covalent chemistry has expanded both in utility and scope, with the most popular reactions including transesterification, transimination, Diels-Alder cycloaddition, conjugate addition–elimination, disulfide exchange, metathesis, and boronic ester exchange.[2-3] The reversibility of these reactions enables applications in combinatorial library development, molecular recognition, self-healing polymers, 2- and 3-D covalent organic frameworks, and matrices for 3D cell-culture.[2, 4-9] With insight into the reaction mechanism, DCC equilibria can be adjusted by structural modification of exchange partners, providing materials with a wide range of properties. In stimuli-responsive materials, these equilibria are influenced by stimuli such as light, temperature, pH, and concentration.[10] Light represents an ideal stimulus because it can be applied at readily tuned wavelengths and fluxes with spatiotemporal precision. In applications where sample penetration depth and biocompatibility are of concern, irradiation in the red and near-infrared range is advantageous.[11]

To influence DCC with light, a photoresponsive substrate must be coupled to the exchange reaction.[12-14] Photoswitches are a class of compounds that undergo bidirectional switching in response to light, resulting in a physical change in shape, charge, conjugation, dipole, or pK_a.[15-23] When a photoswitch is coupled to DCC, the state of the switch may influence the dynamic reaction.[24] In 2006, Branda and coworkers realized the first example of photoswitchable DCC, demonstrating that the Diels-Alder cycloaddition between a diarylethene photoswitch and a dienophile could be turned on or off (gated) depending upon the isomerization of the photoswitch (Figure 1a).[25] In the open isomer, the diarylethene can undergo a [4+2] cycloaddition with a dienophile. The product could be photoswitched via a 6π electrocyclization to yield a closed "locked" isomer, which is unable to participate in the Diels-Alder equilibrium. This work was further developed by Hecht, who applied this reactivity in photoactivatable maleimide prodrugs and self-healing polymer networks.[26-29]In these reports, the DCC is either on or off.

We envisioned an alternative approach that modulates the overall equilibrium of a dynamic covalent bond using different wavelengths of light (Figure 1b). In this case, the equilibrium can operate in both states of the photoswitch, but to different extents. This system will enable bidirectional tuning of the reversible bond between small molecules and polymers to our photoswitch. In a complementary study, Hecht and coworkers investigated the effect of photoswitches on the rate of formation of imine dynamic covalent bonds, but did not study the photoswitches' influence on the bond equilibrium.[30] We identified boronic esters as an ideal dynamic covalent bond for this purpose because the exchange occurs at room temperature with many different diol structures and is compatible with aqueous environments (Figure 1c). These attributes have found utility in molecular sensors, stress-relaxing hydrogels, and recyclable thermosets.[31-39] Previous work has shown that the boronic acid–ester equilibrium is highly sensitive to the boronic acid structure.[40-44] We anticipated that photoswitch isomerization could provide the reversible structural change capable of influencing this equilibrium.

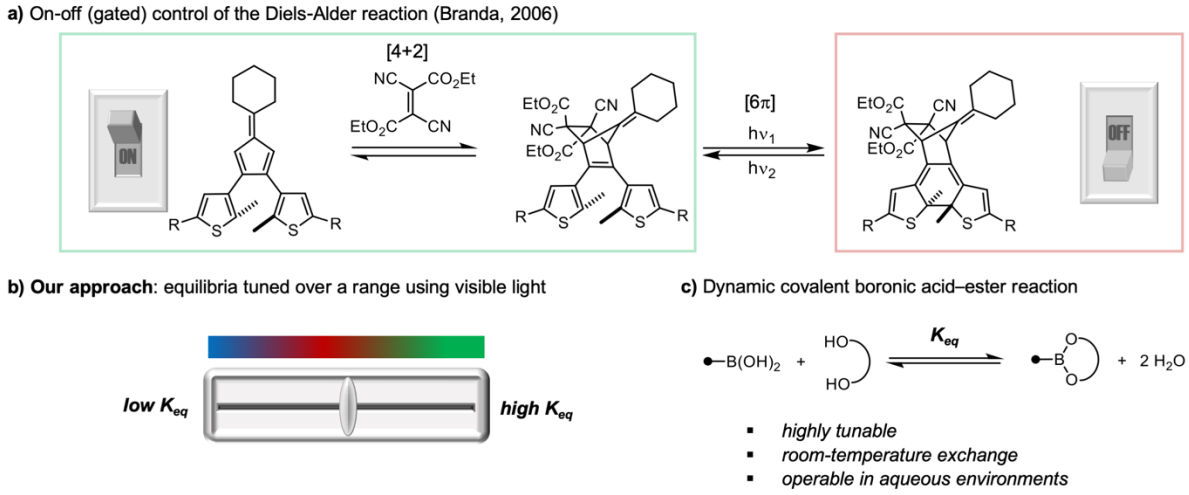

Figure 1. (a) The [4+2] cycloaddition between a diarylethene and dieneophile can be turned on or off via a 6π electrocylization. (b) In this work, different wavelengths of irradiation tune the extent of an equilibrium. (c) The reversible reaction of boronic acids and diols forms boronic esters.

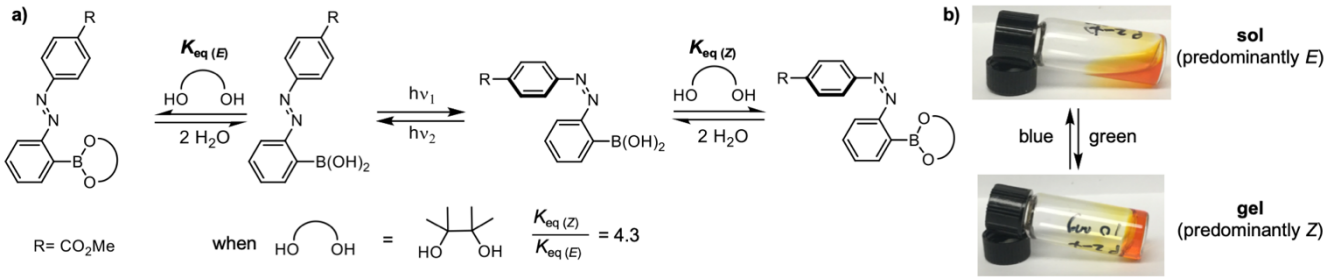

Figure 2. (a) The equilibrium between *ortho*-substituted azobenzene boronic acids and diols is influenced by the isomerization of the photoswitch, with the *Z* isomer displaying a higher binding affinity with diols than the *E* isomer. When the diol is pinacol, the *Z* binding constant is 4 times greater than the *E* binding constant. (b) Reversible sol-gel transitions of poly(ethylene glycol) hydrogels crosslinked with azobenzene boronic esters mediated by green and blue light (10 w/v%, 0.1 M PBS, pH 7.5).

Towards this goal, we synthesized *ortho*-substituted azobenzene boronic acids (Figure 2a).[45-46] As azobenzenes undergo substantial changes in structure upon *E*→*Z* isomerization, we hypothesized that the boronic acid–ester equilibrium could be affected by the photoswitch state. Accordingly, we discovered that these compounds have isomerism-dependent equilibria with diols, wherein the *Z* isomer has a higher binding affinity than the *E* isomer ($K_{eq(Z)} > K_{eq(E)}$, Figure 2a).[47] When incorporated into poly(ethylene glycol) networks, this preferential binding translated to reversible sol-gel transitions upon *E*→*Z* photoisomerization (Figure 2b). Interestingly, this dramatic physical change arose from a relatively modest difference in binding affinity to diols (~4:1 for pinacol). We thus sought structural modifications of the azobenzene boronic acid that could increase the difference in binding affinity between the *E* and *Z* isomers, allowing us to expand the tunability of this photocontrolled dynamic covalent bond and its potential applications.

In this report, we demonstrate that simple modifications of the azobenzene boronic acid allow us to tune the relative binding affinity of *Z* vs. *E* azobenzene boronic acids to diols, $K_{rel} = K_{eq(Z)}/K_{eq(E)}$, from 2.4 to over 20. Experimental results and computed structures suggest that the differences in K_{rel} between a series of azobenzene boronic acids are due to both the stabilization of the *E* boronic acids and the destabilization of the *E* boronic esters, which can be tuned by azobenzene substitution. Our optimized azobenzene boronic acid can be photoswitched with red light and the *Z* isomer has a long thermal half-life. Using the azobenzene boronic acid with the largest K_{rel}, the equilibrium between boronic acid and boronic ester can be tuned with different wavelengths of light. We demonstrate that this azobenzene boronic acid can "catch and release" a fluorescently tagged polyol in aqueous buffer. Lastly, we reversibly tune the stiffness of a covalent adaptable hydrogel with several wavelengths of visible light, including red light.

RESULTS AND DISCUSSION

Ortho substitution increases the difference in binding affinity between E and Z isomers

The equilibrium between boronic acids and diols strongly depends on the concentration of water and diol. Therefore, we designed ^{1}H and ^{19}F NMR equilibrium competition binding experiments to compare the relative binding affinity between *E* and *Z* isomers in the same NMR tube, ensuring that the concentration of water and diol are the same for both isomers (Figure 3a; see Supporting Information (SI), section IV for details and derivation). Our investigations commenced with compound **1**, a para-tolyl azobenzene boronic acid (Figure 3b). The para-methyl substituent was

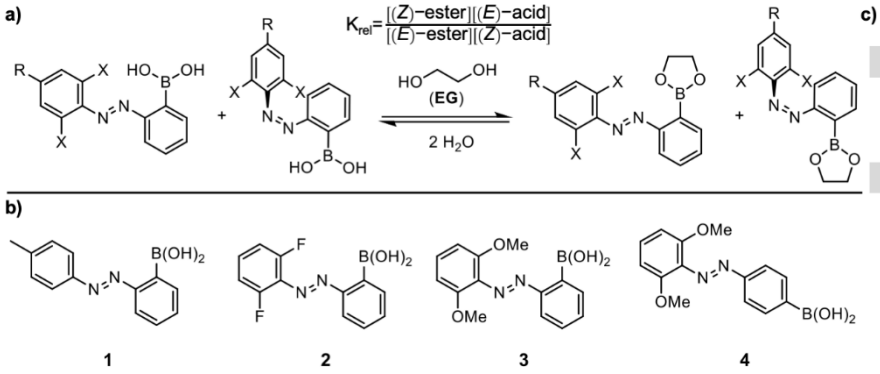

c)

compound	1	2	3	4
K_{rel}	2.4	4.2	21.5	1.1
$t_{1/2}$ (days)	3.5	70	24	--
irradiation λ	PSS (% Z)			
626 nm (red)	< 2	< 6	54	--
525 nm (green)	--	67	67	--
470 nm (blue)	26	50	36	--
365 or 390 nm (UV)	48	59	44	--

Figure 3. (a) Equilibrium competition binding experiment to compare the relative equilibrium binding constants of *E* and *Z* azobenzene boronic acids with diol. (b) Library of photoswitches synthesized and subjected to the above competition binding experiment. (c) Competition binding experiment results in DMSO-d_6 at 25 °C, thermal half-lives (days) and photostationary states (%*Z*) of azobenzene boronic-acids.

used in place of the phenyl analog, which exhibits overlapping ^{1}H NMR signals for the *E* and *Z* isomers. When a mixture of (*E*)-**1** and (*Z*)-**1** was treated with excess ethylene glycol (EG) and D_2O in DMSO-d_6 and allowed to equilibrate for 12 hours, we observed that (*Z*)-**1** binds EG approximately 2.4 times better than (*E*)-**1** (Krel = 2.4) (Figure S8).

For our design of photoswitchable equilibria, the ideal photoswitch should feature visible-light bidirectional photoswitching, high photostationary states, and a long thermal half-life for the *Z* isomer. Unfortunately, in addition to a modest difference between *E* and *Z* binding affinities, compound **1** only reached an appreciable photostationary state (PSS, 48% *Z*) with ultraviolet (UV) irradiation at 365 nm (Figure 3c). By measuring the rate of thermal relaxation of (*Z*)-**1** to (*E*)-**1** at different temperatures and fitting to an Arrhenius plot (Figures S4), we could extrapolate the room-temperature (25 ºC) half-life to be 3.5 days. Previous work has established that electronic and steric modifications of the azobenzene can alter key photochemical properties, which has been summarized well by Bandara and Burdette.[16] We anticipated that these modifications could simultaneously alter the equilibrium of the dynamic covalent bond. First, we sought to optimize the photochemical properties to achieve bidirectional visible-light photoswitching. Secondly, we aimed to increase the thermal stability of the *Z* isomers.

A common strategy to enable azobenzene isomerization with visible light is substituting the aryl rings with resonance electron-donating and -withdrawing groups, creating "push-pull" azobenzenes. These substitution patterns red-shift the π→π* of the *E* isomer through a charge-transfer mechanism. Unfortunately, the *Z* isomers tend to undergo rapid thermal isomerization (< seconds), due to a low activation barrier in the ground state,[48] which would occur much faster than the dynamic covalent reaction. Hecht, Woolley, and others have installed halides or methyl ethers at the *ortho* positions, which separates the n→π* absorption bands of the *E* and *Z* isomers and enables visible-light *E*→*Z* photoisomerization with enhanced *Z* thermal stability.[49-55] Inspired by this work, we synthesized *ortho*-difluoro-substituted azobenzene **2** and dimethoxy analog **3** to access visible-light photoswitching (Figure 3b). **2** exhibited a higher PSS (67% *Z*) with green light (525 nm) irradiation and a dramatically enhanced thermal half-life relative to **1** ($\tau_{½}$ = 70 days, Figure S5). The relative binding affinity, as determined by the equilibrium competition binding experiment with EG, increased by a factor of 1.8 relative to **1**, to K_{rel} = 4.2 (Figure 3c, Figure S9). When the fluorine atoms were replaced with methyl ethers in compound **3**, photoswitching with red LEDs at 626 nm yielded PSS up to 54%, albeit with a modest decrease in thermal half-life ($\tau_{½}$ = 24 days, Figure S6). The competition experiment for compound **3** also revealed a dramatic increase in relative binding, where the *Z* isomer binds EG with over an order of magnitude higher affinity than the *E* isomer (K_{rel} = 21.5, Figure S10). Figure 4 shows the ^{1}H NMR spectrum for the competition experiment of compound **3** with EG, in which (*Z*)-**3** is predominantly bound, while (*E*)-**3** is mainly unbound.

As a control, we synthesized an azobenzene derivative with the boronic acid at the 4' (para) position (compound **4**). This compound exhibited little difference in binding affinities between the *E* and *Z* isomers (K_{rel}= 1.1, Figure S12). Thus, the proximity of the boronic acid to the phenylazo group is essential for the isomerism-dependent changes in binding affinity.

Ortho substitution influences the esterification equilibrium of the *E* isomers

We next set out to understand the origin of the dramatic increase in K_{rel} for compound **3** compared to compounds **1** and **2**. As K_{rel} is defined as the ratio of $K_{eq(Z)}$ to $K_{eq(E)}$, this trend could originate in an *increase* in $K_{eq(Z)}$, a *decrease* in $K_{eq(E)}$, or a combination of both effects. We performed an equilibrium competition binding experiment to compare (*E*)-**1** and (*E*)-**2**, and a separate experiment comparing (*E*)-**2** and (*E*)-**3** (Figure S13). The *E* isomers for **1**–**3** displayed significantly different binding affinities for EG, following

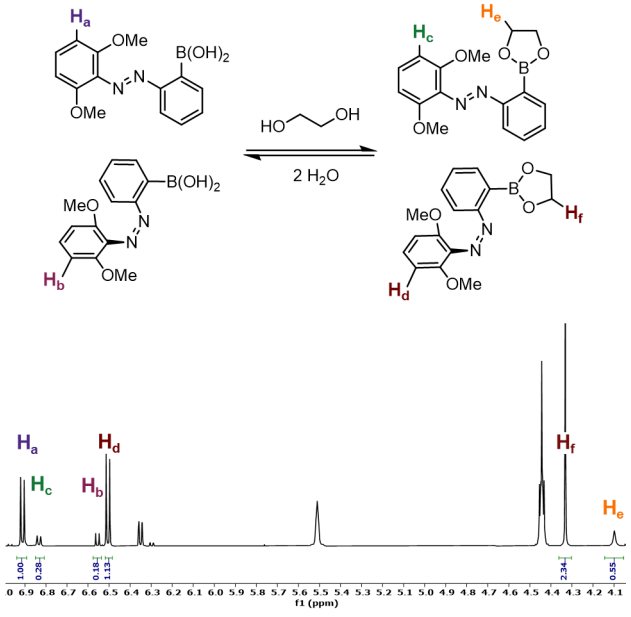

Figure 4. ^{1}H NMR of **3** and EG subjected to equilibrium competition binding conditions in DMSO-d_6.

the K_{eq} trend (*E*)-**3** << (*E*)- **2** < (*E*)-**1**, consistent with the overall changes in K_{rel}. In contrast, equilibrium competition experiments for the *Z* isomers of **1**–**3** revealed similar binding affinities to EG (Figure S14). Therefore, we concluded that the changes in $K_{eq(E)}$, and not $K_{eq(Z)}$, lead to the observed differences in K_{rel} between compounds **1**–**3**.

Calculated structures and control experiments suggest a combination of reactant stabilization and product destabilization disfavors *E* esterification

Why do *E* isomers of azobenzene boronic acids consistently display lower binding affinities for diols than their corresponding *Z* isomers? Why does (*E*)-**3** bind EG significantly worse than (*E*)-**2** and (*E*)-**1**? Structural changes that result in the stabilization of the (*E*)-acid, destabilization of destabilization of the (*E*)-ester, or a combination will correspond to less negative ΔG and decreased diol binding affinity (Figure 5a-b). We hypothesized that there are two main structural parameters influencing the degree of conjugation through the system and therefore the energy of the azobenzene boronic acid and ester. The first is the planarity of the azobenzene, which is described by the dihedral angle between the aryl rings and diazo (CCNN, Φ) (Figure 5c). For unsubstituted azobenzene, the energy is lowest when this angle is 0° and highest at 90° (Figure S29). The second parameter is the coplanarity of the azobenzene and the boronic acid or ester, which can be described by the CCBO dihedral angle ψ . This parameter correlates with the degree of conjugation between the boronic acid or ester with the adjacent aryl group (Figure 5c). Previous reports suggest that arylboronic acids and esters are stabilized when the non-bonding oxygen lone pairs and vacant p orbital are in conjugation with the π-system of the aryl group, with a CCBO dihedral angle of 0°. We performed geometry scans of phenylboronic acid and the corresponding ester, confirming an energetic maximum at 90° and a minimum at 0°, when conjugation is enhanced. (Figure S29).

To understand which scenario might be responsible for the decrease in $K_{eq}(E)$ from **1>2>>3**, we calculated the optimized structures of (*E*)-**1**, **2**, and **3** in their bound and unbound forms with the B3LYP/6-31+G** level of theory and performed frequency calculations to determine the lowest-energy rotamers. We modeled the boronic acids and esters in their trigonal planar form based on ^{11}B NMR studies (Figure S11). We first examined the geometry-optimized structures of (*E*)-**1** through (*E*)-**3** in their unbound forms (Figure 6a). Each azobenzene is nearly planar, and the two CCNN dihedrals angles Φ (Ar^1) and Φ (Ar^2) are between 11° and 17° for

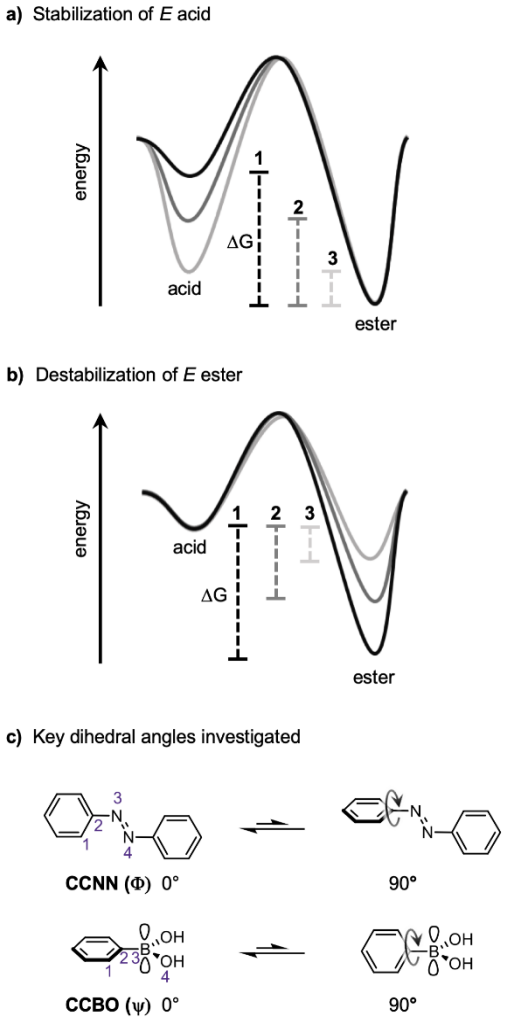

Figure 5. (a,b) Energy diagrams portraying two potential origins of the observed trend in Keq, (*E*)-**1** > (*E*)-**2** > (*E*)-**3**. (c) Key bond rotations that can influence the energy of azobenzene boronic acids and esters.

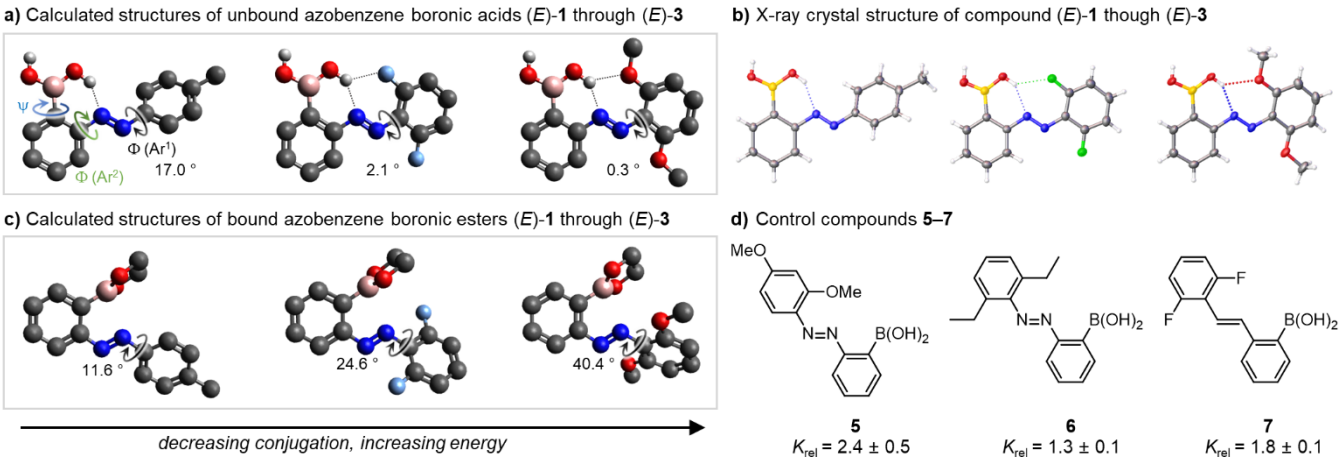

Figure 6. (a) Energy-minimized structures of boronic acids (*E*)-**1** through (*E*)-**3**. Φ (Ar^1, black), Φ (Ar^2, green) and ψ (blue) represent the two CCNN and one CCBO dihedral angles investigated, respectively. (b) Crystal structure of compound **1- 3** showing intramolecular hydrogen bonds. (c) Energy-minimized structures of boronic esters (*E*)-**1** through (*E*)-**3**. (d) Structure of control comounds **5-7** and their experimentally determined K_{rel} values.

(*E*)-**1** and between 0° and 2° for (*E*)-**2** and (*E*)-**3**. The CCBO dihedral angles ψ are close to 0° for **1**–**3**, and an intramolecular hydrogen bond is present between the boronic acid proton and the proximal azobenzene nitrogen.

The boronic acid protons in the calculated structures of (*E*)-**2** and (*E*)-**3** also engage in H-bonding with one of the *ortho*-heteroatom substituents (fluorine or methoxy, respectively). This additional H-bonding interaction was confirmed in the single-crystal X-ray structures of (*E*)-**2** and (*E*)-**3** (Figure 6b). We hypothesize that the additional hydrogen bonds stabilize the boronic acid and lead to a less negative Δ*G* for esterification. While the O-H···F-C interaction in **2** is expected to be much weaker than with the methoxy group in **3**, the H–F distance of 2.27 Å is consistent with previously reported H-bonding interactions involving a C–F acceptor.[56-57] In both **2** and **3**, these additional hydrogen bonds assist in keeping the azobenzene nearly planar, whereas (*E*)-**1**, which lacks H-bond acceptors at the *ortho* positions, is slightly more twisted. Again, these features were corroborated by the single-crystal X-ray structure of (*E*)-**1**, in which Φ (Ar^1) is 19.8º.

Binding of EG to the (*E*)-azobenzene boronic acids is accompanied by varying degrees of twisting of the aryl rings and deviation of the CCNN dihedral angles from 0°. In the calculated structures, *ortho*-unsubstituted (*E*)-**1** remains slightly twisted after binding EG (11.6°), while (*E*)-**2** and (*E*)-**3** display more significant twisting, exemplified by Φ (Ar^1) angles of 24.6° and 40.4°, respectively (Figure 6c, see Figure S31 for full list of angles). This twisting likely arises from repulsive steric interactions between the halide or methoxy *ortho* substituents and the boronic ester. For all compounds, we observe that the boronic ester is nearly perpendicular to the aryl ring ($75° \leq \psi \leq 84°$), which avoids Van der Waals repulsion between the ester oxygen and distal nitrogen. We hypothesize that the large conformational changes engendered by diol binding reduce the degree of conjugation in the azobenzene and raise the energy of the boronic ester relative to the boronic acid. Since these conformational changes become more significant across the series **1** < **2** < **3**, Δ*G* becomes correspondingly less negative across this series, and the esterification becomes less favorable for **3** compared to **1** and **2**. Alternative rotamers for the esters of (*E*)-**1** through (*E*)-**3** (Figure S31) are less than 3 kcal/mol higher in energy but follow similar trends to those shown here, with the smallest conformational changes upon binding occurring for (*E*)-**1** and the largest changes occurring for (*E*)-**3**.

The optimized structures for the *Z* isomers place the boronic acids away from the *ortho* substituents. Each boronic acid still displays an intramolecular hydrogen bond with the proximal nitrogen; however, there are no additional H-bonds with the *ortho*-fluoro or methoxy substituents in (*Z*)-**2** and **3.** The absence of steric interactions between the boronic esters and *ortho* substituents in the *Z* isomers allows diol binding to occur with minimal structural rearrangement for compounds (*Z*)-**1** through (*Z*)-**3**, as exemplified by small changes in Φ(Ar^1), Φ(Ar^2), and ψ upon diol binding (Figure 7 for **3**; see Figure S32 for compounds **1**-**2**). These small changes are consistent with the similar diol binding affinities exhibited by the *Z* isomers of **1**–**3** in equilibrium competition binding experiments. Additionally, the boronic esters maintain conjugation with the aryl ring ($0.6° \leq \psi \leq 20°$) after binding EG. This favorable conformation, combined with the absence of repulsive interactions with the *ortho* groups, likely underlies the improved binding of *Z* azobenzene boronic acids compared to their *E* isomers.

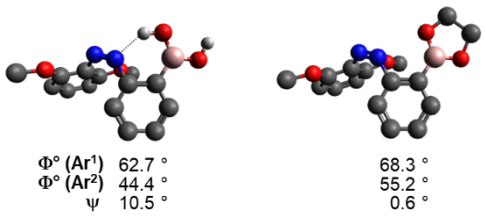

Figure 7. Calculated structure of (*Z*)-**3** before and after binding EG.

Based on the calculated structures, we designed control compounds to experimentally demonstrate that the high K_{rel} for **3** arises from a combination of (i) H-bonding to the azo group, which stabilizes the (*E*)-boronic acid; (ii) additional H-bonding to one of the *ortho*-methoxy groups, providing further stabilization; and (iii) steric destabilization of the (*E*)-boronic ester. First, we synthesized compound **5**, in which one of the methoxy substituents was moved from the *ortho* position to the *para* position. When **5** was subjected to the competition experiment, K_{rel} was determined to be 2.4, almost an order of magnitude lower than that of **3** (see Figure S15 for ^{1}H NMR). The calculated structures of **5** show that the boronic acid and ester both adopt planar conformations. (Figure S33-34). This control experiment suggests that stabilization of the boronic acid by double H-bonding only partially disfavors esterification; steric interactions that destabilize the ester are also required to achieve high K_{rel}.

Next, we synthesized di-*ortho*-ethyl azobenzene **6**, which is sterically comparable to compound **3,** but lacks the ability to participate in additional hydrogen bonding with the *ortho* positions. When subjected to the competition experiment, K_{rel} was determined to be only 1.3 (Figure S16). Calculated structure of **6** show significant twisting in both the boronic acid (Φ (Ar^1) = 43°, Figure S35) and boronic ester (Φ (Ar^1) = 42°). This control experiment demonstrates that steric interactions alone cannot explain the K_{rel} trend for **1**–**3**; H-bonding to stabilize the boronic acid and planarize the (*E*)-azobenzene are essential.

Lastly, we synthesized stilbene **7**, which is sterically comparable to **2** and capable of *E*→*Z* isomerization but is unable to engage in intramolecular hydrogen bonding (Figure S36). For compound **7**, K_{rel} was determined to be only 1.8 (Figure S17). This modest K_{rel} value likely arises from steric effects alone. Stilbene **7** also allowed us to experimentally probe the relative effect of intramolecular H-bonding on the thermodynamics of boronic acid esterification for *E* vs. *Z* isomers. We performed an equilibrium competition binding experiment between **2** and **7** and observed that the stilbenes have higher binding affinities for diols compared to their azobenzene analogs. Specifically, *E* stilbene bound EG 6-fold more than the *E* azobenzene, whereas the *Z* stilbene bound EG 2.6-fold more than the Z azobenzene. While the O–H···N H-bond is present in both *E* and *Z* azobenzene isomers, its stabilizing influence is more significant in the *E* isomer; furthermore, the *E* isomer presents multiple H-bond acceptors.

In summary, calculated structures, supported by experimental results with control compounds **5**–**7**, lead us to the following conclusions:

1) Stabilization of boronic acids by adjacent H-bond acceptors can disfavor esterification. This effect is further exacerbated by the presence of multiple H-bond acceptors, as in the case of **3** and, to a lesser extent, **2**, in which both the proximal azo *N* and the *ortho* groups of the distal arene act as H-bond acceptors.

2) In *E* azobenzenes, the degree of twisting away from the planar conformation imposed by steric interactions offers an additional synthetic handle to tune the stability of dynamic covalent bonds. Previous approaches have considered the effect of photoswitch conjugation on its propensity to form a dynamic bond;[30] our work suggests a complementary design principle, in which the structure of the dynamic bond can also affect the stabilization of the photoswitch by conjugation.

3) The twisted structure of *Z* azobenzenes requires fewer conformational changes to accommodate boronic acid esterification, and also precludes additional H-bonding interactions. Thus, esterification is more favorable for the *Z* isomer than for the *E* isomer.

While previous studies have probed the structural features that affect the thermodynamics of the boronic acid–ester dynamic bond in detail, they have generally focused on parameters such as the electronics of the boronic acid, the presence of proximal basic amines, or the diol structure.[39, 41-42, 44, 58] The insights gained from our studies provide a framework for future designs of boronic acids where proximal functional groups can enhance or disrupt the stability of the dynamic bond.

Diol binding can be tuned through irradiation with different wavelengths of light

We selected **3** as the optimal photoswitch to tune diol binding because of its large K_{rel} and favorable photochemical properties. We envisioned that the ratio of the *E* and *Z* isomers should dictate the overall boronic acid–ester equilibrium, wherein the amount of bound diol should increase as the ratio of (*Z*)-**3** to (*E*)-**3** increases. As the PSS (%*Z*) is wavelength dependent, the ratio of *Z* to *E* can be tuned by irradiation with different wavelengths of light. We prepared a solution of (*E*)-**3** and EG (1:1) in DMSO-d_6, in which the azobenzene bound 30% of the available EG prior to irradiation (Figure 8a, see Figure S19 for ^{1}H NMR spectrum). Irradiating the sample with blue, red, or green irradiation yielded different photostationary states, and higher photostationary states correlated linearly with increased diol binding. Up to 70% of the diol could be bound with green light. The high barrier for *Z*→*E* thermal isomerization ensures that the resulting equilibrium is maintained for the duration of the experiment (24 hours), such that continuous irradiation is not required. By irradiating with a wavelength of light corresponding to a lower PSS, the equilibrium can be shifted to favor boronic acid and enables release of diol into solution. Figure 8b shows the UV-Vis absorbance spectrum of **3** before and after irradiation with green light. The ability to achieve high PSS for both *E*→*Z* and *Z*→*E* isomerization arises from the separation of the n-π* transitions of the *E* and *Z* isomers (Figure 8b, inset).

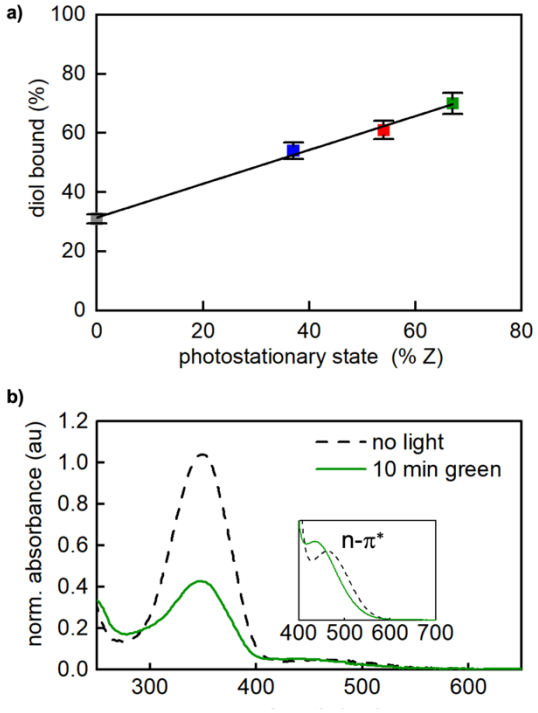

Figure 8. (a) Percent diol binding as a function of PSS, which is achieved thermally (gray) or with blue, red, or green light. Error bars represent integration error, and the line is the least squares fit. (b) UV-Vis profile of **3** in acetonitrile before (black) and after (green) irradiation with green LEDs for 10 minutes.

Photoswitching modulates boronic ester equilibria with different diols

Next, we investigated the generality of photoswitchable binding to boronic acid **3** with different diols. Using **3**, we observed K_{rel} values between 6 and 20 for a variety of diols, including a 1,3-diol (**8**), simple cyclic diols (**9**-**10**), nitro-catechol (**11**), and a variety of complex and biologically relevant diols, including glucose (**14**), adenosine (**15**), and the chemotherapeutic drug capecitabine (**16**) (Figure 9). Phenylboronic acid-containing polycarbonates have previously been used for the pH-dependent release of diols including capecitabine.[59] We envision **3** could provide a complementary light-driven strategy. Diols of interest could first be bound in the *Z* state, where release could be controlled by isomerization to the *E* isomer.

We qualitatively observed that some diols bound **3** poorly in the standard NMR assay conditions (<1% D_2O in DMSO-d_6); when exogenous water was added to the 4-nitrocatechol (**9**) equilibrium competition binding experiment, we exclusively observed only boronic acid for both isomers. In contrast, some cyclic diols and polyols (such as *cis*-1,2-cylcopentanediol (**9**) and gluconolactone derivative (**13**)) have higher binding constants, and additional exogenous water (6% in DMSO-d_6) was needed in the competition experiment to observe any unbound acid, consistent with previous studies using simple arylboronic acids.[41] These results demonstrate that while the *relative* binding affinities between *Z* and *E* are

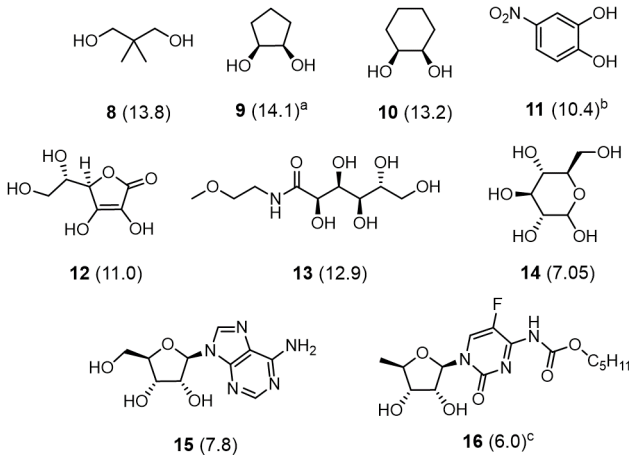

Figure 9. K_{rel} (reported in parentheses) between (*Z*)-**3** and (*E*)-**3** with various diols (20 mM in DMSO-d_6 with 2 µL D_2O). Standard deviations were between 0.1 and 2.4 and are reported in Figures S20 through S28. [a]Excess D_2O was necessary due to high binding affinity. [b]No additional D_2O was used due to low binding affinity. [c]Lower concentration (8 mM) was used due to sample requirements.

similar across a range of diols, the *absolute* equilibrium constants are highly dependent on diol structure. For applications of **3** in an aqueous environment, cyclic diols such as **9** or polyols such as **13** will be optimal.

Azobenzene boronic acids reversibly bind diols in fully aqueous environments

To overcome the low aqueous solubility of small molecule **3**, we designed and synthesized a carboxylate analog of **3**, SI-**11**, and coupled it to amine-terminated 4-arm poly(ethylene glycol) (PEG, M_w 5 kg/mol) (polymer **P1**, Figure 10a; see SI for details). While installing the electron-withdrawing ester shortens the thermal half-life of the *Z* azobenzene to 2.2 days by creating push-pull character (Figure S7), it increases the PSS (%*Z*). SI-**10**, the methyl ester of compound SI-**11**, reaches 76% *Z* after red light irradiation, and returns to 29% *Z* after blue light irradiation (Table S4).

We also synthesized a coumarin-tagged gluconolactone derivative (compound **17**) to provide a fluorescent output for reversible binding. The gluconolactone tag was chosen based on the performance of **13** in the presence of excess water, suggesting esterification would be favorable in an aqueous environment. The ratio of bound **17** should be increased after irradiation to predominantly *Z* isomer with red light and decreased after irradiation to predominantly *E* isomer with blue light. We mixed the boronic acid polymer **P1** and compound **17** in a 1:4 molar ratio (1:1 boronic acid:**17**) in a phosphate buffered saline (PBS) solution at pH 7.5. To analyze the amount of unbound **17**, we filtered the mixture with a 3.0 kDa molecular weight cut-off (MWCO) centrifugal filter such that only free fluorophore (MW 383 g/mol) can pass through the membrane.

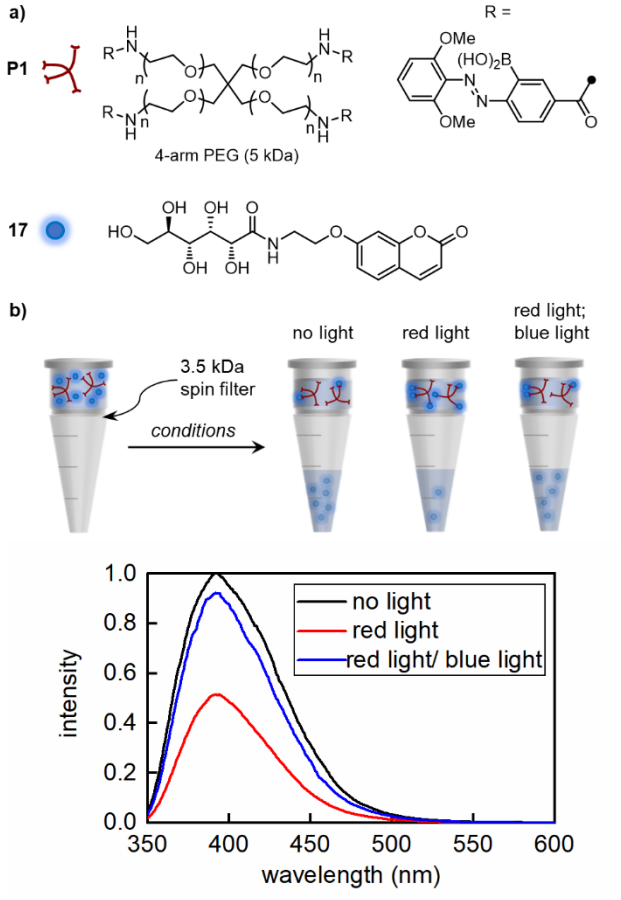

Figure 10. (a) Structures of **P1** and gluconolactone-tagged coumarin **17**. (b) Illustration of experimental setup and fluorescence spectra of eluents after irradiating and spin filtering each solution.

We next performed UV-vis and fluorescence spectroscopy of the resulting dialysate. Without any irradiation, we observed strong fluorescence in the dialysate indicating that unbound **17** had passed through the filter (Figure 10b). When the solution was irradiated with red light for 60 minutes before spin filtering, we observed decreased emission, indicating more fluorophore was bound to **P1** and unable to pass through the filter. In an analogous experiment, we first irradiated the mixture with red light for 60 minutes, then with blue light for 10 minutes, before centrifugal filtration. In this case, the fluorescence of the dialysate increased to nearly the same level as the no-irradiation control, demonstrating that the fluorophore bound to red-irradiated **P1** was released by blue light.

Reversible changes in binding affinity lead to reversible stiffening of hydrogels

Lastly, we sought to translate the reversible changes in binding affinity to control crosslink density in a hydrogel network. Previously, we demonstrated that reversible changes in binding affinity could lead to sol-gel transitions in a boronic ester crosslinked poly(ethylene glycol) hydrogel, with stiffening occurring with UV or green light and softening occurring with blue light. Based on the photochemical properties of compound **3**, we reasoned that its incorporation as a crosslink into hydrogels would enable stiffening with red light. We prepared diol-terminated polymer **P2** by ring-opening glucono-δ-lactone with amine- terminated 4-arm poly(ethylene glycol) (M_w= 5 kDa), according to a previous literature procedure.[32] . When **P1** and **P2** were mixed in a 1:1 ratio in 0.1 M phosphate-buffered saline at pH 7.5 (10 w/v%), a sol was observed, according to the flow-inversion method. Irradiation with red LEDs (626 nm) for 3 hours promotes the *E*→*Z* isomerization of the terminal azobenzene boronic acids and leads to the gelation of the mixture. Irradiating this gel for 5 minutes with blue LEDs promotes *Z*→*E* isomerization and returns the mixture to the sol state (Figure 11a). By alternating irradiation with red and blue light, we could continue to cycle the gel between sol and gel states. Addition of excess free diol **13** leads to the dissolution of the network, presumably by outcompeting **P2** and disrupting the boronic ester crosslinks.

Toward our lab's effort to design photoreversible matrices for 3D cell culture, we prepared a hydrogel with **P1** and **P2** (10 w/v%) in Dulbecco's Modified Eagle Medium (DMEM), a common growth medium for a variety of cell types. While the glucose, amino acids, or vitamins in DMEM could interfere with the boronic ester dynamic bond, we were gratified to observe that gelation can still occur in this medium. Bulk mechanical characterization of this hydrogel was performed by oscillatory photorheology at constant strain in the linear viscoelastic region. We first investigated the frequency-dependent properties of this hydrogel from 100 to 0.1 rad/s, which yields information on the dynamics of the crosslinks. The storage modulus (G') represents the material's ability to store energy elastically like a solid, while the loss modulus (G") represents the material's able to dissipate energy into the surrounding environment like a liquid. In materials that behave as elastic solids, such as permanently crosslinked hydrogels, G' and G" are frequency independent. Viscoelastic materials display both solid- and liquid-like behaviors, which depend upon the frequency of the deformation. At high frequencies (> 1 rad/s), where deformation is faster than the dynamic bond exchange, the **P1**/**P2** gel has solid-like behavior, wherein G' > G''. The crossover point (where G' = G") occurs at 0.5 rad/s, and below this frequency the gel flows like a liquid due to the reversible hydrolysis of boronic ester crosslinks (Figure 11b). Interestingly, this hydrogel does not undergo sol-gel transitions by the flow inversion method, which are observed when PBS is the solvent. We hypothesize that the additives in DMEM reduce the rate of exchange of the dynamic crosslinks, shifting the crossover point to lower frequencies. The relationship between molecular kinetics and the crossover frequency is the subject of ongoing studies in our laboratory.

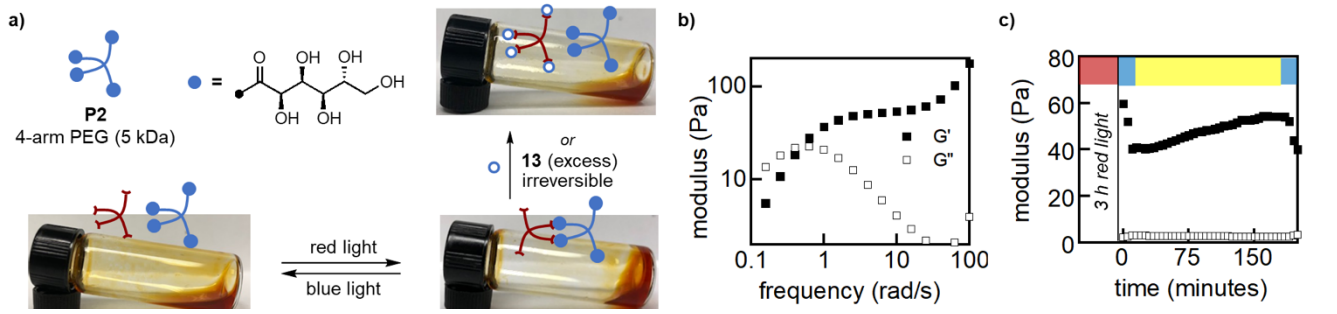

Figure 11. (a) Structure of **P2** and reversible gelation of **P1** and **P2** with red and blue light (10 w/v%, PBS pH 7.5). (b) Frequency sweep of **P1** and **P2** in DMEM (10 w/v%, 10% strain) after stiffening with red light for 3 hours. (c) Reversible mechanical response of **P1** and **P2** in DMEM (10 w/v%, 10% strain, 25 rad/s) to different wavelengths of visible light.

The hydrogel in DMEM also demonstrates photodependent changes in stiffness (Figure 11c). The gel was stiffened for three hours with red light, yielding a G' of 60 Pa. Irradiation for 10 minutes with blue light led to a softer gel, decreasing G' by 33%. The gel could be stiffened again with yellow light irradiation, increasing G' to 54 Pa after 3 hours. We propose that the photo-dependent changes in stiffness arise from changes in the hydrogel crosslink density. We hypothesize that the softness of these gels, compared to those previously reported in the literature,[31-32, 47, 60] is due to the unusually low binding of the *E* azobenzene. While these hydrogels may be practical as tools for studying soft tissue mechanics, we envision that increasing the binding constant of the *Z* isomer while maintaining high K_{rel} will enable larger ranges of photocontrolled stiffness.

CONCLUSIONS

We have shown how multiple wavelengths of light can be used to tune the equilibrium of a dynamic covalent bond by harnessing the photostationary state of a photoswitch. While previous reports of photocontrolled dynamic covalent chemistry turn equilibria on or off, our approach offers the ability to modulate the boronic acid/ester equilibrium depending upon the isomerism of an azobenzene photoswitch. The binding equilibrium becomes more favorable as the percentage of *Z* isomer is increased. Moreover, we show that the range of equilibrium binding constants achieved by a single photoswitch is highly dependent upon *ortho,ortho*-substitution of the distal ring. In addition to increasing the difference in *E* and *Z* binding constants, these *ortho* substituents impart improved photochemical properties including longer thermal half-lives, increased photostationary states, and visible light photoswitching, making them promising for biomedical applications. The optimized azobenzene identified in these studies can reversibly bind a range of biologically relevant diols. We further demonstrated the application of photoswitchable equilibria to a dynamic covalent hydrogel that can be stiffened with red light. Tuning equilibria with photoswitches represents a powerful approach to noninvasively control the interaction between molecular and macromolecular species. While this work applies this concept to boronic acid–ester exchange, the underlying principles may be used to impart photocontrol on other dynamic reactions, such as imine exchange or thia-Michael addition.

ASSOCIATED CONTENT

Supporting Information

Synthetic procedures; characterization data for new compounds; UV-vis spectra; Arrenhius plots; ^{1}H NMR for competition experiments; XYZ coordinates of calculated structures; single-crystal X-ray data; rheological data.

AUTHOR INFORMATION

Corresponding Author

jkalow@northwestern.edu

Present Addresses

†Department of Chemistry and Biochemistry, Montana State University, Bozeman, Montana 59717, United States.

Notes

J. A. K. and J. V. A. have filed a provisional patent application (U.S. Prov. 62/673,312).

ACKNOWLEDGMENT

This material is based upon work supported by the National Science Foundation under CAREER CHE-1847948 and a 3M Non-Tenured Faculty Award (J.A.K.). The authors thank the Dichtel Laboratory for use of their fluorimeter, as well as Jacob Ishibashi, Pradipta Das, Boyeong Kang, and Christopher Eckdahl for helpful comments. This work made use of NMR and MS instrumentation at the Integrated Molecular Structure Education and Research Center (IMSERC) at Northwestern, which has received support from the NSF (NSF CHE-9871268); Soft and Hybrid Nanotechnology Experimental (SHyNE) Resource (NSF ECCS-1542205); the State of Illinois and International Institute for Nanotechnology. This research was supported in part through the computational resources and staff contributions provided for the Quest high performance computing facility at Northwestern University, which is jointly supported by the Office of the Provost, the Office for Research, and Northwestern University Information Technology. Rheological measurements were performed at the MatCI Facility, which receives support from the MRSEC Program (NSF DMR-1720139) of the Materials Research Center at Northwestern University.

REFERENCES

1. Jin, Y. H.; Yu, C.; Denman, R. J.; Zhang, W., Recent advances in dynamic covalent chemistry. *Chem. Soc. Rev.* **2013,** *42*, 6634-6654.
2. Winne, J. M.; Leibler, L.; Du Prez, F. E., Dynamic covalent chemistry in polymer networks: a mechanistic perspective. *Polym. Chem.* **2019,** *10*, 6091-6108.
3. Zhang, W.; Jin, Y., *Dynamic covalent chemistry : principles, reactions, and applications*. First edition. ed.; Wiley,: Hoboken, NJ, 2017; p. 1 online resource.
4. Wojtecki, R. J.; Meador, M. A.; Rowan, S. J., Using the dynamic bond to access macroscopically responsive structurally dynamic polymers. *Nat. Mater.* **2011,** *10*, 14-27.
5. Boehnke, N.; Cam, C.; Bat, E.; Segura, T.; Maynard, H. D., Imine Hydrogels with Tunable Degradability for Tissue Engineering. *Biomacromolecules* **2015,** *16*, 2101-2108.
6. Lohse, M. S.; Bein, T., Covalent Organic Frameworks: Structures, Synthesis, and Applications. *Adv. Funct. Mater.* **2018,** *28*, 1705553

7. Liu, Y.; Lehn, J. M.; Hirsch, A. K. H., Molecular Biodynamers: Dynamic Covalent Analogues of Biopolymers. *Acc. Chem. Res.* **2017,** *50*, 376-386.
8. Rottger, M.; Domenech, T.; van der Weegen, R.; Nicolay, A. B. R.; Leibler, L., High-performance vitrimers from commodity thermoplastics through dioxaborolane metathesis. *Science* **2017,** *356*, 62-65.
9. Gu, R. R.; Flidrova, K.; Lehn, J. M., Dynamic Covalent Metathesis in the C=C/C=N Exchange between Knoevenagel Compounds and Imines. *J. Am. Chem. Soc.* **2018,** *140*, 5560-5568.
10. Maeda, T.; Otsuka, H.; Takahara, A., Dynamic covalent polymers: Reorganizable polymers with dynamic covalent bonds. *Prog. Polym. Sci.* **2009,** *34*, 581-604.
11. Rapp, T. L.; DeForest, C. A., Visible Light-Responsive Dynamic Biomaterials: Going Deeper and Triggering More. *Adv. Healthc. Mater.* **2020**.
12. Scott, T. F.; Schneider, A. D.; Cook, W. D.; Bowman, C. N., Photoinduced plasticity in cross-linked polymers. *Science* **2005,** *308*, 1615-1617.
13. Worrell, B. T.; McBride, M. K.; Lyon, G. B.; Cox, L. M.; Wang, C.; Mavila, S.; Lim, C. H.; Coley, H. M.; Musgrave, C. B.; Ding, Y.; Bowman, C. N., Bistable and photoswitchable states of matter. *Nat. Commun.* **2018,** *9*, 2804.
14. Liu, J. H.; Butt, H. J.; Wu, S., Reconfigurable Surfaces Based on Photocontrolled Dynamic Bonds. *Adv. Funct. Mater.* **2019**, 30, 1907605
15. Gong, T.; Feng, J. C.; Wei, W.; Huang, W., Recent progress in diarylethene as a photoswitching unit. *Prog. Chem.* **2006,** *18*, 698-706.
16. Bandara, H. M. D.; Burdette, S. C., Photoisomerization in different classes of azobenzene. *Chem. Soc. Rev.* **2012,** *41*, 1809-1825.
17. Helmy, S.; Leibfarth, F. A.; Oh, S.; Poelma, J. E.; Hawker, C. J.; de Alaniz, J. R., Photoswitching Using Visible Light: A New Class of Organic Photochromic Molecules. *J. Am. Chem. Soc.* **2014,** *136*, 8169-8172.
18. Klajn, R., Spiropyran-based dynamic materials. *Chem. Soc. Rev.* **2014,** *43*, 148-184.
19. van Dijken, D. J.; Kovaricek, P.; Ihrig, S. P.; Hecht, S., Acylhydrazones as Widely Tunable Photoswitches. *J. Am. Chem. Soc.* **2015,** *137*, 14982-14991.
20. Gerwien, A.; Reinhardt, T.; Mayer, P.; Dube, H., Synthesis of Double-Bond-Substituted Hemithioindigo Photoswitches. *Org. Lett.* **2018,** *20*, 232-235.
21. Kortekaas, L.; Browne, W. R., The evolution of spiropyran: fundamentals and progress of an extraordinarily versatile photochrome. *Chem. Soc. Rev.* **2019,** *48*, 3406-3424.
22. Liu, D.; Sponza, A. D.; Yang, D. D.; Chiu, M., Modulating Polymer Dispersity with Light: Cationic Polymerization of Vinyl Ethers Using Photochromic Initiators. *Angew. Chem. Int. Ed.* **2019,** *58*, 16210-16216.
23. Lvov, A. G.; Yadykov, A. V.; Lyssenko, K. A.; Heinemann, F. W.; Shirinian, V. Z.; Khusniyarov, M. M., Reversible Shifting of a Chemical Equilibrium by Light: The Case of Keto-Enol Tautomerism of a beta-Ketoester. *Org. Lett.* **2020,** *22*, 604-609.
24. Kathan, M.; Hecht, S., Photoswitchable molecules as key ingredients to drive systems away from the global thermodynamic minimum. *Chem. Soc. Rev.* **2017,** *46*, 5536-5550.
25. Lemieux, V.; Gauthier, S.; Branda, N. R., Selective and sequential photorelease using molecular switches. *Angew. Chem. Int. Ed.* **2006,** *45*, 6820-6824.
26. Gostl, R.; Hecht, S., Photoreversible Prodrugs and Protags: Switching the Release of Maleimides by Using Light under Physiological Conditions. *Chem. Eur. J.* **2015,** *21*, 4422-4427.
27. Fuhrmann, A.; Gostl, R.; Wendt, R.; Kotteritzsch, J.; Hager, M. D.; Schubert, U. S.; Brademann-Jock, K.; Thunemann, A. F.; Nochel, U.; Behl, M.; Hecht, S., Conditional repair by locally switching the thermal healing capability of dynamic covalent polymers with light. *Nat. Commun.* **2016,** *7*. 13623
28. Asadirad, A. M.; Boutault, S.; Erno, Z.; Branda, N. R., Controlling a Polymer Adhesive Using Light and a Molecular Switch. *J. Am. Chem. Soc.* **2014,** *136*, 3024-3027.
29. Kathan, M.; Eisenreich, F.; Jurissek, C.; Dallmann, A.; Gurke, J.; Hecht, S., Light-driven molecular trap enables bidirectional manipulation of dynamic covalent systems. *Nat. Chem.* **2018,** *10*, 1031-1036.
30. Kathan, M.; Kovaříček, P.; Jurissek, C.; Senf, A.; Dallmann, A.; Thünemann, A. F.; Hecht, S., Control of Imine Exchange Kinetics with Photoswitches to Modulate Self-Healing in Polysiloxane Networks by Light Illumination. *Angew. Chem. Int. Ed.* **2016,** *55*, 13882-13886.
31. Yesilyurt, V.; Webber, M. J.; Appel, E. A.; Godwin, C.; Langer, R.; Anderson, D. G., Injectable Self-Healing Glucose-Responsive Hydrogels with pH-Regulated Mechanical Properties. *Adv. Mater.* **2016,** *28*, 86-91.
32. Yesilyurt, V.; Ayoob, A. M.; Appel, E. A.; Borenstein, J. T.; Langer, R.; Anderson, D. G., Mixed Reversible Covalent Crosslink Kinetics Enable Precise, Hierarchical Mechanical Tuning of Hydrogel Networks. *Adv. Mater.* **2017,** *29*, 1605947.
33. Guan, Y.; Zhang, Y., Boronic acid-containing hydrogels: synthesis and their applications. *Chem. Soc. Rev.* **2013,** *42*, 8106-8121.
34. Cromwell, O. R.; Chung, J.; Guan, Z. B., Malleable and Self-Healing Covalent Polymer Networks through Tunable Dynamic Boronic Ester Bonds. *J. Am. Chem. Soc.* **2015,** *137*, 6492-6495.
35. Hargrove, A. E.; Reyes, R. N.; Riddington, I.; Anslyn, E. V.; Sessler, J. L., Boronic Acid Porphyrin Receptor for Ginsenoside Sensing. *Org. Lett.* **2010,** *12*, 4804-4807.
36. Ni, N. T.; Laughlin, S.; Wang, Y. J.; Feng, Y.; Zheng, Y. J.; Wang, B. H., Probing the general time scale question of boronic acid binding with sugars in aqueous solution at physiological pH. *Bioorg. Med. Chem.* **2012,** *20*, 2957-2961.
37. Chapin, B. M.; Metola, P.; Vankayala, S. L.; Woodcock, H. L.; Mooibroek, T. J.; Lynch, V. M.; Larkin, J. D.; Anslyn, E. V., Disaggregation is a Mechanism for Emission Turn-On of ortho-Aminomethylphenylboronic Acid-Based Saccharide Sensors. *J. Am. Chem. Soc.* **2017,** *139*, 5568-5578.
38. Sun, X. L.; James, T. D.; Anslyn, E. V., Arresting "Loose Bolt" Internal Conversion from -B(OH)(2) Groups is the Mechanism for Emission Turn-On in ortho-Aminomethylphenylboronic Acid-Based Saccharide Sensors. *J. Am. Chem. Soc.* **2018,** *140*, 2348-2354.
39. Sun, X. L.; Chapin, B. M.; Metola, P.; Collins, B.; Wang, B. H.; James, T. D.; Anslyn, E. V., The mechanisms of boronate ester formation and fluorescent turn-on in ortho-aminomethylphenylboronic acids. *Nat. Chem.* **2019,** *11*, 768-778.
40. Monajemi, H.; Cheah, M. H.; Lee, V. S.; Zain, S. M.; Abdullah, W. A. T. W., On the kinetics and reaction mechanisms of boronic acid in interaction with diols for non-enzymatic glucose monitoring applications: a hybrid DFT study. *RSC Adv.* **2014,** *4*, 10505-10513.
41. Marinaro, W. A.; Prankerd, R.; Kinnari, K.; Stella, V. J., Interaction of Model Aryl- and Alkyl-Boronic Acids and 1,2-Diols in Aqueous Solution. *J. Pharm. Sci.* **2015,** *104*, 1399-1408.
42. Brooks, W. L. A.; Deng, C. C.; Sumerlin, B. S., Structure-Reactivity Relationships in Boronic Acid-Diol Complexation. *ACS Omega* **2018,** *3*, 17863-17870.
43. Martinez-Aguirre, M. A.; Flores-Alamo, M.; Medrano, F.; Yatsimirsky, A. K., Examination of pinanediol-boronic acid ester formation in aqueous media: relevance to the relative stability of trigonal and tetrahedral boronate esters. *Org. Biomol. Chem.* **2020,** *18*, 2716-2726.

44. Furikado, Y.; Nagahata, T.; Okamoto, T.; Sugaya, T.; Iwatsuki, S.; Inamo, M.; Takagi, H. D.; Odani, A.; Ishihara, K., Universal Reaction Mechanism of Boronic Acids with Diols in Aqueous Solution: Kinetics and the Basic Concept of a Conditional Formation Constant. *Chem. Eur. J.* **2014,** *20*, 13194-13202.

45. Kano, N.; Yoshino, J.; Kawashima, T., Photoswitching of the Lewis Acidity of a Catecholborane Bearing an Azo Group Based on the Change in Coordination Number of Boron. *Org. Lett.* **2005,** *7*, 3909-3911.

46. Yoshino, J.; Kano, N.; Kawashima, T., Synthesis of organoboron compounds bearing an azo group and substituent effects on their structures and photoisomerization. *Tetrahedron* **2008,** *64*, 7774-7781.

47. Accardo, J. V.; Kalow, J. A., Reversibly tuning hydrogel stiffness through photocontrolled dynamic covalent crosslinks. *Chem. Sci.* **2018,** *9*, 5987-5993.

48. Bahrenburg, J.; Rottger, K.; Siewertsen, R.; Renth, F.; Temps, F., Sequential photoisomerisation dynamics of the push-pull azobenzene Disperse Red 1. *Photochem. Photobiol. Sci.* **2012,** *11*, 1210-1219.

49. Bléger, D.; Schwarz, J.; Brouwer, A. M.; Hecht, S., o-Fluoroazobenzenes as Readily Synthesized Photoswitches Offering Nearly Quantitative Two-Way Isomerization with Visible Light. *J. Am. Chem. Soc.* **2012,** *134*, 20597-20600.

50. Samanta, S.; McCormick, T. M.; Schmidt, S. K.; Seferos, D. S.; Woolley, G. A., Robust visible light photoswitching with ortho-thiol substituted azobenzenes. *Chem. Commun.* **2013,** *49*, 10314-10316.

51. Knie, C.; Utecht, M.; Zhao, F.; Kulla, H.; Kovalenko, S.; Brouwer, A. M.; Saalfrank, P.; Hecht, S.; Bléger, D., ortho-Fluoroazobenzenes: Visible Light Switches with Very Long-LivedZIsomers. *Chem. Eur. J.* **2014,** *20*, 16492-16501.

52. Dong, M. X.; Babalhavaeji, A.; Samanta, S.; Beharry, A. A.; Woolley, G. A., Red-Shifting Azobenzene Photoswitches for in Vivo Use. *Acc. Chem. Res.* **2015,** *48*, 2662-2670.

53. Ahmed, Z.; Siiskonen, A.; Virkki, M.; Priimagi, A., Controlling azobenzene photoswitching through combined ortho-fluorination and -amination. *Chem. Commun.* **2017,** *53*, 12520-12523.

54. Dong, M.; Babalhavaeji, A.; Collins, C. V.; Jarrah, K.; Sadovski, O.; Dai, Q. Y.; Woolley, G. A., Near-Infrared Photoswitching of Azobenzenes under Physiological Conditions. *J. Am. Chem. Soc.* **2017,** *139*, 13483-13486.

55. Konrad, D. B.; Savasci, G.; Allmendinger, L.; Trauner, D.; Ochsenfeld, C.; Ali, A. M., Computational Design and Synthesis of a Deeply Red-Shifted and Bistable Azobenzene. *J. Am. Chem. Soc.* **2020,** *142*, 6538-6547.

56. Schneider, H. J., Hydrogen bonds with fluorine. Studies in solution, in gas phase and by computations, conflicting conclusions from crystallographic analyses. *Chem. Sci.* **2012,** *3*, 1381-1394.

57. Taylor, R., The hydrogen bond between N-H or O-H and organic fluorine: favourable yes, competitive no. *Acta Cryst. B* **2017,** *73*, 474-488.

58. Collins, B. E.; Metola, P.; Anslyn, E. V., On the rate of boronate ester formation in ortho-aminomethyl-functionalised phenyl boronic acids. *Supramol. Chem.* **2013,** *25*, 79-86.

59. Aguirre-Chagala, Y. E.; Santos, J. L.; Huang, Y. X.; Herrera-Alonso, M., Phenylboronic Acid-Installed Polycarbonates for the pH-Dependent Release of Diol-Containing Molecules. *ACS Macro Lett.* **2014,** *3*, 1249-1253.

60. Tang, S. C.; Ma, H.; Tu, H. C.; Wang, H. R.; Lin, P. C.; Anseth, K. S., Adaptable Fast Relaxing Boronate-Based Hydrogels for Probing Cell-Matrix Interactions. *Adv. Sci.* **2018,** *5*, 1800638.

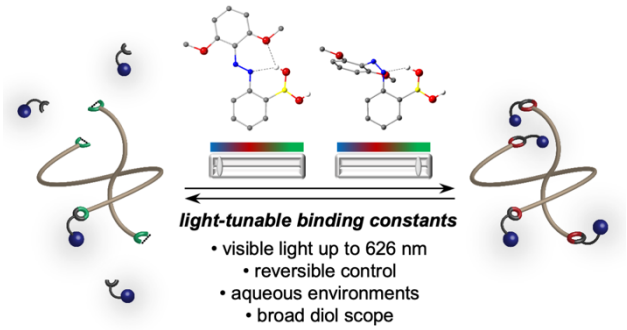
light-tunable binding constants
• visible light up to 626 nm
• reversible control
• aqueous environments
• broad diol scope

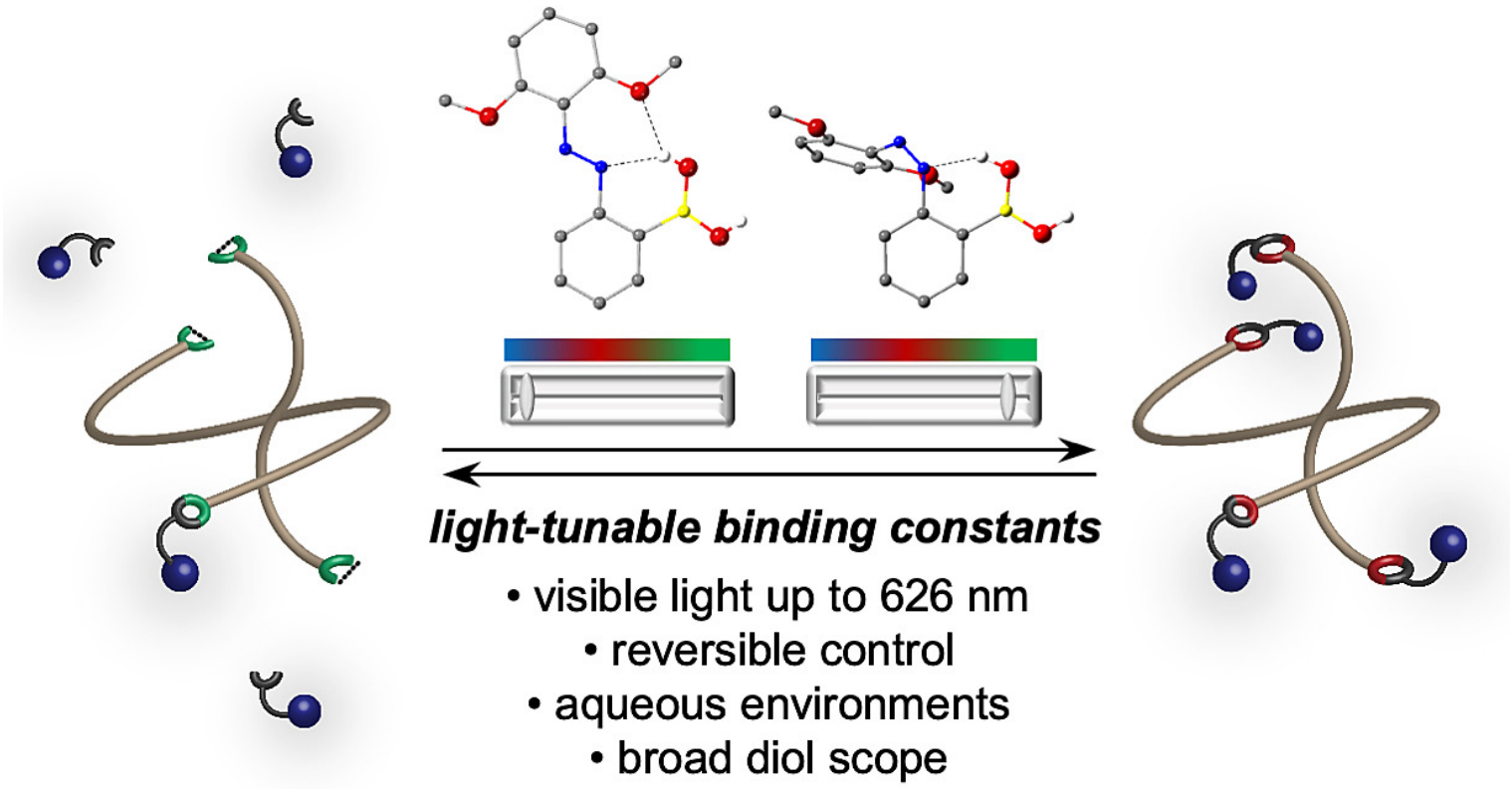

TOC jak.png (217.79 KiB)

Supporting Information

Using visible-light to tune boronic acid–ester equilibria

Joseph Accardo, Emily McClure, Martín A. Mosquera and Julia A. Kalow*

Department of Chemistry, Northwestern University
2145 Sheridan Rd, Evanston, IL 60208

E-mail: jkalow@northwestern.edu

Contents

I. General information

General procedures. Unless otherwise noted, reactions were performed under N_2 atmosphere in oven-dried (150 ºC) glassware. Reaction progress was monitored by thin layer chromatography (Merck silica gel 60 F_{254} plates), visualizing with fluorescence quenching, $KMnO_4$, or ninhydrin stains. Automated column chromatography was performed using SiliCycle SiliaFlash F60 (40-63 μm, 60 Å) in SNAP cartridges on a Biotage Isolera One. Organic solvents were removed *in vacuo* using a rotary evaporator (Büchi Rotovapor R-100, ~20–300 torr) and residual solvent was removed under high vacuum (<200 mtorr). Water-soluble polymers were purified by dialysis using SnakeSkin Dialysis Tubing (3.5 kDa cutoff, 16 mm diameter) purchased from Fisher Scientific.

Materials. Commercial reagents were purchased from Sigma-Aldrich, Acros, Alfa Aesar, TCI, or Oakwood and used as received. 4-Arm PEG-NH_2 HCl salt (M_w 5 kDa) was purchased from JenKem, and was melted under high vacuum (<100 mtorr) prior to functionalization.

Instrumentation. Proton nuclear magnetic resonance (^{1}H NMR) spectra and carbon nuclear magnetic resonance (^{13}C NMR) spectra were recorded on Bruker AVANCE-500 spectrometers at 500 MHz and 125 MHz, and referenced to the solvent residual peaks. ^{19}F NMR spectra were recorded on Bruker AVANCE-500 spectrometers at 470 MHz. Boron nuclear magnetic resonance (^{11}B NMR) spectra were recorded on Bruker AVANCE-400 spectrometers at 128 MHz in Wilmad Precision NMR tubes (CFQ, 500 MHz, OD: 5 mm, wall thickness: 0.38 mm). NMR data are represented as follows: chemical shift (δ ppm), multiplicity (s = singlet, d = doublet, t = triplet, q = quartet, m = multiplet), coupling constant in Hertz (Hz) and integration. UV-Vis spectra were collected on a Cary 5000 UV-vis-NIR spectrophotometer with an Hg lamp; cuvettes were 10-mm path length quartz cells (Starna 23-Q-10). Blue LED strip lights (wavelength = 470 nm, power = 6.6 W) green LED strip lights (wavelength = 525 nm, low power = 5.7 W, high power = 16 W), yellow LED strip lights (wavelength= 590 nm), red LED strip lights (wavelength = 626 nm, power = 6.6W), were purchased from superbrightleds.com.Size exclusion chromatography (SEC) measurements were performed in stabilized, HPLC-grade tetrahydrofuran using an Agilent 1260 Infinity II system with variable-wavelength diode array (254, 450, and 530 nm) and refractive index detectors, guard column (Agilent PLgel; 5μm; 50 x 7.5 mm), and three analytical columns (Agilent PLgel; 5μm; 300 x 7.5 mm; 10^5, 10^4, and 10^3 Å pore sizes). The instrument was calibrated with narrow-dispersity polystyrene standards between 640 Da and 2300 kDa (Polymer Standards Service GmbH). All runs were performed at 1.0 mL/min flow rate and 40 ºC. Molecular weight values are calculated based on the refractive index signal.

II. Synthesis

Nitroso compounds were prepared by the oxidation of the aniline precursor using the Oxone method developed by Rück-Braun.[1]

1-bromo-2-nitrosobenzene (SI-1)

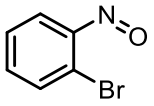

2-bromoaniline (1.00g, 1 Eq, 5.81 mmol) was added to a 100 mL RBF equipped with a stir bar and dissolved in 17 mL of DCM. Oxone (7.15g, 2 Eq, 11.6 mmol) was dissolved into 20 mL of deionized water and added to the reaction, which was left to stir vigorously for 3 hours at ambient temperature. The reaction was diluted with DCM and washed with 1M NaOH (2x) and 1M HCl. The organic layer was collected, dried with sodium sulfate and concentrated. The crude solid was carried on to the following reaction.

(*E*)-1-(2-bromophenyl)-2-(p-tolyl)diazene (SI-2)

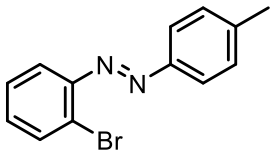

SI-**1** (400 mg, 1 Eq, 2.15 mmol) and p-toluidine (242 mg, 1.05 Eq, 2.26 mmol) were added to a 100 mL round-bottom flask (RBF) equipped with a stir bar. 28 mL of DCM and 7 mL of acetic acid were added and the reaction was stirred at ambient temperature for 4 hours. The reaction mixture was concentrated and dissolved into EtOAc and washed with 1M NaOH to remove acetic acid. The organic fraction was collected, dried with sodium sulfate, and concentrated *in vacuo*. The crude residue was purified by column chromatography (5% EtOAc in hexane) to yield (*E*)-1-(2-bromophenyl)-2-(p-tolyl)diazene (367 mg, 1.33 mmol, 62%) as a red solid.

^{1}H NMR (500 MHz, $CDCl_3$) δ 7.90 (d, *J* = 8.5 Hz, 2H), 7.75 (dd, *J* = 8.0, 1.4 Hz, 1H), 7.67 (dd, *J* = 8.0, 1.7 Hz, 1H), 7.42 – 7.36 (m, 1H), 7.36 – 7.28 (m, 3H), 2.45 (s, 3H).**^{13}C NMR** (125 MHz, $CDCl_3$) δ 150.84, 149.75, 142.29, 133.69, 131.57, 129.84, 127.96, 125.46, 123.44, 117.81, 21.60. **HRMS**: m/z expected for $C_{13}H_{12}BrN_2$ $[M+H]^+$ 275.01, measured 275.02.

(*E*)-(2-(p-tolyldiazenyl)phenyl)boronic acid (1)

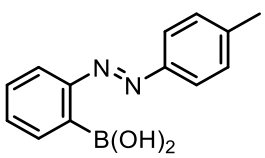

Bis(pinacolato)diboron (299 mg, 1.1 Eq, 1.18 mmol), potassium acetate (316 mg, 3 Eq, 3.22 mmol), and Pd(dppf)Cl_2*dcm (88 mg, 0.1 Eq, 0.107 mmol) were added to a 25-mL Schlenk flask equipped with a stir bar. The reaction was backfilled with nitrogen (3x) and then SI-**2** (295 mg, 1 Eq, 1.07 mmol) was added in 10 mL of dry toluene. The reaction was stirred for 12 hours at 80 °C and then filtered through a Celite plug, concentrated, and re-dissolved into EtOAc. The organic layer was washed with aq. NH_4Cl followed by DI water. The organic layer was collected, dried over sodium sulfate, concentrated and then dissolved in 10 mL of THF and 2 mL of DI water. Sodium periodate (459 mg, 2 Eq, 2.14 mmol) and 1 mL of 1M HCl were added and the reaction was left to stir overnight. The THF was removed *in vacuo* and the crude was re-dissolved in EtOAc. The boronic acid was extracted into water with 1M NaOH. The organic layer was discarded and the aqueous layer was neutralized with 1M HCl leading to boronic acid precipitation. It was further re-extracted with EtOAc and concentrated to give a brown-yellow oil. 25 mL of hexane was added to the oil which was sonicated for 30 minutes leading to the precipitation of a yellow solid. This was collected on a filter to yield (*E*)-(2-(p-tolyldiazenyl)phenyl)boronic acid (70 mg, 0.29 mmol, 27%) as a yellow solid.

^{1}H NMR (500 MHz, DMSO-d_6) δ 7.86 (d, J = 8.0 Hz, 1H), 7.79 (d, J = 8.3 Hz, 2H), 7.57 – 7.46 (m, 3H), 7.42 (d, J = 8.1 Hz, 2H), 2.42 (s, 3H). **^{13}C NMR** (125 MHz, DMSO-d_6) δ 155.21, 149.47, 142.29, 133.15, 130.99, 130.42, 129.62, 122.94, 122.74, 21.53. **HRMS** m/z expected for $C_{13}H_{14}BN_2O_2$ $[M+H]^+$ 241.11, measured 241.11.

1,3-difluoro-2-nitrosobenzene (SI-3)

2,6-difluoroaniline (560 mg, 500 µL, 1 Eq, 4.34 mmol) was added to a 100 mL RBF equipped with a stir bar and dissolved in 14 mL of DCM. Oxone (5.33 g, 2 Eq, 8.67 mmol) was dissolved into 16 mL of DI water, and added to the reaction. The reaction was stirred vigorously for 24 hours at ambient temperature. The reaction was diluted with DCM and washed with 1M NaOH (2x) and 1M HCl. The organic layer was collected, dried with sodium sulfate and concentrated. The crude was carried on to the following reaction.

(*E*)-(2-((2,6-difluorophenyl)diazenyl)phenyl)boronic acid (2)

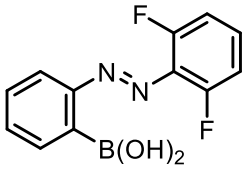

SI-**3** (350 mg, 1 Eq, 2.45 mmol) and 2-(4,4,5,5-tetramethyl-1,3,2-dioxaborolan-2-yl)aniline (536 mg, 1 Eq, 2.45 mmol) were added to a 25 mL RBF equipped with a stir bar. Acetic acid (10 mL) was added and the reaction was stirred at ambient temperature for 24 hours. The reaction was then diluted with DCM and washed with sodium bicarbonate (2x) to remove AcOH. The organic layers were dried with sodium sulfate and concentrated and carried through to the deprotection step without any further

purification. The crude residue was dissolved into 60 mL of THF into a 250 mL RBF, to which sodium periodate (1.57 g, 3 Eq, 7.34 mmol) and 2 mL of 1M HCl were added. The reaction was stirred overnight. The solvent was then removed, and the product was dissolved into EtOAc and washed with water. The organic layer was collected and dried over sodium sulfate. It was then passed through a small silica plug, first with 40:60 EtOAc in hexane to remove the byproduct and then with 5% MeOH in DCM. The MeOH-DCM fractions were collected and concentrated *in vacuo*. The crude boronic acid was further purified with 1M NaOH basic extraction against EtOAc (1x). The basic aqueous layer was then neutralized with 1M HCl and the boronic acid was re-extracted with EtOAc. Finally, the organic layers were collected and concentrated and washed with cold ACN to yield (*E*)-(2-((2,6-difluorophenyl)diazenyl)phenyl)boronic acid (75 mg, 0.29 mmol, 12%) as an orange solid.

^{1}H NMR (500 MHz, DMSO-d_6) δ 8.01 (s, 2H), 7.84 – 7.78 (m, 1H), 7.78 – 7.72 (m, 1H), 7.65 – 7.57 (m, 3H), 7.42 – 7.32 (m, 2H).**^{13}C NMR** (125 MHz, DMSO) δ 156.69, 156.24, 154.65, 134.58, 132.80, 130.44, 119.28, 113.72, 113.56. **HRMS:** m/z expected for $C_{12}H_{10}BF_2N_2O_2$ $[M+H]^+$ 263.07, measured 263.08.

(*E*)-1-(2-bromophenyl)-2-(2,6-dimethoxyphenyl)diazene (SI-4)

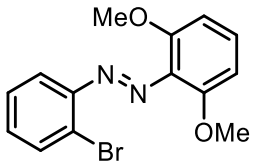

SI-**1** (885 mg, 1 Eq, 4.67 mmol) was added to a flask charged with a stir bar and dissolved in 36 mL of DCM. 2,6-dimethoxyaniline (729 mg, 1 Eq, 4.76 mmol) and acetic acid (5.7 mL, 21 Eq, 100 mmol) were added to the flask which was allowed to stir open to air overnight at ambient temperature. The reaction mixture was then concentrated *in vacuo*, re-dissolved in EtOAc (40 mL) and washed with 40 mL 1 M HCl (3x). The organic layers were collected, dried over sodium sulfate and concentrated *in vacuo*. The resulting crude was purified *via* flash column chromatography (20% EtOAc in hexane) to yield (*E*)-1-(2-bromophenyl)-2-(2,6-dimethoxyphenyl)diazene (835 mg, 55%) as a red powder.

^{1}H NMR (500 MHz, $CDCl_3$) δ 7.73 (dd, *J* = 7.9, 1.3 Hz, 1H), 7.57 (dd, *J* = 7.9, 1.7 Hz, 1H), 7.43 – 7.34 (m, 1H), 7.33 – 7.27 (m, 2H), 6.70 (d, *J* = 8.4 Hz, 2H), 3.89 (s, 6H).**^{13}C NMR** (126 MHz, $CDCl_3$) δ 153.26, 151.43, 135.62, 131.32, 130.70, 127.99, 125.28, 123.84, 118.13, 106.54, 56.70. **HRMS:** m/z expected for $C_{14}H_{14}BrN_2O_2$ $[M+H]^+$ 321.02, measured 321.02.

(*E*)-(2-((2,6-dimethoxyphenyl)diazenyl)phenyl)boronic acid (3)

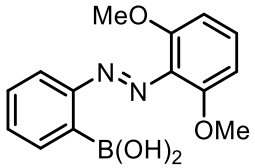

SI-**4** (2.50 g, 1 Eq, 7.78 mmol), bis(pinacolato)diboron (2.17 g, 1.1 Eq, 8.56 mmol), potassium acetate (2.29 g, 3 Eq, 23.4 mmol), and Pd(dppf)Cl_2*dcm (636 mg, 0.1 Eq, 0.778 mmol) were added to a flask equipped with stir bar and degassed and back-filled with nitrogen (3x). Toluene (85 mL) was added

via cannula and the reaction was stirred under nitrogen at 80°C overnight. The solution was filtered through a celite plug, using EtOAc to elute additional product. The product was concentrated *in vacuo*, and diluted with 150 mL of THF and 39 mL of DI water. Sodium periodate (3.33 g, 2 Eq, 15.6 mmol) was added and allowed to stir for 30 minutes before adding 1 M HCl (7.7 mL). The reaction was stirred overnight at ambient temperature. The organic solvent was removed *in vacuo* and the product was washed with EtOAc. The resulting organic layer was extracted with 1 M NaOH. The aqueous layer was neutralized with 1 M HCl and extracted with EtOAc. The resulting organic layer was dried over sodium sulfate and concentrated to yield a crude product that was washed with DCM on a fritted funnel to yield (*E*)-(2-((2,6-dimethoxyphenyl)diazenyl)phenyl)boronic acid (672 mg, 30%) as a free-flowing dark orange powder.

^{1}H NMR (500 MHz, DMSO-d_6) δ 8.52 (s, 2H), 8.00 (dd, J = 7.4, 1.7 Hz, 1H), 7.73 (dd, J = 8.1, 1.2 Hz, 1H), 7.61 – 7.45 (m, 3H), 6.90 (d, J = 8.5 Hz, 2H), 3.90 (s, 6H).**^{13}C NMR** (126 MHz, DMSO-d_6) δ 158.08, 157.71, 154.61, 136.51, 133.64, 131.74, 131.14, 130.52, 114.11, 105.79, 56.62. **HRMS:** m/z expected for $C_{14}H_{16}BN_2O_4$ $[M+H]^+$ 287.11, measured 287.12

1-bromo-4-nitrosobenzene (SI-5)

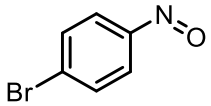

4-bromoaniline (500 mg, 1 Eq, 2.91 mmol) was added to a 100 mL RBF equipped with a stir bar and dissolved in 7 mL of DCM. Oxone (3.57 g, 2 Eq, 5.81 mmol) was dissolved into 28 mL of deionized water and added to the reaction, which was left to stir vigorously for 3 hours at ambient temperature. The reaction was diluted with DCM and washed with 1M NaOH (2x) and 1M HCl. The organic layer was collected, dried with sodium sulfate and concentrated. The crude was carried on to the following reaction.

(*E*)-1-(4-bromophenyl)-2-(2,6-dimethoxyphenyl)diazene (SI-6)

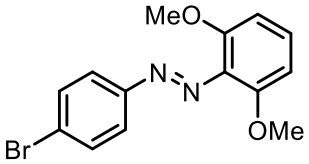

SI-**5** (910 mg, 1.1 Eq, 4.89 mmol) was added to a flask equipped with a stir bar and dissolved in 40 mL of DCM. 2,6-dimethoxy aniline (681 mg, 1.0 Eq, 4.45 mmol) and acetic acid (5.34 mL, 21 Eq, 93.4 mmol) were added and the reaction was left to stir at ambient temperature overnight. The reaction mixture was then concentrated *in vacuo* and diluted with 100 mL EtOAc and washed with 1 M HCl. The aqueous layer was washed with 75 mL EtOAc (3x) and the combined organic layers were dried over sodium sulfate and concentrated *in vacuo*. The resulting crude red oil was purified by column chromatography (30% EtOAc in hexane) to yield (*E*)-1-(4-bromophenyl)-2-(2,6-dimethoxyphenyl)diazene (719.4 mg, 51%) as a red powder.

^{1}H NMR (500 MHz, $CDCl_3$) δ 7.77 – 7.71 (m, 2H), 7.64 – 7.58 (m, 2H), 7.28 – 7.21 (m, 1H), 6.66 (d, J = 8.4 Hz, 2H), 3.82 (s, 6H).**^{13}C NMR** (125 MHz, $CDCl_3$) δ 152.52, 152.19, 133.47, 132.19, 130.00, 125.18, 124.13, 105.12, 56.48 **LRMS:** m/z expected for $C_{14}H_{14}BrN_2O_2$ $[M+H]^+$ 321.02, measured 321.0

(*E*)-(4-((2,6-dimethoxyphenyl)diazenyl)phenyl)boronic acid (4)

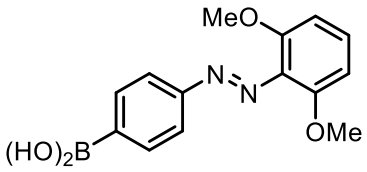

SI-**6** (670 mg, 1 Eq, 2.09 mmol), bis(pinacolato)diboron (583 mg, 1.1 Eq, 2.29 mmol), potassium acetate (614 mg, 3 Eq, 6.26 mmol), and Pd(dppf)Cl2*dcm (170 mg, 0.1 Eq, 0.209 mmol) were added to a flask charged with stir bar and degassed and back-filled with nitrogen (3x). Toluene (20 mL) was added *via* cannula and the reaction was stirred under nitrogen at 80 ºC overnight. It was then filtered through celite, using EtOAc to elute additional product. The filtrate was then concentrated and re-dissolved in THF (27 mL) followed by addition of sodium periodate (892 mg, 2 Eq, 4.17 mmol) in 7 mL of DI water. After 30 minutes of stirring, 1.3 mL of 1 M HCl was added to the reaction mixture and further stirred overnight at room temperature. The organic layer was removed *in vacuo* and the resulting aqueous solution was extracted with EtOAc. The crude was then purified by column chromatography (10% MeOH in DCM), followed by a base extraction and a plug column first with 50% EtOAc in Hexanes then 10% MeOH in DCM to yield (E)-(4-((2,6-dimethoxyphenyl)diazenyl)phenyl)boronic acid (39 mg, 7%) as a dark red powder.

^{1}H NMR (500 MHz, DMSO-d_6) δ 8.23 (s, 2H), 7.97 (d, J = 8.3 Hz, 2H), 7.70 (d, J = 8.3 Hz, 2H), 7.31 (t, J = 8.4 Hz, 1H), 6.81 (d, J = 8.5 Hz, 1H), 3.75 (s, 6H).**^{13}C NMR** (125 MHz, DMSO-d_6) δ 153.67, 151.53, 135.10, 129.66, 121.08, 116.63, 105.27, 104.42, 56.22. **HRMS:** m/z expected for $C_{14}H_{16}BN_2O_4$ $[M+H]^+$ 287.11, measured 287.12

(*E*)-1-(2-bromophenyl)-2-(2,4-dimethoxyphenyl)diazene (SI-7)

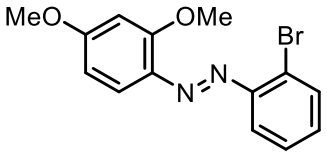

To a flask equipped with a stir bar, SI-**1** (500 mg, 1.2 Eq, 2.69 mmol) in 20 mL of DCM was added followed by 2,4 dimethoxy aniline (343 mg, 1 Eq, 2.24 mmol) and acetic acid (2.69 mL, 21 Eq, 47 mmol). The reaction was left to stir overnight at ambient temperature. The reaction mixture was washed with 75 mL of sodium bicarbonate (3x), followed by 75 mL of 1 M HCl (2x). The combined organic layers were dried over sodium sulfate and concentrated *in vacuo*. The resulting product was purified *via* column chromatography (25% EtOAc in hexane) to yield (*E*)-1-(2-bromophenyl)-2-(2,4-dimethoxyphenyl)diazene (624 mg, 87%) as a red powder.

^{1}H NMR (500 MHz, $CDCl_3$) δ 7.85 (d, *J* = 8.9 Hz, 1H), 7.75 – 7.68 (m, 1H), 7.63 (dd, *J* = 8.0, 1.7 Hz, 1H), 7.35 (ddd, *J* = 8.1, 7.3, 1.4 Hz, 1H), 7.28 – 7.20 (m, 2H), 6.59 – 6.42 (m, 1H), 4.02 (s, 3H), 3.89 (d, *J* = 1.3 Hz, 3H).**^{13}C NMR** (125 MHz, $CDCl_3$) δ 164.34, 159.77, 150.85, 137.44, 134.83, 131.56, 128.91, 124.75, 118.89, 118.33, 106.56, 99.79, 56.41, 55.72. **HRMS:** m/z expected for $C_{14}H_{14}BrN_2O_2$ $[M+H]^+$ 321.02, measured 321.02

(*E*)-(2-((2,4-dimethoxyphenyl)diazenyl)phenyl)boronic acid (5)

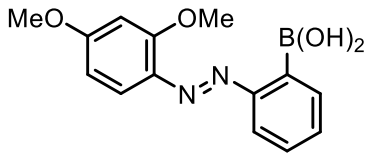

SI-**7** (600 mg, 1 Eq, 1.87 mmol), bis(pinacolato)diboron (522 mg, 1.1 Eq, 2.05 mmol), potassium acetate (550 mg, 3 Eq, 5.60 mmol), and Pd(dppf)Cl2*dcm (137 mg, 0.1 Eq, 0.187 mmol) were added to a flask charged with stir bar and degassed and back-filled with nitrogen (3x). Toluene (20 mL) was added *via* cannula and the reaction was stirred under nitrogen at 80 ºC overnight. The reaction mixture was then filtered through celite, using EtOAc to elute additional product. The filtrate was concentrated and re-dissolved in THF (36 mL). To it sodium periodate (799 mg, 2 Eq, 3.74 mmol) in 9 mL of DI water was added and after 30 minutes of stirring, 0.9 mL of 1 M HCl was added to the reaction mixture which was then left to stir overnight at room temperature. The organic layer was removed *in vacuo* and the resulting aqueous solution was extracted with EtOAc and dried over sodium sulfate. The organic layer was concentrated and purified *via* column chromatography (10% MeOH in DCM). The resulting product was concentrated and re-dissolved in EtOAc, extracted with 1 M NaOH. The basic layer was neutralized with 1 M HCl and extracted with EtOAc, dried over sodium sulfate, and concentrated to yield (E)-(2-((2,4-dimethoxyphenyl)diazenyl)phenyl)boronic acid (181 mg, 34%) as a red powder.

^{1}H NMR (500 MHz, DMSO-d_6) δ 8.27 (s, 2H), 7.79 (dd, J = 7.3, 1.6 Hz, 1H), 7.71 (dd, J = 8.1, 1.2 Hz, 1H), 7.67 (d, J = 8.9 Hz, 1H), 7.52 (td, J = 7.7, 1.6 Hz, 1H), 7.46 (td, J = 7.2, 1.2 Hz, 1H), 6.79 (d, J = 2.6 Hz, 1H), 6.73 (dd, J = 8.9, 2.5 Hz, 1H), 3.96 (s, 3H), 3.89 (s, 3H). **^{13}C NMR** (125 MHz, DMSO-d_6) δ 164.13, 157.22, 156.67, 135.88, 135.07, 130.73, 130.29, 129.76, 124.02, 122.69, 116.32, 106.89, 99.84, 56.48, 56.30. **HRMS:** m/z expected for $C_{14}H_{16}BN_2O_4$ $[M+H]^+$ 287.11, measured 287.12

methyl 3-bromo-4-nitrosobenzoate (SI-8)

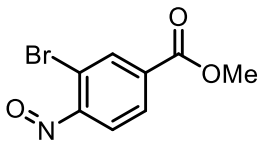

Methyl 4-amino-3-bromobenzoate (230 mg, 1 Eq, 1.00 mmol) was dissolved into 6 mL of DCM into a 50 mL RBF equipped with a stir bar. Oxone (1.84 g, 3 Eq, 3.00 mmol) was dissolved into 24 mL of water, and was added into the RBF. The reaction was left to stir for 36 hours at ambient temperature. The reaction was diluted with DCM and washed with 1M NaOH (2x) and 1M HCl. The organic layer was collected, dried with sodium sulfate and concentrated. The crude was purified by flash

chromatography (10% EtOAc in hexane) to yield the product as a yellow solid, which was carried on to the following reaction.

methyl (*E*)-3-bromo-4-((2,6-dimethoxyphenyl)diazenyl)benzoate (SI-9)

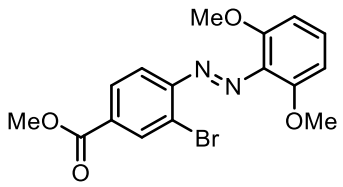

In a 250-mL RBF equipped with a stir bar, SI-**8** (560 mg, 1 Eq, 2.29 mmol) and 2,6-dimethoxyaniline (352 mg, 1 Eq, 2.29 mmol) were dissolved into DCM. To it 10 mL of AcOH was added and the reaction was capped and let stir for 24 hours at ambient temperature. Initially the reaction solution was a dark green color, which quickly became darker and the green color faded away. After 24 hours, the reaction was a deep red/black solution. The reaction was then diluted with DCM and washed with 1M NaOH and then with 1M HCl. The organic layer was collected, dried over sodium sulfate, and concentrated. The crude was purified with flash chromatography (20% EtOAc in hexane) to yield methyl (*E*)-3-bromo-4-((2,6-dimethoxyphenyl)diazenyl)benzoate (301 mg, 35%) as red solid.

^{1}H NMR (500 MHz, $CDCl_3$) δ 8.38 (s, 1H), 8.01 (d, *J* = 8.0 Hz, 1H), 7.54 (d, *J* = 8.3 Hz, 1H), 7.31 (t, *J* = 8.4 Hz, 1H), 6.68 (d, *J* = 8.4 Hz, 2H), 3.93 (s, 3H), 3.89 (s, 6H).**^{13}C NMR** (125 MHz, $CDCl_3$) δ 165.54, 154.20, 153.72, 134.78, 133.00, 132.16, 131.84, 129.35, 123.58, 117.99, 105.12, 56.66, 52.52. **HRMS:** m/z expected for $C_{16}H_{16}BrN_2O_4$ $[M+H]^+$ 379.02, measured 379.03

(*E*)-(2-((2,6-dimethoxyphenyl)diazenyl)-5-(methoxycarbonyl)phenyl)boronic acid (SI-10)

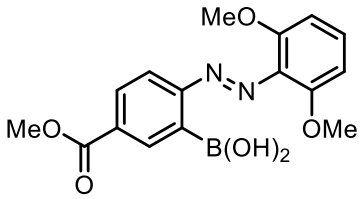

Bis(pinacolato)diboron (222 mg, 1.1 Eq, 873 μmol), potassium acetate (234 mg, 3 Eq, 2.38 mmol) and $Pd(dppf)Cl_2$*dcm (64.8 mg, 0.1 Eq, 79.4 μmol) were added to a 50 mL schlenk flask equipped with a stir rod. The reaction was backfilled (3x) with nitrogen and then SI-**9** (301 mg, 1 Eq, 794 μmol) was added in 35 mL of dry toluene. The reaction was stirred for 18 hours at 80 ºC. Upon completion, the reaction was cooled to room temperature and filtered through a celite plug. The filtrate was then concentrated and re-dissolved in EtOAc. The organic layer was washed with saturated NH_4Cl followed by DI water. Combined organic layers were collected, dried over sodium sulfate, concentrated and then re-dissolved in 10 mL of THF into a 25 mL RBF equipped with a stir bar. 2 mL of DI water and sodium periodate (340 mg, 1.59 mmol) were added to it and stirred overnight. Upon completion, the organic solvent was removed *in vacuo*. The crude was dissolved in EtOAc and washed with saturated NH_4Cl. The organic layer was collected, dried over sodium sulfate and concentrated to yield (*E*)-(2-((2,6-dimethoxyphenyl)diazenyl)-5-(methoxycarbonyl)phenyl)boronic acid (154 mg, 448 μmol, 56%) as a red solid.

^{1}H NMR (500 MHz, DMSO-d_6) δ 8.67 (s, 2H), 8.60 (s, 1H), 8.14 (d, J = 8.5 Hz, 1H), 7.81 (d, J = 8.6 Hz, 1H), 7.55 (t, J = 8.5 Hz, 1H), 6.93 (d, J = 8.5 Hz, 2H), 3.93 (s, 6H), 3.91 (s, 3H). **^{13}C NMR** (125 MHz, DMSO-d_6) δ 166.38, 160.05, 155.04, 137.73, 134.91, 132.54, 131.04, 130.55, 114.60, 105.82, 56.72, 52.78. **HRMS:** m/z expected for $C_{16}H_{17}BN_2O_6$ $[M+H]^+$ 345.12 , measured 345.12.

(*E*)-3-borono-4-((2,6-dimethoxyphenyl)diazenyl)benzoic acid (SI-11)

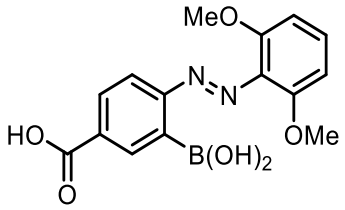

To a 100 mL RBF equipped with a stir bar, compound SI-**10** (200 mg, 1 Eq, 581 μmol) in methanol (21 mL) was added followed by LiOH (41.8 mg, 3 Eq, 1.74 mmol) in 8 mL of water. It was then stirred for 48 hours at ambient temperature, then diluted with EtOAc and DI water (1:1). The product remained in the aqueous layer, so the organic layer was discarded. The aqueous layer was then neutralized with 1M HCl and extracted back into EtOAc. The organic layer was collected, dried over sodium sulfate and concentrated. The product was washed extensively with acetonitrile to yield (*E*)-3-borono-4-((2,6-dimethoxyphenyl)diazenyl)benzoic acid (153 mg, 80%) as an orange solid.

^{1}H NMR (500 MHz, DMSO-d_6) δ 8.67 (s, 2H), 8.58 (s, 1H), 8.11 (dd, J = 8.5, 2.1 Hz, 1H), 7.78 (d, J = 8.4 Hz, 1H), 7.54 (t, J = 8.5 Hz, 1H), 6.92 (d, J = 8.5 Hz, 2H), 3.92 (s, 6H).**^{13}C NMR** (125 MHz, DMSO-d_6) δ 167.47, 159.89, 155.00, 137.93, 134.84, 132.72, 132.22, 130.43, 114.38, 105.77, 56.69. **LRMS:** m/z expected for $C_{15}H_{16}BN_2O_6$ $[M+H]^+$ 331.1 , measured 331.1

7-(2-aminoethoxy)-2H-chromen-2-one hydrochloride (SI-12)

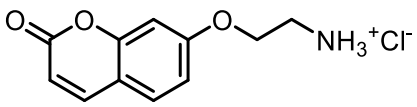

7-Hydroxy-2H-chromen-2-one (635 mg, 1 Eq, 3.92 mmol) and potassium carbonate (388 mg, 1 Eq, 3.92 mmol) were dissolved in acetonitrile (10 mL) into a 25 mL 3-neck RBF equipped with a stir bar and condenser. To it, tert-butyl (2-bromoethyl)carbamate (878 mg, 1 Eq, 3.92 mmol) in 10 mL of dry acetonitrile was added and stirred at refluxing conditions for 20 hours, leading to the formation of bright yellow solid precipitates. Upon completion, the reaction was concentrated and dissolved into EtOAc and washed with saturated $NaHCO_3$. The organic layer was dried and concentrated to about 20 mL, to which 25 drops of concentrated HCl was added. This led to the precipitation of a white solid over two hours which was collected by filtration and characterized as the HCl salt. The salt was then free based by dissolving 50 mg into 10 mL of MeOH followed by addition of 10 eq of solid $NaHCO_3$ and letting stir for 3 hours. After the solvent was removed and the crude was dissolved in DCM and washed with water. The organic layer was dried over sodium sulfate and concentrated. The amino compound was unstable at room temperature, so was immediately carried towards next reaction without any further purification.

Data for compound SI-9 : ^{1}H NMR (500 MHz, DMSO-d_6) δ 8.11 (s, 3H), 8.03 (d, J = 9.5 Hz, 1H), 7.69 (d, J = 8.6 Hz, 1H), 7.06 (d, J = 2.4 Hz, 1H), 7.01 (dd, J = 8.6, 2.4 Hz, 1H), 6.34 (d, J = 9.5 Hz, 1H), 4.29 (t, J = 5.1 Hz, 2H), 3.25 (p, J = 5.4 Hz, 2H). **^{13}C NMR** (125 MHz, DMSO-d_6) δ 161.33, 160.65, 155.73, 144.74, 130.10, 113.40, 113.31, 113.21, 101.97, 65.53, 38.62. **HRMS:** m/z expected for $C_{11}H_{12}NO_3$ $[M+H]^+$ 206.07 , measured 206.08.

2,3,4,5,6-pentahydroxy-N-(2-((2-oxo-2H-chromen-7-yl)oxy)ethyl)hexanamide (17)

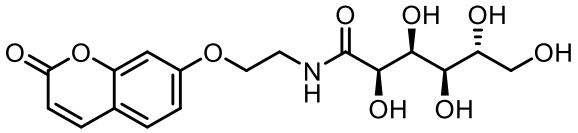

7-(2-Aminoethoxy)-2H-chromen-2-one (30.0 mg, 1 Eq, 146 μmol, free base of **SI-12**) was dissolved into acetonitrile (10 mL) in a 20 mL scintillation vial equipped with a stir bar, and 3,4,5-trihydroxy-6-(hydroxymethyl)tetrahydro-2H-pyran-2-one (24.7 mg, 0.95 Eq, 139 μmol) was added. The reaction was heated to 70 ºC overnight. The reaction was then filtered over Celite and the filtrate was concentrated and washed with MeOH to yield 2,3,4,5,6-pentahydroxy-N-(2-((2-oxo-2H-chromen-7-yl)oxy)ethyl)hexanamide (25 mg, 65 μmol, 45%) as a white solid.

^{1}H NMR (500 MHz, DMSO-d_6) δ 8.06 (d, J = 9.5 Hz, 1H), 7.70 (d, J = 8.6 Hz, 1H), 7.09 (s, 1H), 7.03 (dd, J = 8.6, 2.4 Hz, 1H), 6.36 (d, J = 9.5 Hz, 1H), 4.19 (t, J = 6.1 Hz, 2H), 4.10 (d, J = 3.8 Hz, 1H), 3.99 (s, 1H), 3.66 – 3.49 (m, 6H).**^{13}C NMR** (125 MHz, DMSO-d_6) δ 173.39, 161.96, 160.80, 155.82, 144.81, 130.01, 113.22, 113.01, 112.93, 101.71, 73.81, 72.57, 71.80, 70.43, 67.21, 63.63, 37.81. **LRMS:** m/z expected for $C_{17}H_{20}NO_9$ $[M-H]^-$ 382.12 , measured 382.0.

(*E*)-1-(2-bromophenyl)-2-(2,6-diethylphenyl)diazene (SI-13)

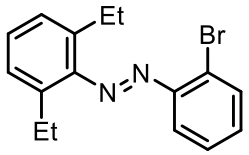

To a 250 mL flask equipped with a stir bar, SI-**1** (872 mg, 1 Eq, 4.69 mmol) and 2,6-diethylaniline (735 mg, 811 μL, 1.05 Eq, 4.92 mmol) were dissolved into 60 mL of DCM, to which 15 mL of AcOH was added to. The reaction was left to run for 7 days at ambient temperature, which was then diluted with DCM and washed with 1M NaOH (2x). The organic fraction was collected, dried with sodium sulfate, and concentrated. The crude was dissolved into hexane and passed through a silica plug with hexane. The eluent was collected, concentrated, and then passed through an alumina plug with hexane. The hexane was concentrated to approximately 10 mL and cooled to –20 °C, which led to the crystallization of an impurity. The product was collected as a dark red oil, (*E*)-1-(2-bromophenyl)-2-(2,6-diethylphenyl)diazene (187 mg, 0.53 mmol, 11%, >90% ^{1}H NMR purity), and carried on to the next reaction without further purification. **^{1}H NMR** (500 MHz, $CDCl_3$) δ 7.70 (dd, J = 7.9, 1.3 Hz, 1H), 7.53 (dd, J = 8.0, 1.7 Hz, 1H), 7.34 (ddd, J = 8.0, 7.2, 1.4 Hz, 1H), 7.26 (ddd, J = 7.8, 7.2, 1.7 Hz, 1H), 7.20 – 7.16 (m, 1H), 7.11 (d, J = 7.6 Hz, 2H).

(*E*)-1-(2,6-diethylphenyl)-2-(2-(4,4,5,5-tetramethyl-1,3,2-dioxaborolan-2-yl)phenyl)diazene (6)

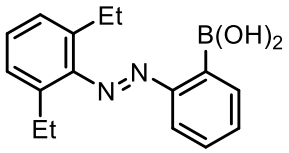

Bis(pinacolato)diboron (165 mg, 1.1 Eq, 648 μmol), potassium acetate (174 mg, 3 Eq, 1.77 mmol) and Pd(dppf)Cl_2*dcm (48.1 mg, 0.1 Eq, 58.9 μmol) were added to a 25 mL schlenk flask equipped with a stir rod. The reaction was backfilled (3x) with nitrogen and then SI-**13** (187 mg, 1 Eq, 589 μmol) was added in 8 mL of dry toluene. The reaction was stirred for 18 hours at 80 ºC. Upon completion, the reaction was cooled to room temperature and filtered through a celite plug. The solvent was removed, the crude was diluted in DCM and washed with water. The organic layer was dried with sodium sulfate, and concentrated. The crude was dissolved into 9 mL of THF into a 100 mL RBF equipped with a stir bar, to which 2.25 mL of water and sodium periodate (379 mg, 3 Eq, 1.77 μmol) were added to. 0.5 mL of 1M HCl was added and the reaction was left to react overnight at ambient temperature. After the reaction was diluted with EtOAc and washed with water. The organic layer was collected, dried with sodium sulfate, and concentrated. The crude was purified by flash chromatography (20% EtOAc in hexane) to yield , (*E*)-(2-((2,6-diethylphenyl)diazenyl)phenyl)boronic acid (99 mg, 350 μmol, 59%) as a red oil.

^{1}H NMR (500 MHz, DMSO-d_6) δ 7.94 – 7.87 (m, 1H), 7.69 – 7.57 (m, 3H), 7.33 (dd, *J* = 8.4, 6.6 Hz, 1H), 7.30 – 7.23 (m, 2H), 2.69 (q, *J* = 7.5 Hz, 4H), 1.14 (t, *J* = 7.5 Hz, 6H). **^{13}C NMR** (125 MHz, DMSO) δ 155.14, 150.96, 136.36, 133.08, 131.20, 129.57, 128.70, 127.71, 122.24, 24.72, 16.23. **LRMS:** m/z expected for $C_{16}H_{19}BN_2O_2$ $[M+H]^+$ 283.15 , measured 283.1

(*E*)-2-(2-bromostyryl)-1,3-difluorobenzene (SI-14)

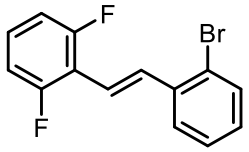

A 25 mL schlenk flask equipped with a stir rod was charged with dimethyl (2,6-difluorobenzyl)phosphonate (150 mg, 1.00 Eq, 635 μmol), to which 33 mg of NaH powder (57% NaH) was added to slowly on ice, leading to a cloudy yellow reaction. After 30 minutes, 2-bromobenzaldehyde (118 mg, 74.1 μL, 1.00 Eq, 635 μmol) was added to the reaction, which was allowed to warm to room temperature. After 15 hours the reaction appeared as a clear yellow solution. The THF was removed *in vacuo* and the solution was diluted with EtOAc and washed with DI water 2x. The organic layer was collected and dried with sodium sulfate and concentrated to yield a light yellow oil, ((*E*)-2-(2-bromostyryl)-1,3-difluorobenzene (114 mg, 386 μmol, 61%) and carried through to the next reaction.

Crude **^{1}H NMR** (500 MHz, $CDCl_3$) δ 7.80 (d, J = 16.6 Hz, 1H), 7.69 (dd, J = 7.9, 1.7 Hz, 1H), 7.60 (dd, J = 8.0, 1.3 Hz, 1H), 7.34 (tdd, J = 7.9, 1.3, 0.7 Hz, 1H), 7.22 – 7.12 (m, 2H), 7.06 (d, J = 16.6 Hz, 1H), 6.98 – 6.90 (m, 2H).

(*E*)-(2-(2,6-difluorostyryl)phenyl)boronic acid (7)

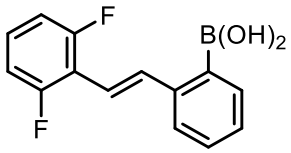

(SI-**14**) (136 mg, 1 Eq, 461 μmol) was dissolved into 3 mL of dry THF and transferred into a 25 mL schlenk flask equipped with a stir rod. The solution was cooled to -78 °C for 15 minutes and n-butyllithium (44.3 mg, 278 μL, 1.5 Eq, 691 μmol) was added dropwise. This was allowed to stir for 30 minutes, to which triisopropyl borate (130 mg, 0.16 mL, 1.5 Eq, 691 μmol) was added. The reaction was allowed to warm to room temperature and run for 12 hours. The reaction was quenched with 1M HCl and allowed to run for an hour. The organic solvent was removed and the product was diluted in EtOAc and washed with 1M HCl and DI water (2x). The organic layer was dried with sodium sulfate and concentrated. The product was dissolved in DCM in a RBF layered with hexane and purified by slow evaporation of the DCM *in vacuo* to yield the product as a white powder: (*E*)-(2-(2,6-difluorostyryl)phenyl)boronic acid (33 mg, 0.13 mmol, 28%).

^{1}H NMR (500 MHz, DMSO) δ 7.87 (dd, *J* = 16.8, 2.4 Hz, 1H), 7.74 (d, *J* = 7.9 Hz, 1H), 7.51 (dd, *J* = 7.4, 1.5 Hz, 1H), 7.42 – 7.31 (m, 2H), 7.31 – 7.25 (m, 1H), 7.19 – 7.11 (m, 2H), 6.99 (d, *J* = 16.8 Hz, 1H).**^{13}C NMR** (125 MHz, DMSO) δ 161.54, 159.62, 140.52, 137.39, 133.87, 129.55, 129.36, 127.69, 124.74, 114.92, 112.61. **LRMS:** m/z expected for $C_{14}H_{11}BF_2O_2$ $[M+FA]^-$ 305.06, measured 305.1

P1

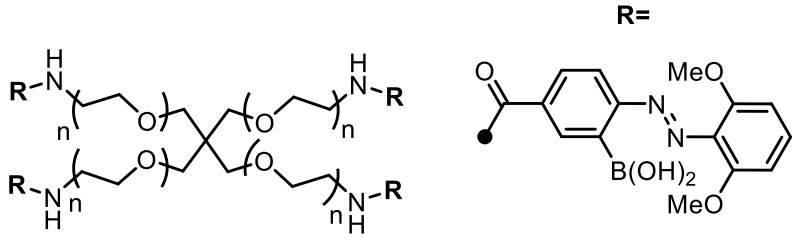

P1

125 mg of 4-arm PEG amine hydrochloride salt (MW = 5000) was added to a Schlenk flask (25 mL) and melted under high vaccum (2x) to remove excess water. 2-methoxyethan-1-aminium (0.125 g, 1 Eq, 23.6 μmol), HOBt (36.1 mg, 10 Eq, 236 μmol), and (E)-3-borono-4-((2,6-dimethoxyphenyl)diazenyl)benzoic acid (77.9 mg, 10 Eq, 236 μmol) were then added as solids along with a stir bar, the vessel was sealed and backfilled with nitrogen (3x). 2 mL of DCM and 2 mL of DMF were then added to solubilize the reagents leading to a clear red solution. TEA (23.9 mg, 33 μL, 10 Eq, 236 μmol) was then added to the solution, which was stirred at room temperature for 24 hours. Upon completion, the reaction was diluted with DCM and filtered through a glass-fritted filter. The filtrate was concentrated *in vacuo* and then diluted with EtOAc and water (1:1). The EtOAc layer was separated and further washed with DI water (3x). Combined aqueous layers were concentrated *in vacuo* to ~30 mL and dialyzed for 3 days against DI water (MWCO = 3.5 kDa) while the water being changed daily. The sample was then lyophilized for 48 hours to yield 88 mg of the polymer product.

NOTE: Addition of NaCl was useful for clearing the emulsion at the organic/water interface.

P2

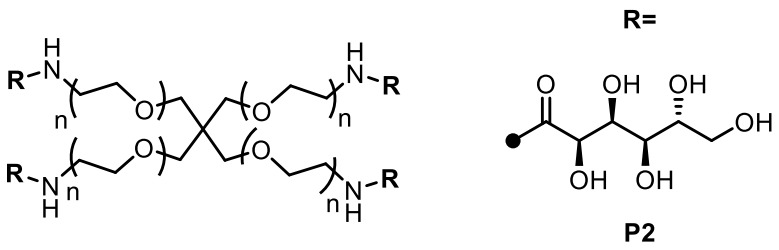

P2 was prepared following a literature procedure.[2]

III. Photochemical characterization

Determination of Photostationary state (PSS): PSS were determined by irradiating the respective azobenzene with either the UV (390 nm) blue (470 nm), green (535 nm), or red (626 nm) LEDs for at least 30 minutes and then immediately subject to ^{1}H or ^{19}F NMR. The percentage of *Z* isomer was recorded.

Wavelength	% Z isomer
626 nm (red)	< 2
525 nm (green)	26
450 nm (blue)	26
365 nm (UV)	48

Wavelength	% Z isomer
6260 nm (red)	< 6
525 nm (green)	67
450 nm (blue)	50
365 nm (UV)	59

Table S1 (left) and Table S2 (right): Photostationary states (% *Z*) of **1** and **2** after 30 minutes irradiation with various wavelengths of light.

Wavelength	% Z isomer
626 nm (red)	56
590 nm (yellow)	72
525 nm (green)	67
450 nm (blue)	36
390 nm (UV)	44

Wavelength	% Z isomer
626 nm (red)	76
525 nm (green)	61
450 nm (blue)	29
390 nm (UV)	51

Table S3 (left) and Table S4 (right): Photostationary states (% *Z*) of **3** and **SI-7** after 30 minutes irradiation with various wavelengths of light.

UV-Vis Spectrum of compound 1-3 and controls before (black) and (green) after irradiation with green LEDs.

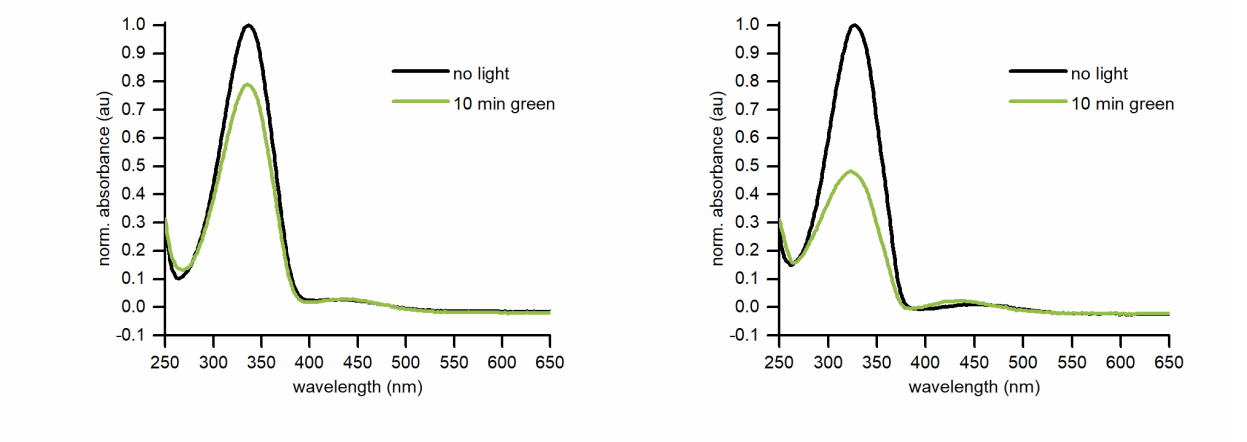

Figure S1. Left: Normalized UV-Vis absorbance spectra of (*E*)-**1** (33 µM in acetonitrile) before (black) and after (green) ten minutes of irradiation. **Right:** Normalized UV-Vis of (*E*)-**2** (15 µM in acetonitrile) before (black) and after (green) ten minutes of irradiation.

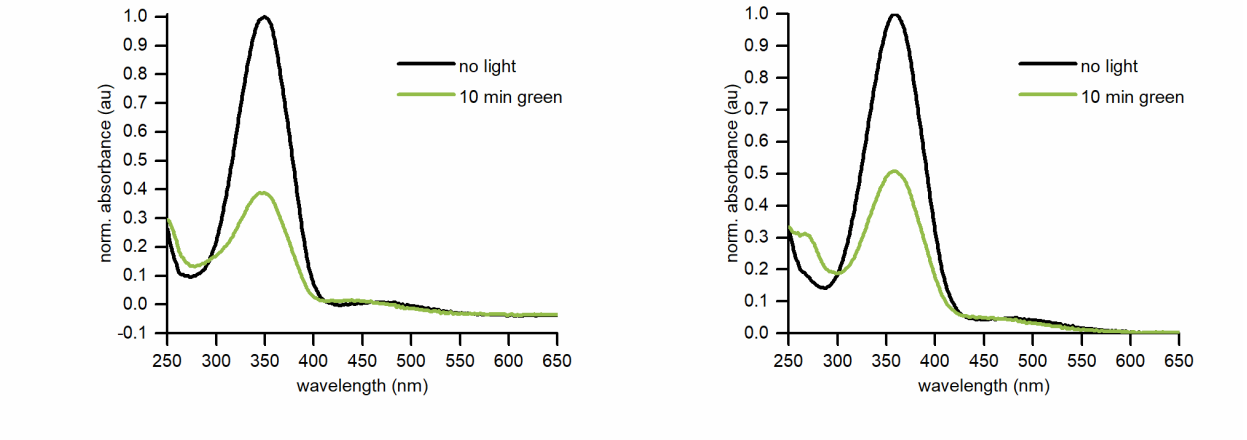

Figure S2. Left: Normalized UV-Vis absorbance spectra of (*E*)-**3** (21 µM in acetonitrile) before (black) and after (green) ten minutes of irradiation. **Right:** Normalized UV-Vis absorbance spectra of (*E*)-**4** (12 µM in acetonitrile) before (black) and after (green) ten minutes of irradiation.

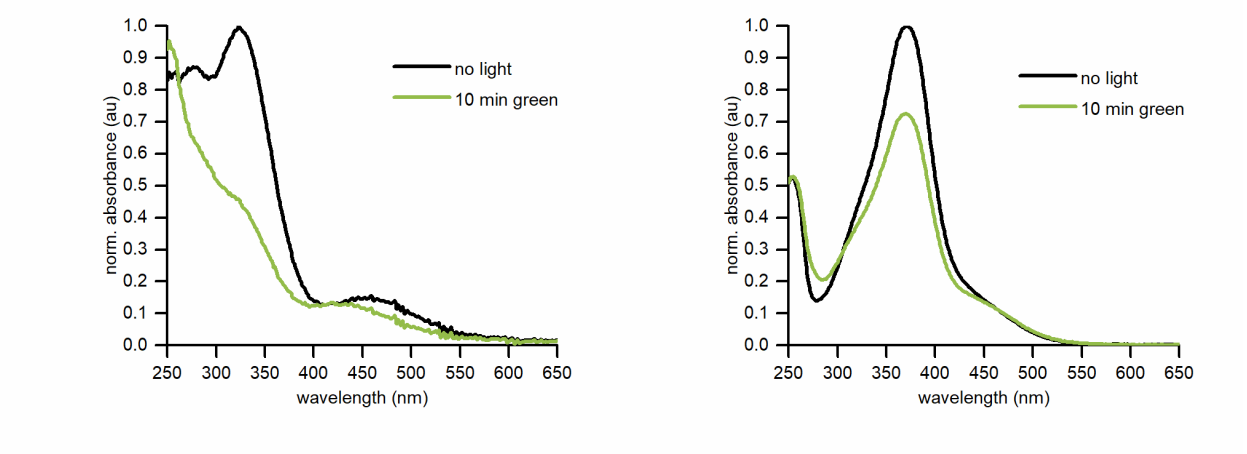

Figure S3. Left: Normalized UV-Vis absorbance spectra of (*E*)-**4** (14 µM in acetonitrile) before (black) and after (green) ten minutes of irradiation. **Right:** Normalized UV-Vis absorbance spectra of (*E*)-**5** (35 µM in acetonitrile) before (black) and after (green) ten minutes of irradiation.

Determination of thermal half-lives: The respective azobenzene (at a concentration of between 1-4 mg/mL) was irradiated with green or red LEDs for at least 30 minutes to reach the PSS and placed into the NMR which was set to a given temperature (typically between 40-80 °C). ^{1}H or ^{19}F NMR spectrum were recorded every five minutes at variable temperatures between 30 and 80 °C to monitor the thermal conversion of azobenzene from the *Z* to *E* isomer. Rate constants for the first order thermal isomerization were determined from exponential fits and Arrhenius plots were constructed for the rate of isomerization versus temperature. Thermal half-lives at room temperatures (25 °C) were determined by extrapolation of these graphs, where $\tau_{1/2} = \ln(2)/k$.

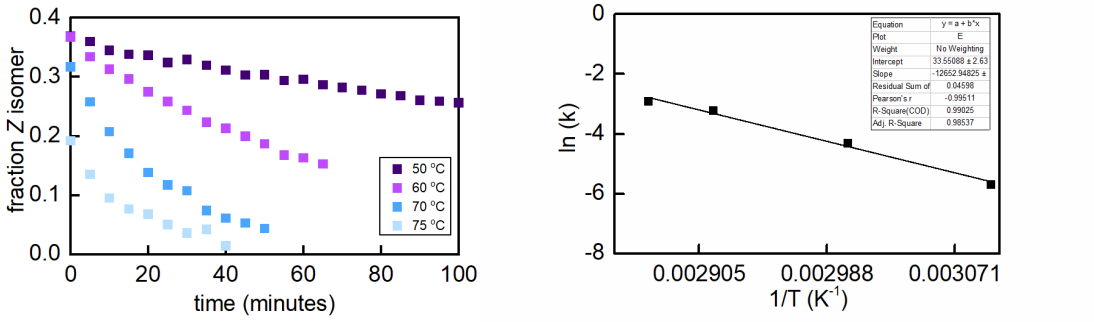

Figure S4. Left: Thermal isomerization of (*Z*)-**1** to (*E*)-**1** as determined by ^{1}H NMR at 50 °C, 60 °C, 70 °C, and 75 °C. **Right:** Arrhenius plot of thermal isomerization of (*Z*)-**1** to (*E*)-**1**. The half-life was determined to 3.5 days at 25 °C.

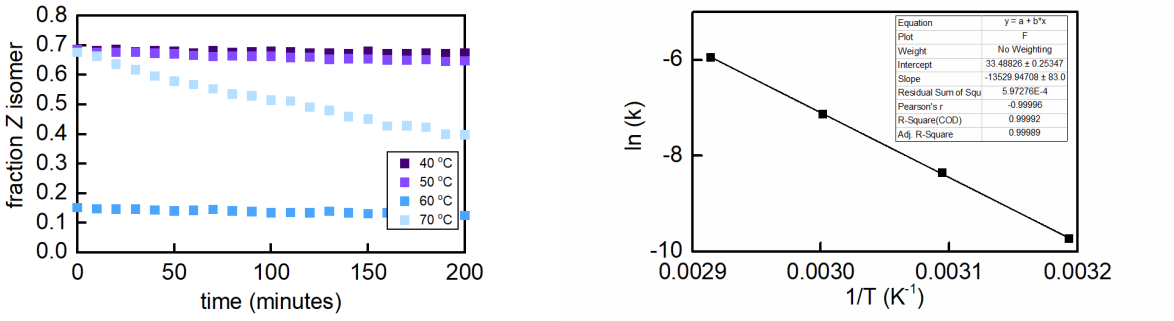

Figure S5. Left: Thermal isomerization of (*Z*)-**2** to (*E*)-**2** as determined by ^{1}H NMR at 40 °C, 50 °C, 60 °C, and 70 °C. **Right:** Arrhenius plot of thermal isomerization of (*Z*)-**2** to (*E*)-**2**. The half-life was determined to 70 days at 25 °C.

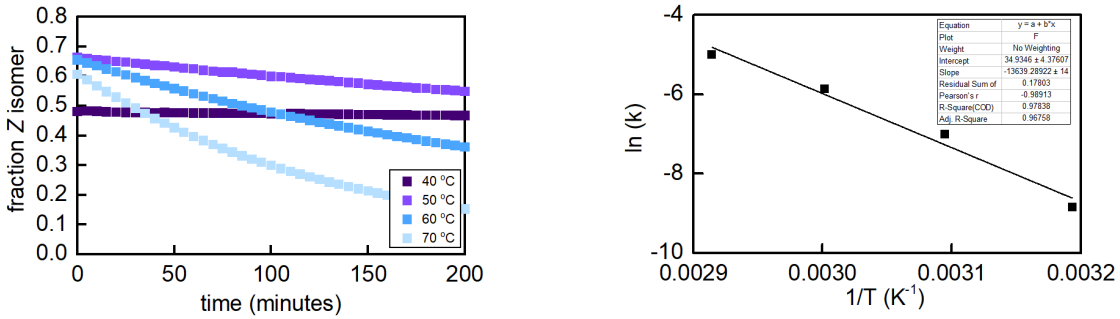

Figure S6. Left: Thermal isomerization of (*Z*)-**3** to (*E*)-**3** as determined by ^{1}H NMR at 40 °C, 50 °C, 60 °C, and 70 °C. **Right:** Arrhenius plot of thermal isomerization of (*Z*)-**3** to (*E*)-**3**. The half-life was determined to 24 days at 25 °C.

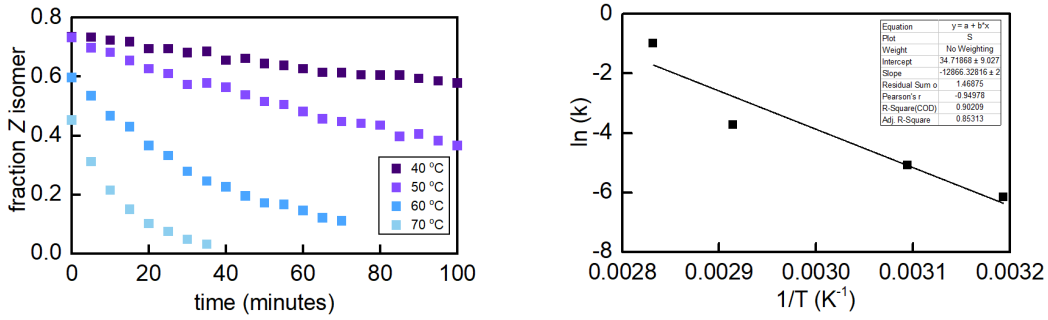

Figure S7. Left: Thermal isomerization of (*Z*)-**SI-10** to (*E*)-**SI-10** as determined by ^{1}H NMR at 40 °C, 50 °C, 60 °C, and 70 °C. **Right:** Arrhenius plot of thermal isomerization of (*Z*)-**1** to (*E*)-**1**. The half-life was determined to 2.2 days at 25 °C

IV. Competition experiments

General procedure for competition experiment: 10 μmol of the given azobenzene boronic acid was dissolved into 500 μL of DMSO-d_6 and irradiated with green or red LEDs for 30 minutes to produce a mixture of the *E* and *Z* isomers. 2 equivalence of diol was added to the solution, and 2 μL of D_2O was added. If an internal standard was necessary, cyclooctenediol was added, which is noted in those specific experiments. The solution was left to equilibrate for at least 12 hours and then ^{1}H or ^{19}F (if applicable) NMR spectrum were recorded. The amount of bound and unbound boronic acid for both the *E* and *Z* isomer were determined by integration and the relative K_{eq} (K_{rel}) was determined from below formula. Protons that could be accurately assigned have been included.

$K_{eq}(E)$ is expressed by equation 1 and $K_{eq}(Z)$ is expressed by equation 2. Because both equilibria are present in the same NMR tube, the concentration of water and diol are the same, and the K_{rel} can be simplified as in equation 3.

$$\mathrm{K_{eq}}(E) = \frac{[(E)\text{-ester}][\mathrm{H_2O}]^2}{[(E)\text{-acid}][\mathrm{diol}]} \quad (1)$$

$$\mathrm{K_{eq}}(Z) = \frac{[(Z)\text{-ester}][\mathrm{H_2O}]^2}{[(Z)\text{-acid}][\mathrm{diol}]} \quad (2)$$

$$\mathrm{K_{rel}} = \frac{\mathrm{K_{eq}}(Z)}{\mathrm{K_{eq}}(E)} = \frac{[(Z)\text{-ester}][\mathrm{H_2O}]^2}{[(Z)\text{-acid}][\mathrm{diol}]} * \frac{[(E)\text{-acid}][\mathrm{diol}]}{[(E)\text{-ester}][\mathrm{H_2O}]^2} = \frac{[Z\text{-ester}][E\text{-acid}]}{[Z\text{-acid}][E\text{-ester}]} \quad (3)$$

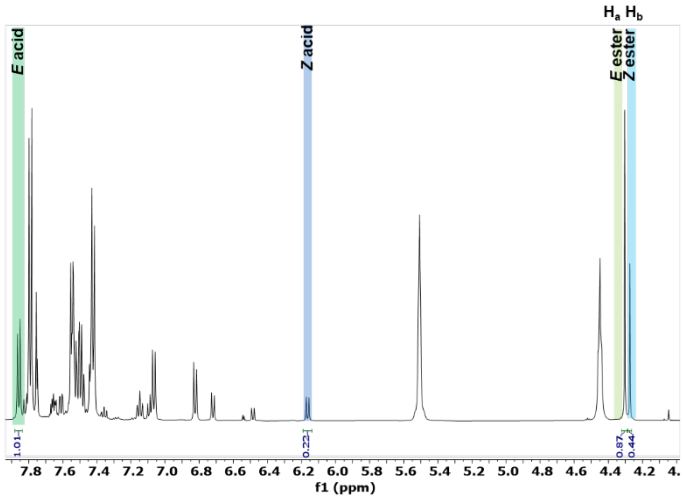

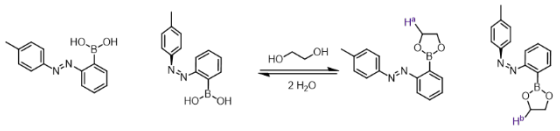

Trial 1	Trial 2	Trial 3	Average	St. Dev
2.4	2.3	2.4	2.4	0.1

Figure S8. Competition experiments to determine K_{rel} of compound **3** with EG.

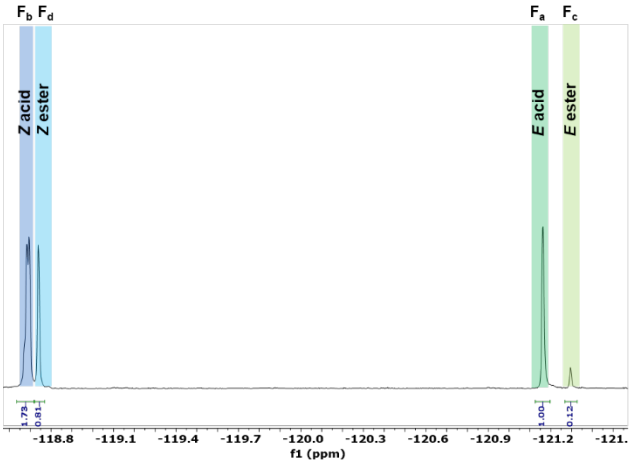

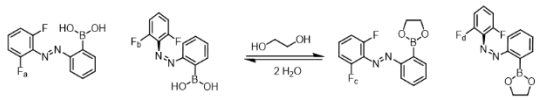

Trial 1	Trial 2	Trial 3	Average	St. Dev
4.2	3.9	3.9	4.0	0.2

Figure S9. Competition experiments to determine K_{rel} of compound **2** with EG.

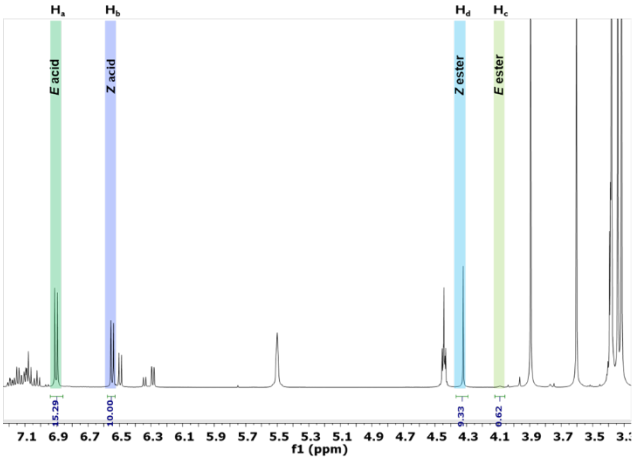

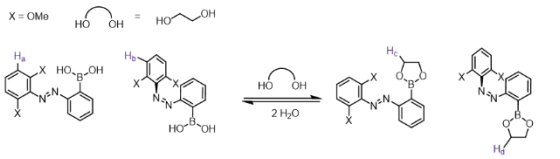

Trial 1	Trial 2	Trial 3	Average	St. Dev
22.7	23	18.8	21.5	2.4

Figure S10. Competition experiments to determine K_{rel} of compound **3** with EG. X = OMe.

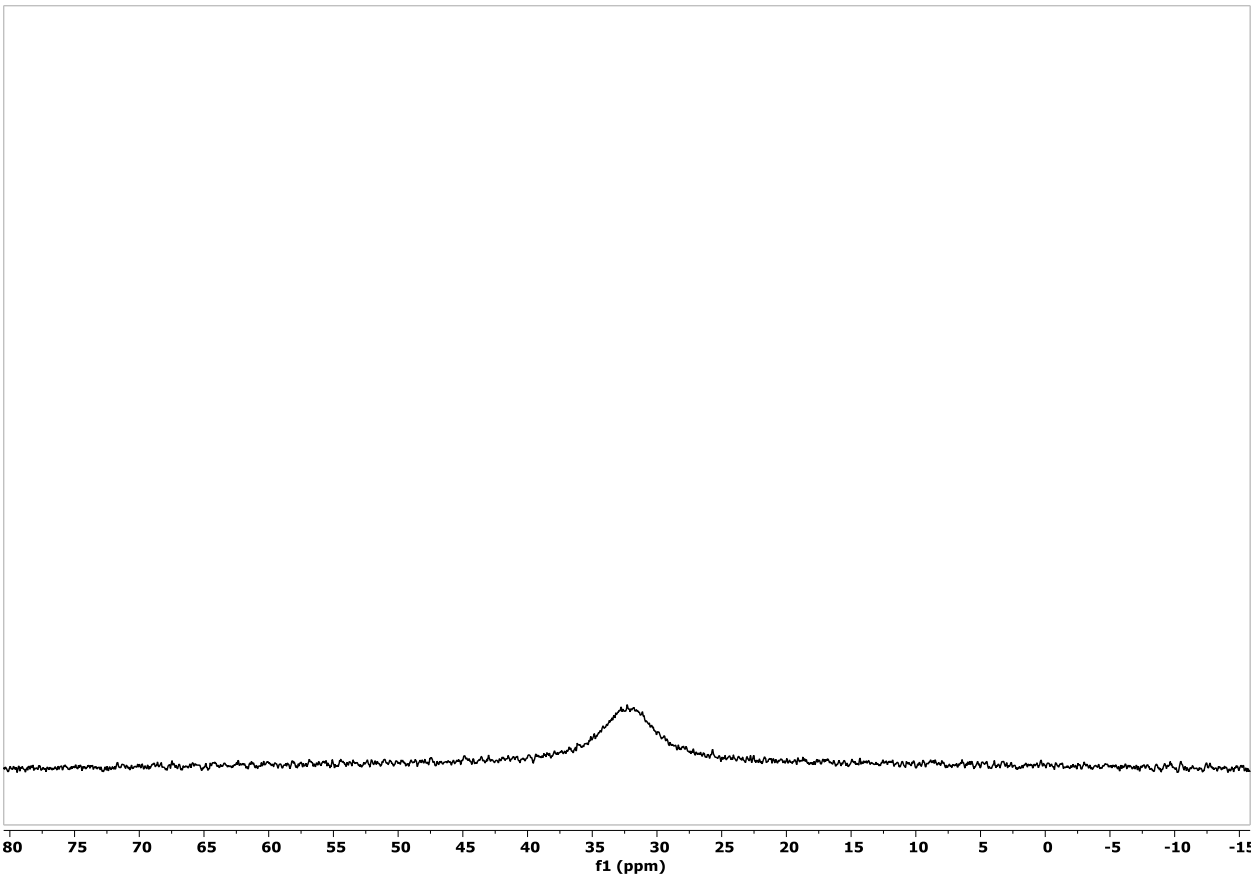

Figure S11. ^{11}B NMR spectrum of competition experiment between (*E*)-**3** and (*Z*)-**3** with EG in DMSO-d_6.

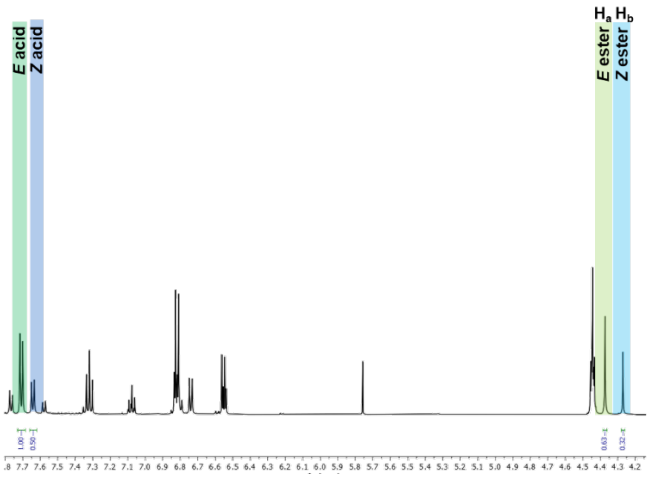

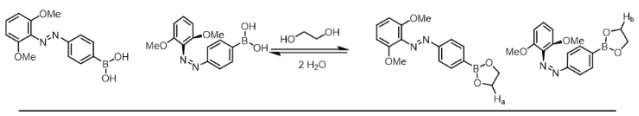

Trial 1	Trial 2	Trial 3	Average	St. Dev
1.1	0.96	1.01	1.0	0.1

Figure S12. Competition experiment between (*E*)-**4** and (*Z*)-**4** with EG.

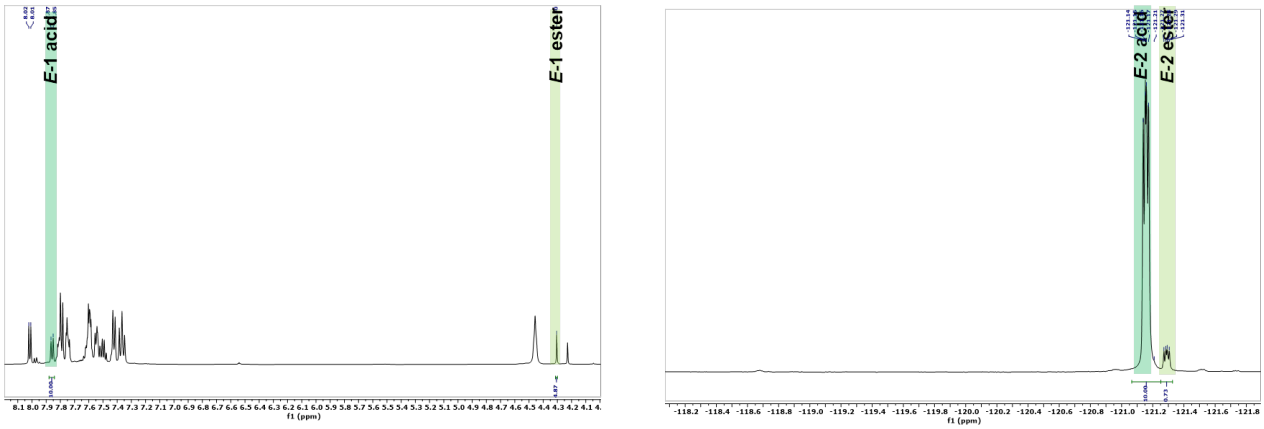

$$\frac{K_{eq(E)}\,\mathbf{1}}{K_{eq(E)}\,\mathbf{2}} = 1.77$$

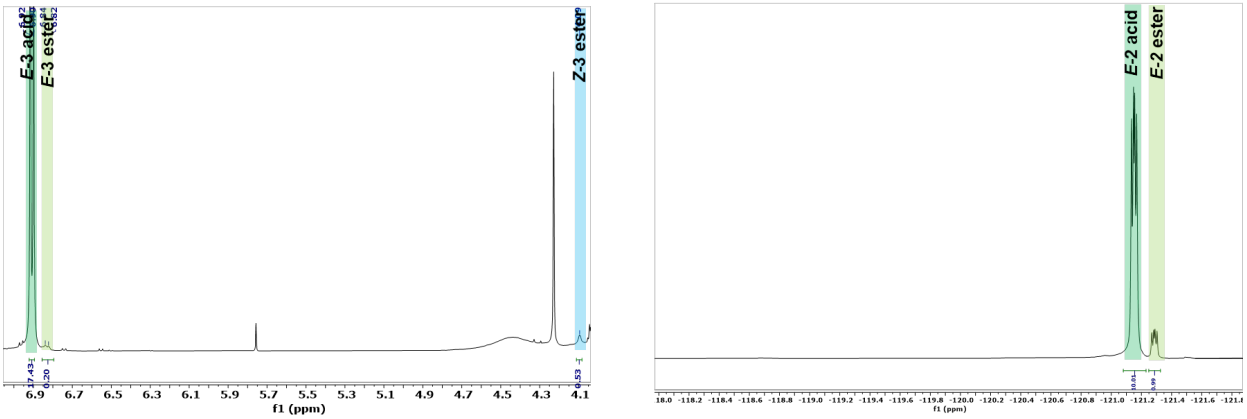

$$\frac{K_{eq(E)}\,\mathbf{2}}{K_{eq(E)}\,\mathbf{3}} = 5.6$$

Figure S13. (top) Competition experiment between (*E*)-**1** and (*E*)-**2** with EG. (bottom) Competition experiment between (*E*)-**2** and (*E*)-**3** with EG.

$K_{eq(E)}$ **1** and $K_{eq(E)}$ **3** were determined from the left ^{1}H NMR spectra and and $K_{eq(E)}$ **2** nd $K_{eq(Z)}$ **2** was determined by the right ^{19}F NMR spectra. The difference in binding for (*E*)-**3** and (*E*)-**2** was determined to be between 4.2 and 6.9 (due to integration error), so the average of 5.6 was taken to be the change in binding affinity.

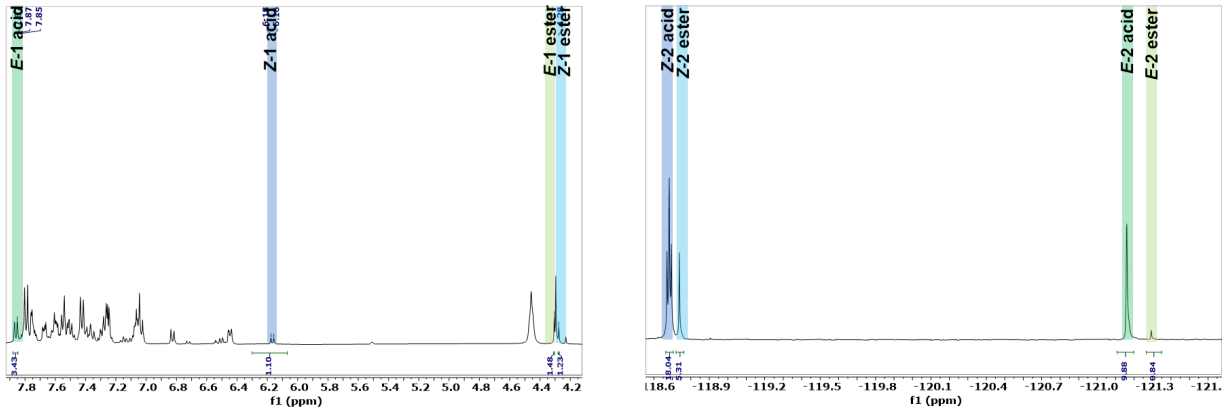

$$\frac{K_{eq(Z)}\,\mathbf{1}}{K_{eq(Z)}\,\mathbf{2}} = 0.95$$

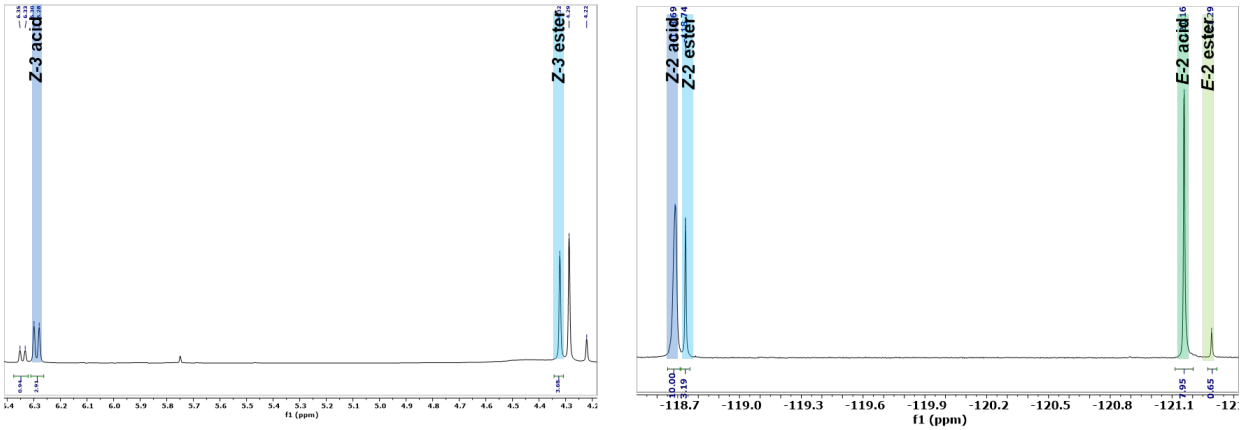

$$\frac{K_{eq(Z)}\,\mathbf{2}}{K_{eq(Z)}\,\mathbf{3}} = 1.01$$

Figure S14. (top) Competition experiment between (*Z*)-**1** and (*Z*)-**2** with EG. (bottom) Competition experiment between (*Z*)-**2** and (*Z*)-**3** with EG.
$K_{eq(Z)}$ **1** and $K_{eq(Z)}$ **3** were determined from the left ^{1}H NMR spectra $K_{eq(Z)}$ **2** was determined by the right ^{19}F NMR spectra.

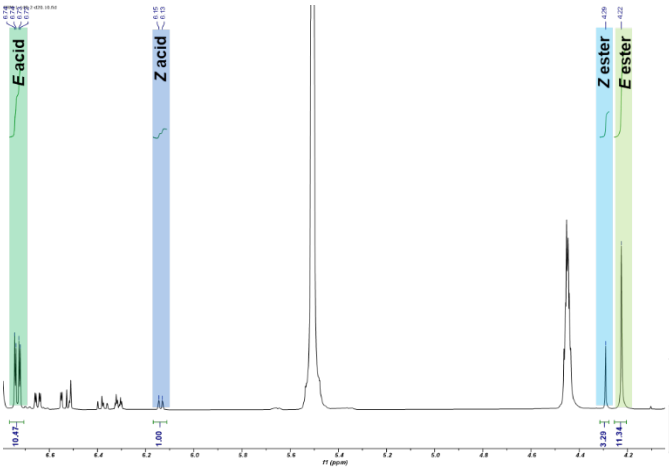

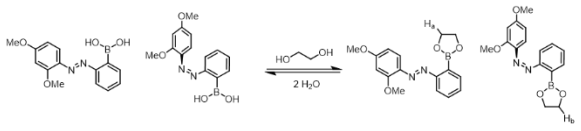

Trial 1	Trial 2	Trial 3	Average	St. Dev
2.2	3.0	2.1	2.4	0.5

Figure S15. Competition experiment between (*E*)-**5** and (*Z*)-**5** with EG.

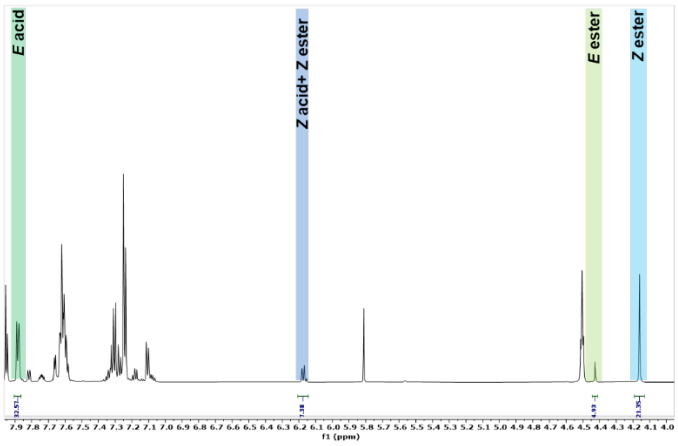

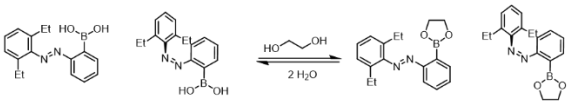

Trial 1	Trial 2	Trial 3	Average	St. Dev
1.22	1.26	1.34	1.27	0.1

Figure S16. Competition experiment between (*E*)-**6** and (*Z*)-**6** with EG.

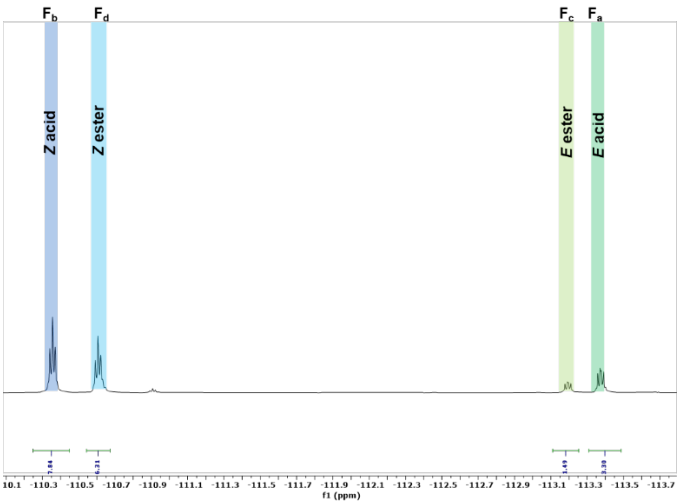

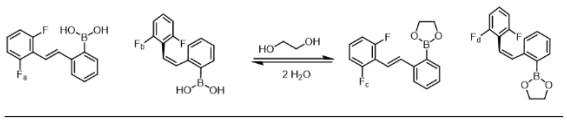

Trial 1	Trial 2	Trial 3	Average	St. Dev
1.77	1.80	--	1.79	0.1

Figure S17. Competition experiment between (*E*)-**7** and (*Z*)-**7** with EG. The *Z* isomer was accessed by irradiation of the solution with 305 nm light for 20 minutes.

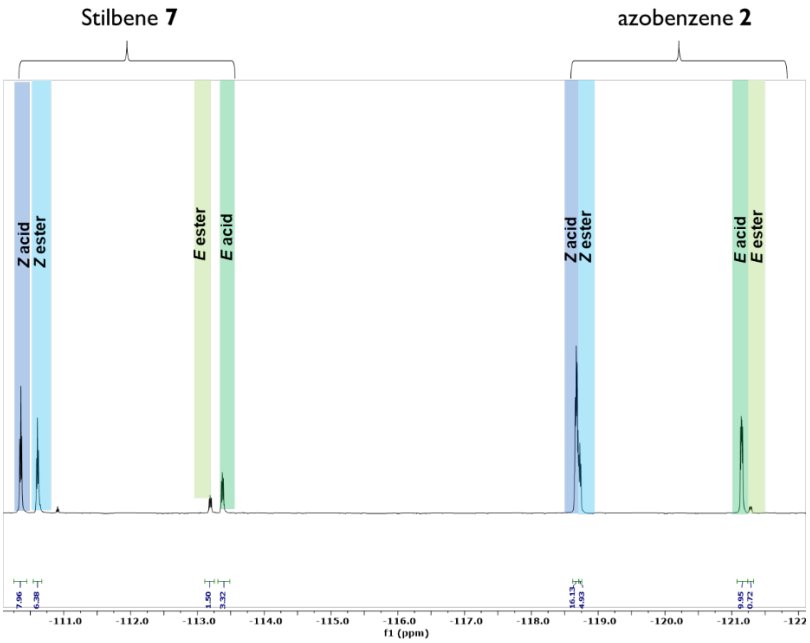

Figure S18. Competition experiment between **2** and **7** with EG.

Wavelength-dependent diol binding with compound 3 and ethylene glycol

10 μmol of compound **3** was dissolved into 500 μL of DMSO-d_6 to which 1 Eq of ethylene glycol was added. After equilibrating for 12 hours a ^{1}H NMR spectrum was recorded to determine how much of the ethylene glycol was bound, relative to total amount of ethylene glycol in solution. This was repeated after the sample was irradiated with blue, green, and red LEDs to determine the amount of diol bound as a function of irradiation wavelength.

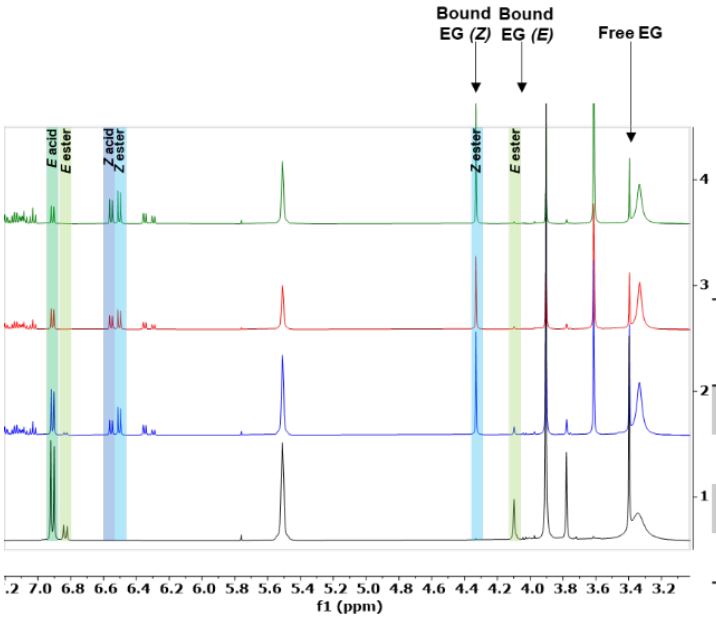

irradiation color	% Z isomer	% diol bound
None (Δ)	0	30
blue	45	54
green	74	70
red	59	63

Figure S19 (left): ^{1}H Spectrum highlighting bound and unbound (*E*)- and (*Z*)-**3** with EG after irradiation with no light (black trace), blue light (blue trace), red light (red trace), and green light (green trace). Right: Table of PSS of **3** with different wavelengths of irradiation and the % diol bound.

Binding experiments with compound 3 and various diols

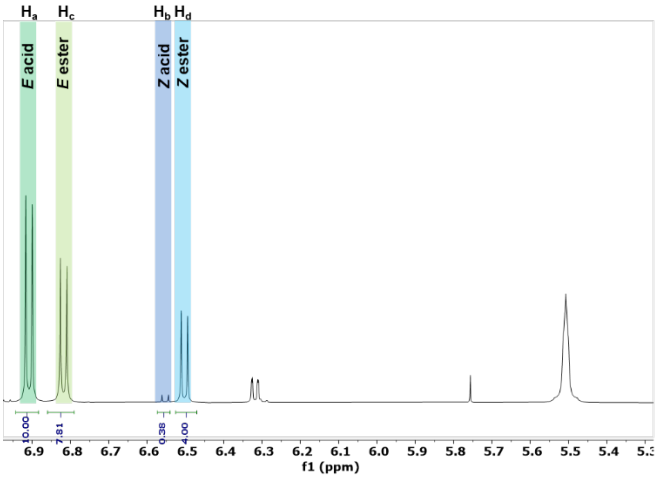

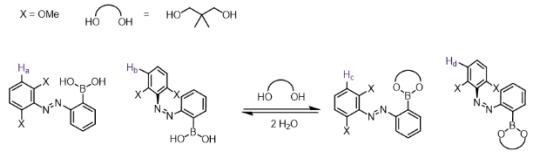

Trial 1	Trial 2	Trial 3	Average	St. Dev
13.9	13.5	14.1	13.8	0.3

Figure S20. Competition experiment between (*E*)-**3** and (*Z*)-**3** with neopentyl glycol (**6**).

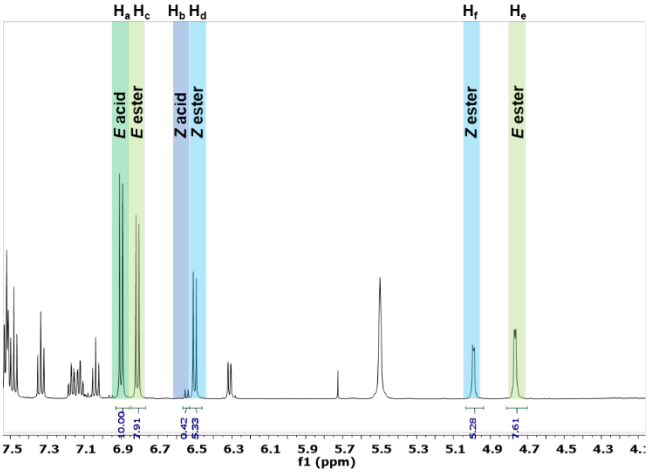

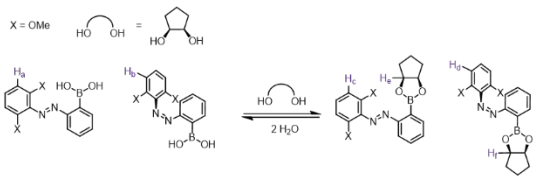

Trial 1	Trial 2	Trial 3	Average	St. Dev
15.7	13.0	16.0	14.9	1.7

Figure S21. Competition experiment between (*E*)-**3** and (*Z*)-**3** with *cis*-1,2-cyclopentanediol (**7**).

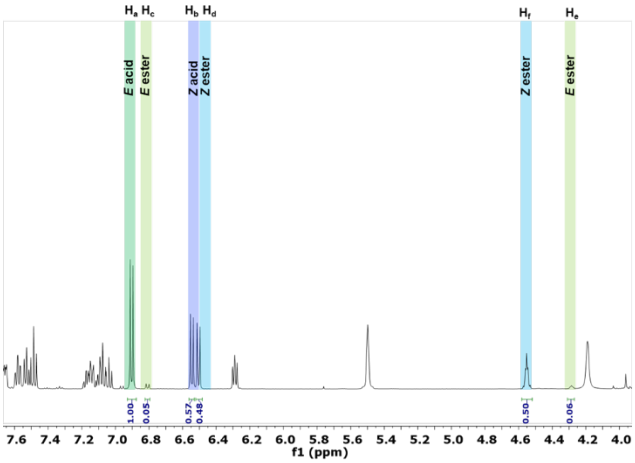

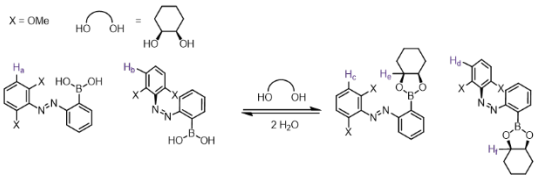

Trial 1	Trial 2	Trial 3	Average	St. Dev
16.2	16.8	14.6	15.9	1.2

Figure S22. Competition experiment between (*E*)-**3** and (*Z*)-**3** with *cis*-1,2-cyclohexanediol (**8**).

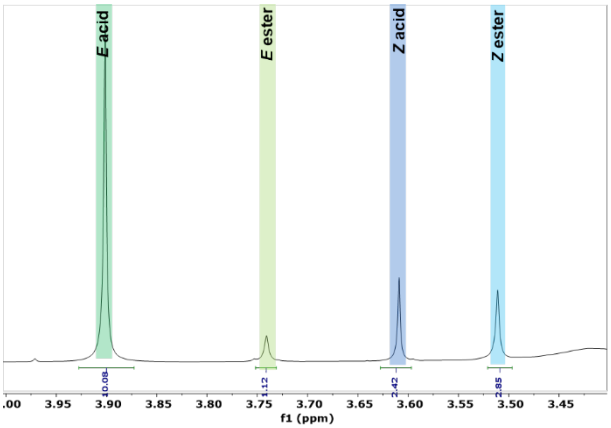

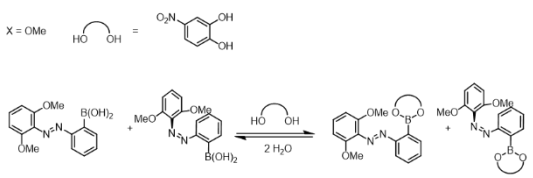

Trial 1	Trial 2	Trial 3	Average	St. Dev
9.6	10.5	11.2	10.4	0.8

Figure S23. Competition experiment between (*E*)-**3** and (*Z*)-**3** with 4-nitrocatechol (**9**).

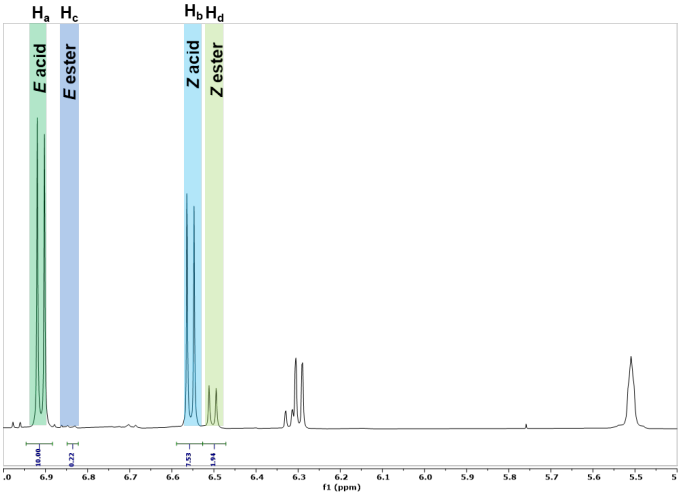

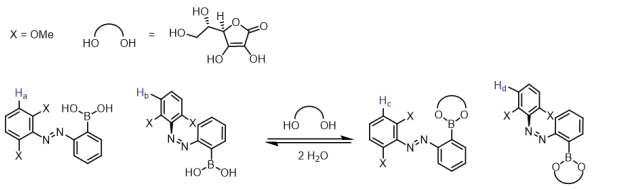

Trial 1	Trial 2	Trial 3	Average	St. Dev
10.0	11.7	11.3	11.0	0.1

Figure S24. Competition experiment between (*E*)-**3** and (*Z*)-**3** with L-ascorbic acid (**10**).

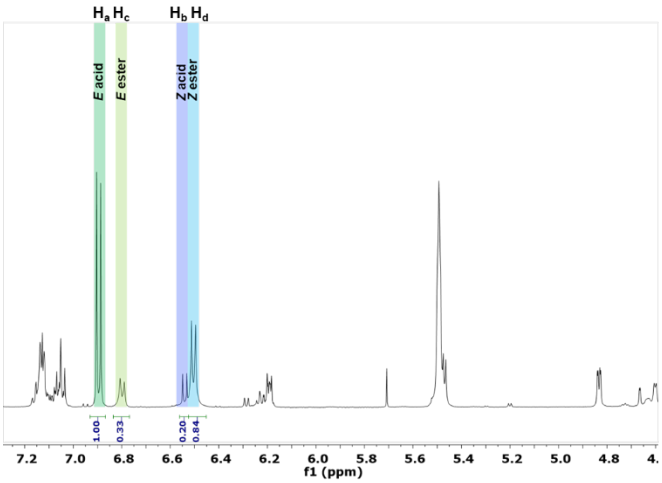

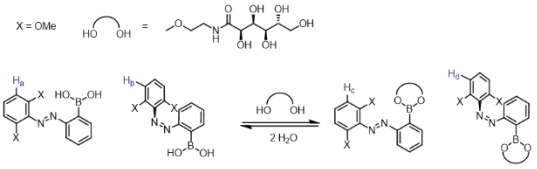

Trial 1	Trial 2	Trial 3	Average	St. Dev
14.0	12.0	12.7	12.9	1.0

Figure S25. Competition experiment between (*E*)-**3** and (*Z*)-**3** with gluconolactone derivative (**11**).

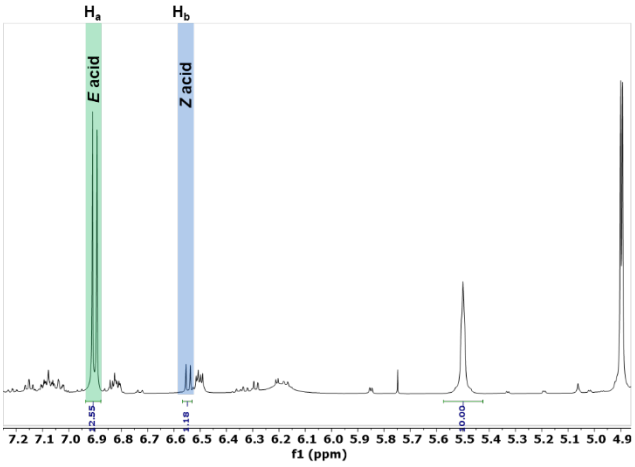

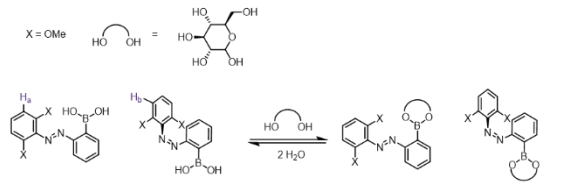

Trial 1	Trial 2	Trial 3	Average	St. Dev
5.9	5.5	9.8	7.0	2.4

Figure S26. Competition experiment between (*E*)-**3** and (*Z*)-**3** with glucose (**12**).

NOTE: Competition experiments with glucose were complicated to analyze due to multiple binding modes of glucose which was evident by ^{1}H NMR. To account for these, we let the experiments equilibrate and determined the amount of unbound boronic acid relative to a cyclooctadiene internal standard. Afterwards, excess D_2O was added to the experiment to hydrolyze all the boronic ester. We then compared the integration of the boronic acids to the internal standard to determine how much boronic acid was consumed prior to hydrolysis. The ^{1}H NMR shows the peaks that were used in the integration as the unbound *E* or *Z* azobenzene boronic acid and the COD internal standard.

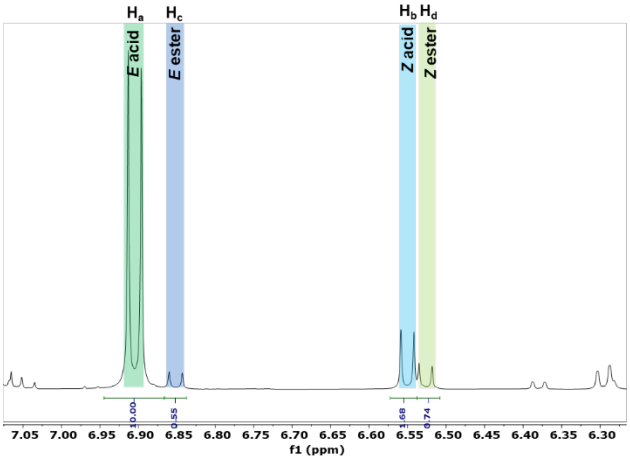

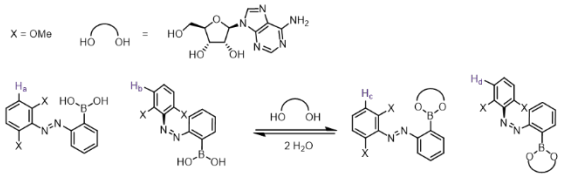

Trial 1	Trial 2	Trial 3	Average	St. Dev
7.5	8.0	8.0	7.8	0.3

Figure S27. Competition experiment between (*E*)-**3** and (*Z*)-**3** with adenosine (**13**).

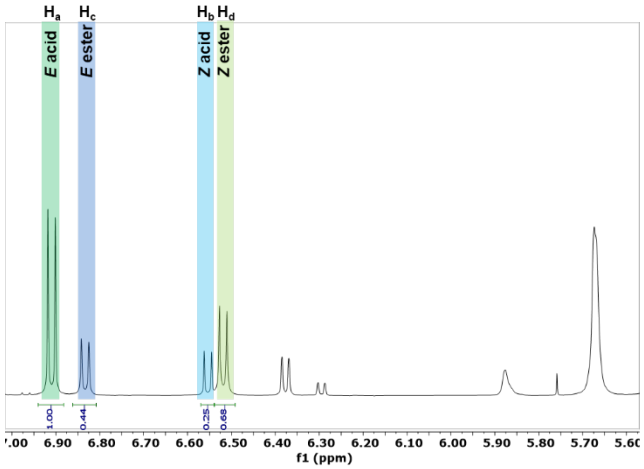

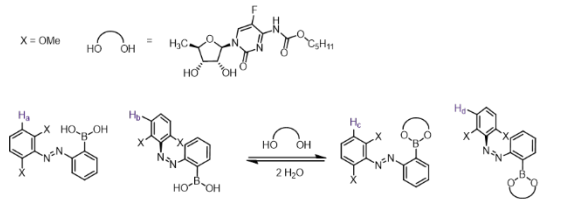

Trial 1	Trial 2	Trial 3	Average	St. Dev
5.5	6.2	6.3	6.0	0.5

Figure S28. Competition experiment between (*E*)-**3** and (*Z*)-**3** with capecitabine (**14**).

V. Computational calculation details

Calculations were performed on the Northwestern University's 'Quest' computational cluster. Preliminary optimizations were performed using the restricted Hartree-Fock theory with the def2-SVP basis set, the input files were generated by Avogadro, and were then further optimized using B3LYP hybrid functional and the 6-31+G** basis set as implemented in Orca.[3] Frequency scans, which were employed to compute the relative energy of the rotamers, were performed with a 6-31+G** basis set and B3LYP method. Geometry scans were performed with a 6-31+G** basis set and B3LYP method from 0–180º in 9.5º intervals.

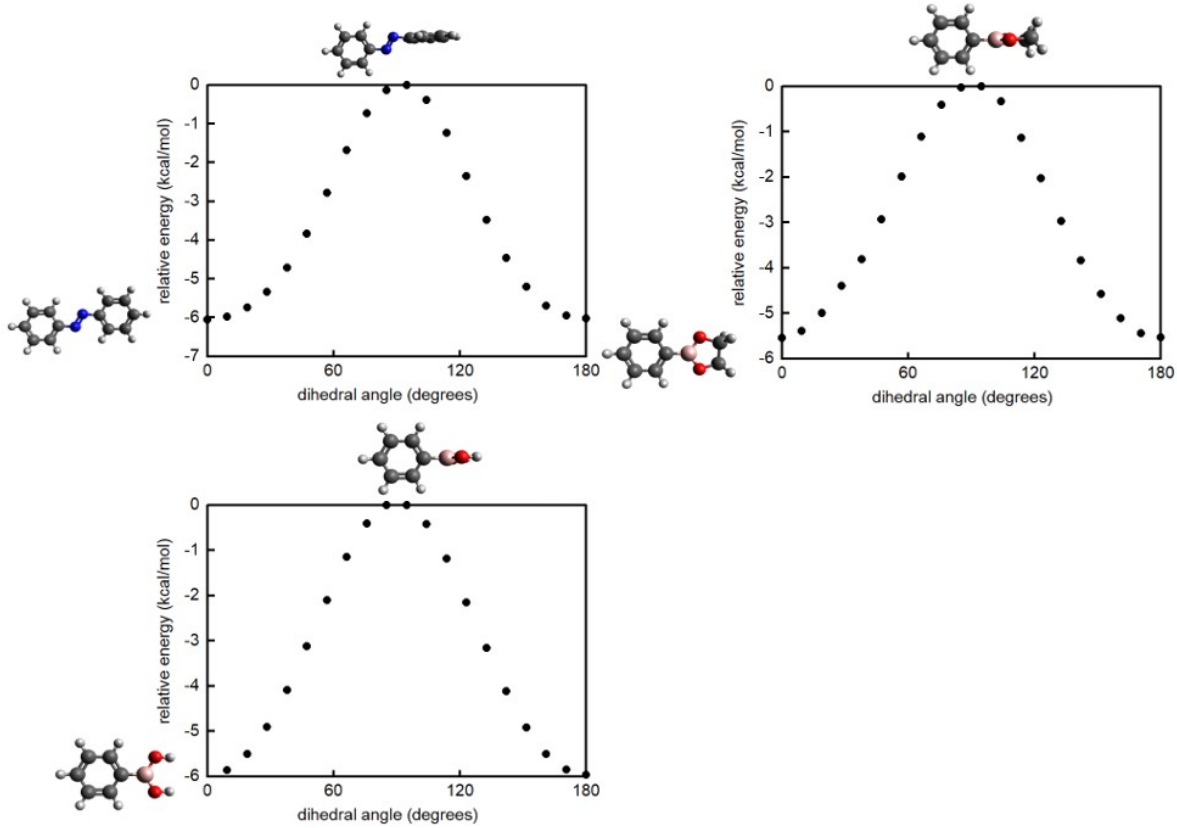

Figure S29. (top left) Geometry scan of azobenzene dihedral angle **Φ** from 0 to 180º in 9.5º intervals. (top right) Geometry scans of phenyl boronic acid ethylene glycol ester. Dihedral angle ψ (bottom right) from 0 to 180º in 9.5º intervals. (bottom left) Geometry scan of phenyl boronic acid from dihedral angle ψ (bottom right) from 0 to 180º in 9.5º intervals. The optimized structures are depicted for the compounds at 0º and 85º.

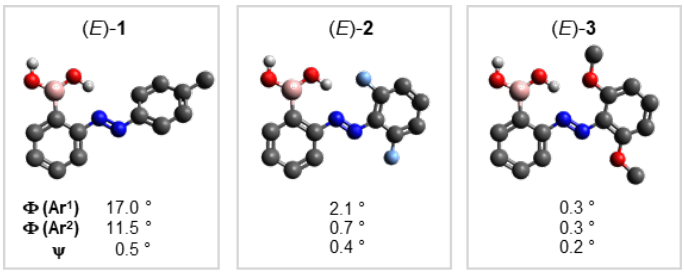

Figure S30. Geometry-optimized structures of (*E*)-**1** through (*E*)-**3** unbound.

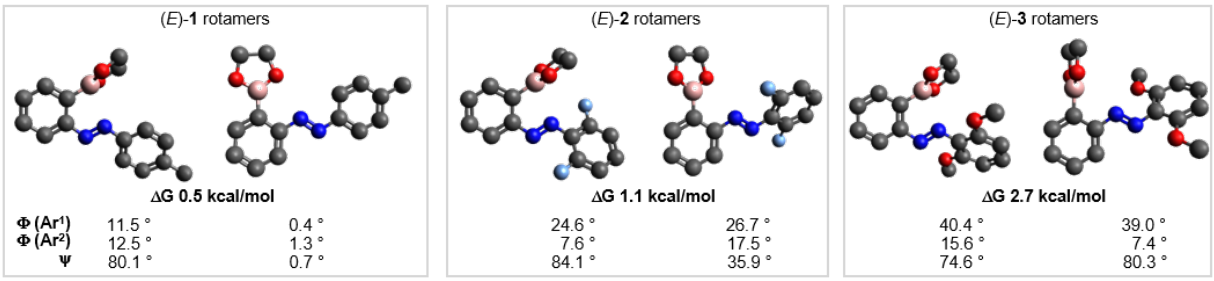

Figure S31. Geometry-optimized rotamers of (*E*)-**1** through (*E*)-**3** bound with EG. The most stable rotamers (rotamers 1) are the left structures in each box, and the differences in energy between the rotamers are reported below (ΔG). The less stable isomers ("rotamer 2", shown on the right side of each box) follow a similar trend to Figure 6, with the smaller conformation changes upon binding occurring for compound **1** and the largest changes for compound **3**.

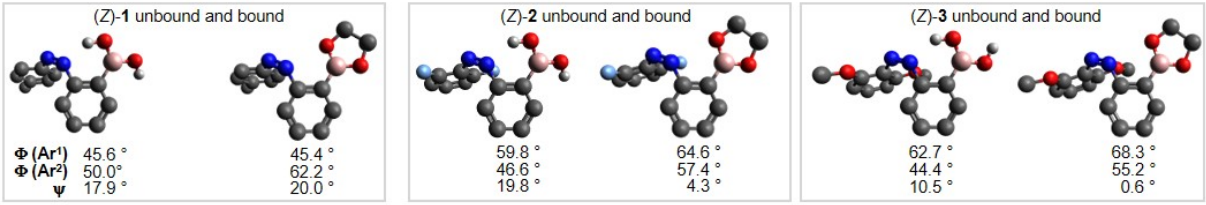

Figure S32. Geometry-optimized rotamers and relative energies of (*Z*)-**1** through (*Z*)-**3**.

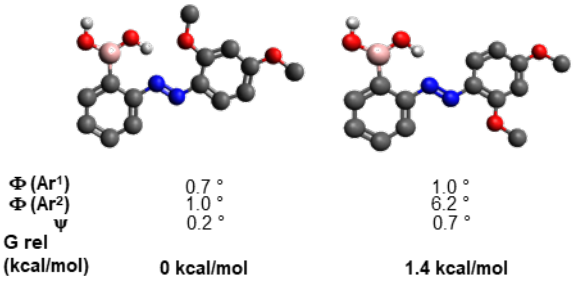

Figure S33. Geometry-optimized rotamers and relative energies of unbound (*E*)-**5.**

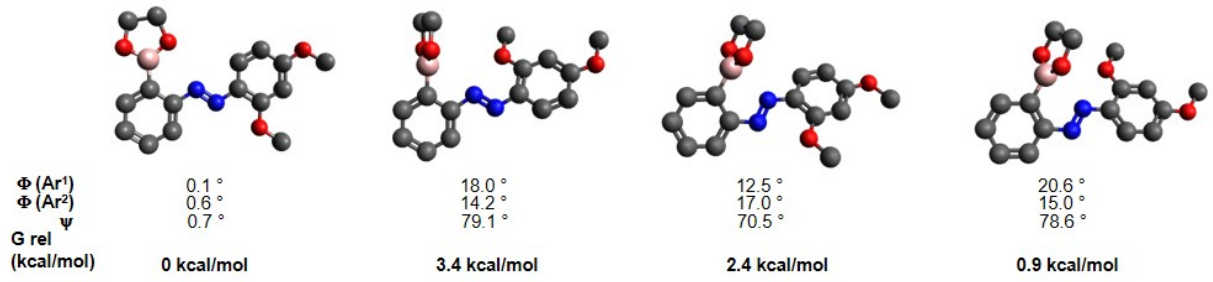

Figure S34. Geometry-optimized rotamers and relative energies of bound (*E*)-**5.**

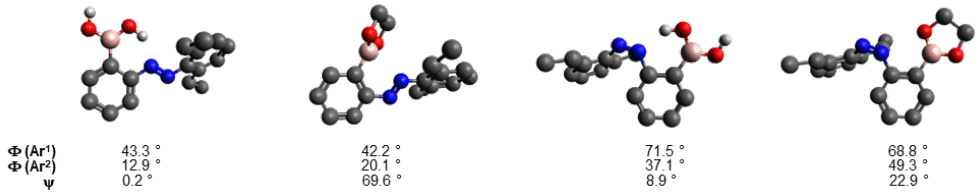

Figure S35. Geometry optimized structures of (*E*)-**6** and (*Z*)-**6.**

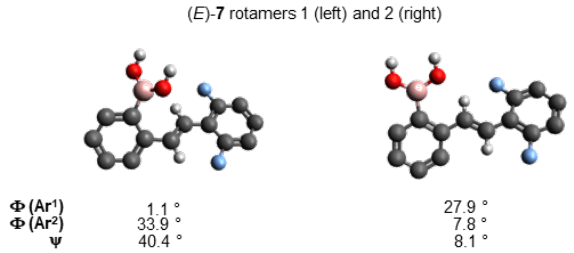

Figure S36. Geometry optimized rotamers of (*E*)-**7** showing the absence of any intramolecular hydrogen bond.

XYZ coordinates of ground state optimized geometries

(*E*)-**1** unbound

```
O -6.0010460000 1.4416190000 4.4030960000
O -4.2112380000 0.4830540000 3.1996130000
N -7.3996820000 5.0027090000 3.6878310000
N -6.8035700000 3.9096640000 3.4986180000
C -11.6261420000 5.2849730000 7.5674580000
C -8.8694630000 6.2413310000 5.0961940000
C -9.8867480000 6.3383150000 6.0457850000
C -10.5160090000 5.1907000000 6.5479580000
C -10.0943130000 3.9357640000 6.0650170000
C -9.0741280000 3.8238670000 5.1282730000
C -8.4405940000 4.9850910000 4.6433430000
C -5.6343830000 4.9873180000 1.5984840000
C -4.6375580000 4.9378780000 0.6300550000
C -3.7944410000 3.8209930000 0.5464040000
C -3.9602700000 2.7575610000 1.4343570000
C -4.9586240000 2.7694920000 2.4261290000
C -5.7921520000 3.9144740000 2.4951060000
B -5.0832560000 1.5262140000 3.3972150000
H -6.5478110000 2.2548360000 4.3987000000
```

H -4.3579020000 -0.2298930000 3.8350510000
H -12.5527890000 4.8388650000 7.1867570000
H -11.3649780000 4.7475340000 8.4871040000
H -11.8376730000 6.3240200000 7.8337940000
H -8.7813160000 2.8493280000 4.7535390000
H -8.3854590000 7.1287250000 4.6995760000
H -6.2997490000 5.8400430000 1.6753810000
H -10.2000800000 7.3181560000 6.3967090000
H -10.5839200000 3.0348040000 6.4273730000
H -4.5177810000 5.7656790000 -0.0645800000
H -3.3085480000 1.8912870000 1.3675320000
H -3.0168070000 3.7812870000 -0.2122120000

(*E*)-**1** bound rotamer 1

O -0.3029680000 3.9273400000 1.3293140000
O 0.1651730000 3.5614400000 -0.8922940000
N -2.5671660000 5.2277670000 -0.2136110000
N -3.5928760000 4.5324730000 0.0027560000
C -2.9874660000 10.9589840000 -0.1017030000
C 1.3426170000 4.1801630000 -0.3433630000
C 0.9180960000 4.6401040000 1.0718410000
C -1.7618570000 8.8008030000 -0.6158130000
C -1.6784040000 7.4100360000 -0.6293770000
C -2.9061260000 9.4502770000 -0.1237590000
C -3.9669560000 8.6574710000 0.3504190000
C -3.8996860000 7.2667270000 0.3355900000
C -2.7480190000 6.6317710000 -0.1596760000
C -3.3595110000 3.1348850000 -0.0191960000
C -2.0638170000 2.5678900000 -0.0058540000
C -1.9757900000 1.1712020000 -0.0695970000
C -3.1192610000 0.3623470000 -0.1267360000
C -4.3898330000 0.9444520000 -0.1176750000
C -4.5089680000 2.3329900000 -0.0598040000
B -0.7615750000 3.4374360000 0.1224190000
H -0.7977320000 6.9050080000 -1.0153700000
H -4.7203740000 6.6622780000 0.7057750000
H -2.1955200000 11.3906790000 0.5224850000
H -2.8693450000 11.3776070000 -1.1084340000
H -3.9482680000 11.3023630000 0.2930180000
H -0.9293240000 9.3915890000 -0.9913520000
H -4.8588960000 9.1429350000 0.7403990000
H -3.0143460000 -0.7187750000 -0.1716010000
H -5.2795470000 0.3223430000 -0.1570970000
H -0.9965610000 0.6977000000 -0.0682570000
H -5.4801840000 2.8191680000 -0.0568320000
H 1.6502170000 5.0089880000 -0.9890640000
H 2.1488590000 3.4369760000 -0.3182300000
H 0.7140730000 5.7170280000 1.1150220000
H 1.6507140000 4.3878140000 1.8445850000

(*E*)-**1** bound rotamer 2

O -2.5123990000 2.2349240000 -0.2084720000
O -1.7095570000 4.3807760000 -0.2713990000
N 2.2860140000 5.1061920000 -0.0847050000
N 1.1835980000 4.4989050000 -0.1017240000
C 2.1951010000 10.8529810000 -0.1528350000
C -3.6786650000 3.0737000000 -0.1777960000
C -3.1342780000 4.4961450000 -0.4430180000
C 3.3923890000 7.2274890000 -0.0759530000
C 3.3931170000 8.6211160000 -0.0903430000
C 2.1887440000 9.3419300000 -0.1331300000

```
C 0.9817520000 8.6188260000 -0.1605510000
C 0.9652340000 7.2269740000 -0.1461260000
C 2.1806700000 6.5202630000 -0.1030060000
C 1.2612590000 3.0817310000 -0.0826140000
C 2.4827350000 2.3851760000 -0.0205880000
C 2.4937520000 0.9948260000 0.0018380000
C 1.2868870000 0.2829630000 -0.0356460000
C 0.0776880000 0.9750390000 -0.0959080000
C 0.0288240000 2.3842590000 -0.1224850000
B -1.3899640000 3.0449200000 -0.1999480000
H 2.7219810000 11.2602500000 0.7187870000
H 2.7058980000 11.2363460000 -1.0450440000
H 1.1789660000 11.2573600000 -0.1499090000
H -4.1509000000 2.9817740000 0.8077750000
H -4.3859610000 2.7343560000 -0.9404860000
H -3.5193510000 5.2411860000 0.2594980000
H -3.3350800000 4.8376700000 -1.4653320000
H -0.8560800000 0.4215980000 -0.1235590000
H 3.4400040000 0.4615900000 0.0506350000
H 1.2924520000 -0.8039540000 -0.0164650000
H 3.4050810000 2.9543750000 0.0107430000
H 0.0345000000 6.6689900000 -0.1681470000
H 0.0399290000 9.1626620000 -0.1941770000
H 4.3392800000 9.1577510000 -0.0676670000
H 4.3211700000 6.6649900000 -0.0427130000
```

(*E*)-**2** unbound

```
F 1.3736400000 8.5415580000 0.3027720000
F -3.3702760000 8.8567290000 0.1149910000
O -4.7387200000 6.2742120000 -0.2651310000
O -5.4734140000 4.0512600000 -0.4908650000
N -0.9023440000 7.1840140000 0.1199340000
N -1.9716090000 6.5249990000 -0.0054020000
C 0.2383740000 9.2663450000 0.2964590000
C 0.3448640000 10.6467490000 0.3858590000
C -0.8243780000 11.4100430000 0.3809680000
C -2.0742920000 10.7918910000 0.2882040000
C -2.1412230000 9.4090530000 0.1988040000
C -0.9949180000 8.5808100000 0.1981660000
C -1.8024110000 5.1138460000 -0.0774820000
C -0.5348030000 4.5042520000 0.0011860000
C -0.4274580000 3.1211270000 -0.0778780000
C -1.5786410000 2.3358910000 -0.2354960000
C -2.8314100000 2.9449560000 -0.3120060000
C -2.9819440000 4.3423930000 -0.2351470000
B -4.4431290000 4.9478250000 -0.3305560000
H -0.7633870000 12.4917460000 0.4509880000
H -3.9324590000 6.8117990000 -0.1510820000
H -6.3270720000 4.5013210000 -0.5413260000
H -2.9976320000 11.3609850000 0.2842150000
H 1.3278780000 11.0988820000 0.4574320000
H -1.4946360000 1.2538770000 -0.2986570000
H -3.7213500000 2.3354710000 -0.4342410000
H 0.3437100000 5.1273360000 0.1223900000
H 0.5504710000 2.6506980000 -0.0169690000
```

(*E*)-**2** bound rotamer 1

```
F -1.5375010000 6.1672990000 -0.9959340000
F 2.5814160000 5.6473970000 1.3159090000
O 2.8536640000 2.2782150000 0.9738530000
O 2.5395460000 2.7333520000 -1.2584030000
```

```
N 0.4631370000 4.3948600000 0.2283150000
N -0.6748990000 3.8661240000 0.1178100000
C 3.8677650000 3.1995780000 -0.9606360000
C 4.1280570000 2.7516160000 0.5014530000
C 1.6308480000 6.4288880000 0.7559110000
C 1.8205520000 7.8029070000 0.7704940000
C 0.8477870000 8.6169220000 0.1850770000
C -0.2870740000 8.0525550000 -0.4023400000
C -0.4495900000 6.6726690000 -0.3850990000
C 0.4960850000 5.8027210000 0.2029910000
C -0.8755760000 -0.3220150000 0.0656650000
C 0.3852210000 0.2896520000 0.0130130000
C 0.5300050000 1.6825100000 0.0144200000
C -0.6562420000 2.4512430000 0.0859410000
C -1.9221760000 1.8481360000 0.1303280000
C -2.0333620000 0.4583170000 0.1224230000
B 1.9651980000 2.3196890000 -0.0752720000
H 3.8918500000 4.2896990000 -1.0703110000
H 4.5673740000 2.7560460000 -1.6759520000
H 4.4622020000 3.5732930000 1.1414180000
H 4.8508260000 1.9299880000 0.5685410000
H 1.2716620000 -0.3386660000 -0.0337190000
H -3.0121010000 -0.0117810000 0.1606740000
H -0.9494710000 -1.4067420000 0.0583000000
H -2.7977800000 2.4887500000 0.1754380000
H 0.9764350000 9.6951390000 0.1820800000
H -1.0486760000 8.6613530000 -0.8779400000
H 2.7131180000 8.2111960000 1.2316820000
```

(*E*)-**2** bound rotamer 2

```
F 0.1406860000 6.5857480000 1.4009430000
F 4.0166070000 6.5267000000 -1.3457530000
O -2.5553140000 2.3458680000 0.1612250000
O -1.6587660000 4.0514420000 -1.0840490000
N 2.1519540000 5.0505640000 -0.1028120000
N 1.0720880000 4.4236760000 0.0603130000
C -3.6848960000 3.0725420000 -0.3599650000
C -3.0671780000 4.3361820000 -1.0053780000
C 3.0758570000 7.1975320000 -0.6485380000
C 3.1482650000 8.5828670000 -0.6114730000
C 2.1779720000 9.2830860000 0.1097160000
C 1.1598940000 8.5984570000 0.7784090000
C 1.1112360000 7.2114990000 0.7065780000
C 2.0599390000 6.4539720000 -0.0146300000
C 1.1979940000 3.0083810000 0.0361790000
C 2.4309800000 2.3535000000 0.2050900000
C 2.4784610000 0.9630190000 0.2389730000
C 1.2981390000 0.2178100000 0.1167990000
C 0.0755710000 0.8730750000 -0.0436620000
C -0.0055660000 2.2771140000 -0.0945110000
B -1.4072900000 2.9337020000 -0.3292130000
H -4.3718700000 3.3007340000 0.4600010000
H -4.2016030000 2.4375170000 -1.0894170000
H -3.2061490000 5.2318510000 -0.3892540000
H -3.4487270000 4.5346900000 -2.0109560000
H -0.8375360000 0.2905410000 -0.1284580000
H 3.4311140000 0.4576300000 0.3749810000
H 1.3319510000 -0.8680000000 0.1562880000
H 3.3301230000 2.9488430000 0.3208470000
H 0.4058770000 9.1196150000 1.3587510000
H 2.2176990000 10.3673810000 0.1556100000
H 3.9509490000 9.0874640000 -1.1379040000
```

(*E*)-**3** unbound

```
O 0.7843370000 -0.7060310000 7.4753550000
O 1.2757030000 -0.5036100000 5.1758660000
O -2.7922900000 -0.2821800000 0.1865920000
O 1.4481050000 -0.2727760000 2.3057910000
N -0.9065950000 -0.4772510000 3.5383660000
N -1.4630670000 -0.4106150000 2.4060810000
C 2.8757410000 -0.2144850000 2.2666820000
C -3.6110840000 -0.2255180000 -0.9767480000
C -1.2089920000 -0.6867090000 5.9234990000
C -1.8025020000 -0.6135180000 4.6383300000
C -3.1997580000 -0.6749080000 4.4771290000
C -4.0192160000 -0.8096860000 5.5924480000
C -3.4562660000 -0.8830300000 6.8750300000
C -2.0711520000 -0.8213570000 7.0284670000
C 1.3552200000 -0.0846830000 -0.0991620000
C 0.5750980000 -0.0258910000 -1.2525660000
C -0.8164130000 -0.0888820000 -1.1972560000
C -1.4465970000 -0.2146790000 0.0465480000
C -0.6841680000 -0.2804200000 1.2564280000
C 0.7397870000 -0.2108830000 1.1544340000
B 0.3527310000 -0.6265680000 6.1698530000
H 1.0646600000 0.0724040000 -2.2177110000
H 3.2874940000 -1.0535400000 1.6933630000
H 3.2185960000 0.7350270000 1.8385670000
H 3.1888880000 -0.2867070000 3.3081040000
H -3.4802030000 0.7226190000 -1.5138530000
H -3.4043660000 -1.0642700000 -1.6533360000
H -4.6373940000 -0.2968890000 -0.6135270000
H 1.7476100000 -0.6592170000 7.5316930000
H 0.8234980000 -0.4566290000 4.3020940000
H -3.6136520000 -0.6153220000 3.4767250000
H -5.0984100000 -0.8584270000 5.4671260000
H -4.0973000000 -0.9882750000 7.7464210000
H -1.6346640000 -0.8787110000 8.0212660000
H 2.4335240000 -0.0316640000 -0.1800980000
H -1.3934130000 -0.0396760000 -2.1116290000
```

(*E*)-**3** bound rotamer 1

```
O -4.7042730000 6.4312870000 0.7476270000
O -0.5689780000 6.7021490000 -1.5002980000
O -1.1243980000 4.0190110000 1.8908390000
O 0.3453870000 3.5258740000 0.1912320000
N -2.4555830000 5.1938560000 -0.4668000000
N -3.4759530000 4.4887110000 -0.6783730000
C 1.1193570000 4.2117810000 1.1899560000
C 0.0716430000 4.7565530000 2.1884550000
C 0.5176920000 7.4287610000 -2.0606190000
C -5.7306280000 7.0113170000 1.5441450000
C -1.6314430000 8.7838540000 -0.8221370000
C -1.5853410000 7.3871460000 -0.9123690000
C -2.7262190000 9.3872460000 -0.2013310000
C -3.7705590000 8.6311590000 0.3287280000
C -3.7429120000 7.2309410000 0.2250910000
C -2.6438210000 6.5892180000 -0.4062240000
C -3.2156260000 3.0945770000 -0.6252070000
C -2.0402960000 2.5529870000 -0.0554780000
C -1.8834090000 1.1616230000 -0.1116420000
C -2.8593840000 0.3335180000 -0.6825590000
C -4.0258000000 0.8904280000 -1.2157570000
```

```
C -4.2057790000 2.2734300000 -1.1819210000
B -0.9570910000 3.4511900000 0.6406240000
H -0.8361590000 9.3958460000 -1.2287050000
H -2.7658120000 10.4709810000 -0.1287740000
H -4.6008050000 9.1298420000 0.8129870000
H -2.7101210000 -0.7431830000 -0.7031760000
H -4.7880070000 0.2522180000 -1.6543660000
H -0.9863850000 0.7096280000 0.3052680000
H -5.0964220000 2.7408430000 -1.5916220000
H 1.7047470000 5.0036710000 0.7125320000
H 1.8067870000 3.4939910000 1.6544850000
H -0.1253610000 5.8253510000 2.0370040000
H 0.3454370000 4.5906140000 3.2351720000
H 1.0418040000 8.0216080000 -1.2995070000
H 1.1946460000 6.6744850000 -2.4648040000
H 0.1813180000 8.0893030000 -2.8701150000
H -6.3685240000 7.6784420000 0.9506190000
H -6.3254100000 6.1719910000 1.9072030000
H -5.3140000000 7.5615940000 2.3975490000
```

(*E*)-**3** bound rotamer 2

```
O 3.3450510000 4.6932760000 -0.3472940000
O 2.1595190000 5.0002000000 -2.2890320000
O -2.5904870000 8.8715540000 -0.6259900000
O 1.8544050000 8.3363410000 0.8704960000
N -0.7045710000 7.2589630000 0.2314730000
N 0.1955020000 6.4236750000 -0.0430970000
C 4.3208120000 5.0685830000 -1.3386890000
C 3.4830310000 5.4897160000 -2.5697540000
C -3.7109100000 9.6745010000 -0.9760700000
C 3.0386790000 8.8707380000 1.4500060000
C 0.8895790000 9.1877930000 0.4370230000
C 1.0705040000 10.5785330000 0.3781870000
C 0.0218280000 11.3975190000 -0.0379090000
C -1.2226940000 10.8683340000 -0.3820660000
C -1.4194210000 9.4835980000 -0.3074560000
C -0.3654160000 8.6184270000 0.0881400000
C -0.1548780000 5.0634940000 0.1880800000
C 0.8125840000 4.1350740000 -0.2453510000
C 0.5655900000 2.7705910000 -0.0248530000
C -0.6106190000 2.3450560000 0.5983810000
C -1.5620480000 3.2854430000 1.0196000000
C -1.3378180000 4.6447600000 0.8211160000
B 2.1130360000 4.6460770000 -0.9609130000
H 4.9622370000 4.2028230000 -1.5420250000
H 4.9395980000 5.8801800000 -0.9437650000
H 3.8391690000 5.0458730000 -3.5037650000
H 3.4328230000 6.5781110000 -2.6884960000
H -2.0530270000 5.3915410000 1.1480920000
H -3.5248020000 10.2420820000 -1.8969520000
H -4.5316180000 8.9751210000 -1.1426660000
H -3.9778540000 10.3662570000 -0.1664700000
H 2.8098670000 9.5317280000 2.2959730000
H 3.6037910000 8.0065990000 1.8028300000
H 3.6358500000 9.4186420000 0.7094930000
H 0.1776590000 12.4715280000 -0.0955560000
H -2.0184250000 11.5282310000 -0.7031730000
H 2.0204100000 11.0219370000 0.6492480000
H -2.4733960000 2.9524610000 1.5097440000
H 1.2971510000 2.0313070000 -0.3418550000
H -0.7847030000 1.2846910000 0.7630540000
```

(*Z*)-**1** unbound

```
O -8.2581260000 1.3404190000 1.3224050000
O -6.7910390000 2.3456200000 -0.1614520000
N -3.6652450000 0.7699940000 -1.2647260000
N -4.9143330000 0.7018580000 -1.2918190000
C 0.1439220000 -2.8485870000 1.0894230000
C -0.6672250000 -1.3318510000 -0.7725670000
C -0.8897670000 -1.9311470000 0.4791840000
C -2.0858790000 -1.6312870000 1.1496080000
C -3.0499540000 -0.7961620000 0.5848260000
C -1.6003540000 -0.4607430000 -1.3288620000
C -5.3888530000 -1.7093450000 -1.5029440000
C -6.2451170000 -2.7881100000 -1.2930070000
C -7.3983660000 -2.6233730000 -0.5194050000
C -7.6971120000 -1.3669510000 0.0125220000
C -6.8766860000 -0.2431390000 -0.1982060000
C -5.6923640000 -0.4567930000 -0.9461650000
C -2.8183530000 -0.2200020000 -0.6736460000
B -7.3090890000 1.1940250000 0.3391330000
H -6.1063250000 2.1657370000 -0.8329360000
H -8.5692720000 0.5152950000 1.7072560000
H 0.3359260000 -3.7140290000 0.4439960000
H 1.1008500000 -2.3313580000 1.2284790000
H -0.1794040000 -3.2223460000 2.0647110000
H -6.0139190000 -3.7534850000 -1.7343560000
H -8.0694530000 -3.4609550000 -0.3508760000
H -8.6211750000 -1.2585910000 0.5773570000
H -4.4955710000 -1.8295880000 -2.1068600000
H -3.9632310000 -0.5786950000 1.1281860000
H -2.2681300000 -2.0580420000 2.1327150000
H -1.4066480000 0.0362020000 -2.2749320000
H 0.2601820000 -1.5298430000 -1.3053920000
```

(*Z*)-**1** bound

```
O -8.4177770000 1.3218840000 0.7807870000
O -6.2683320000 2.0340970000 0.4042060000
N -3.7833710000 0.6527090000 -1.6952210000
N -5.0241640000 0.5404330000 -1.7613570000
C -6.9127260000 3.1363350000 1.0684970000
C -8.3669280000 2.6544340000 1.3234950000
C -0.0617650000 -2.4827280000 1.3946290000
C -0.7900100000 -1.2922020000 -0.7228110000
C -1.0692230000 -1.6863110000 0.5973640000
C -2.2971060000 -1.2988450000 1.1540350000
C -3.2364250000 -0.5742460000 0.4183120000
C -1.7018220000 -0.5362510000 -1.4552480000
C -5.5170920000 -1.8534300000 -1.7928850000
C -6.3570240000 -2.9213570000 -1.4774610000
C -7.4459350000 -2.7316220000 -0.6204960000
C -7.6898020000 -1.4619200000 -0.0931300000
C -6.8683190000 -0.3600360000 -0.3978210000
C -5.7617030000 -0.5828170000 -1.2490820000
C -2.9498330000 -0.2070970000 -0.9041750000
B -7.1821300000 1.0206040000 0.2502040000
H -6.8637470000 4.0150300000 0.4174450000
H -6.3698690000 3.3533580000 1.9939310000
H -9.1116900000 3.2703900000 0.8097460000
H -8.6192580000 2.6116650000 2.3880490000
H 0.1702390000 -3.4350990000 0.9031400000
H 0.8831060000 -1.9361760000 1.5010310000
```

```
H -0.4340640000 -2.7064820000 2.3983200000
H -6.1609950000 -3.9010200000 -1.9051840000
H -8.1023840000 -3.5615890000 -0.3749070000
H -8.5396230000 -1.3079300000 0.5667760000
H -4.6801750000 -1.9933790000 -2.4702970000
H -4.1730910000 -0.2770340000 0.8753210000
H -2.5247270000 -1.5685300000 2.1825050000
H -1.4679970000 -0.1976120000 -2.4603250000
H 0.1628110000 -1.5624190000 -1.1727540000
```

(*Z*)-**2** unbound

```
F -3.9705770000 -0.2881050000 1.4562180000
F -1.5800800000 -0.1908280000 -2.6142720000
O -8.3268870000 1.2663470000 1.3230200000
O -6.8782220000 2.3569770000 -0.1160860000
N -3.6562640000 0.8240810000 -1.1472660000
N -4.9022810000 0.7629300000 -1.1955260000
C -0.7484380000 -1.4965430000 -0.8288690000
C -0.8934970000 -1.9519080000 0.4855420000
C -1.9847560000 -1.5497320000 1.2599960000
C -2.9285500000 -0.7009350000 0.6972000000
C -1.7055920000 -0.6336520000 -1.3426080000
C -5.3280070000 -1.6448690000 -1.5096940000
C -6.1682960000 -2.7457590000 -1.3491620000
C -7.3477800000 -2.6177820000 -0.6110340000
C -7.6914120000 -1.3786300000 -0.0632980000
C -6.8887470000 -0.2360760000 -0.2223200000
C -5.6778450000 -0.4125850000 -0.9366210000
C -2.8369830000 -0.2281050000 -0.6201870000
B -7.3630820000 1.1769080000 0.3493430000
H -0.1500410000 -2.6199460000 0.9088710000
H -6.1650500000 2.2224710000 -0.7651580000
H -8.6039690000 0.4242330000 1.6968150000
H -5.9063700000 -3.6955900000 -1.8062870000
H -8.0073130000 -3.4714830000 -0.4821100000
H -8.6349060000 -1.3014410000 0.4730840000
H -4.4264630000 -1.7313720000 -2.1063100000
H -2.1135060000 -1.8766660000 2.2858530000
H 0.0887240000 -1.7930790000 -1.4513130000
```

(*Z*)-**2** bound

```
F -4.0766560000 0.1518420000 1.3942640000
F -1.4001260000 -0.2622920000 -2.4735280000
O -8.4440440000 1.1214270000 0.8466760000
O -6.5322570000 2.2655640000 0.2965570000
N -3.5396800000 0.9768760000 -1.2846350000
N -4.7637790000 0.8867610000 -1.4913920000
C -7.2957530000 3.1749710000 1.1101650000
C -8.6546640000 2.4621440000 1.3282220000
C -0.7419340000 -1.3820080000 -0.4984810000
C -0.9952860000 -1.6871670000 0.8427840000
C -2.1256020000 -1.1742310000 1.4834740000
C -2.9945540000 -0.3634140000 0.7634680000
C -1.6303970000 -0.5551590000 -1.1706810000
C -5.1351240000 -1.4995790000 -1.8625570000
C -5.9398260000 -2.6338010000 -1.7466640000
C -7.1187170000 -2.5813190000 -0.9980200000
C -7.4953290000 -1.3832750000 -0.3863390000
C -6.7202040000 -0.2146460000 -0.4985800000
C -5.5150650000 -0.3053650000 -1.2317880000
C -2.7915570000 -0.0368790000 -0.5834710000
```

```
B -7.2182260000 1.0823090000 0.2133980000
H -0.3085420000 -2.3257220000 1.3895160000
H -7.3918050000 4.1282630000 0.5824530000
H -6.7528110000 3.3422070000 2.0467580000
H -9.4653140000 2.9171690000 0.7484320000
H -8.9526700000 2.4204980000 2.3799940000
H -5.6459030000 -3.5535900000 -2.2448920000
H -7.7468290000 -3.4628040000 -0.9036560000
H -8.4164980000 -1.3394400000 0.1874900000
H -4.2340620000 -1.5262300000 -2.4670840000
H -2.3436060000 -1.3888400000 2.5239490000
H 0.1247590000 -1.7692180000 -1.0229340000
```

(*Z*)-**3** unbound

```
O -6.8887400000 2.2203960000 -0.4012660000
O -8.6084770000 0.9824400000 0.6313070000
O -4.0110670000 -0.0988600000 1.4034910000
O -1.4955610000 -0.1316830000 -2.5452520000
N -3.5546510000 0.8324230000 -1.1582870000
N -4.7905240000 0.7130500000 -1.3012110000
C -4.2214470000 -0.4062130000 2.7786450000
C -0.3084330000 -0.3822190000 -3.2914490000
C -0.5874900000 -1.3488470000 -0.6276540000
C -0.7809380000 -1.7380940000 0.6997720000
C -1.9152240000 -1.3515260000 1.4141580000
C -2.8898840000 -0.5615200000 0.7875660000
C -1.5558330000 -0.5518210000 -1.2504970000
C -5.0631490000 -1.7293040000 -1.5889260000
C -5.8592400000 -2.8673870000 -1.4623930000
C -7.1075930000 -2.7843800000 -0.8363670000
C -7.5715030000 -1.5496650000 -0.3755650000
C -6.8120990000 -0.3752880000 -0.5172740000
C -5.5260360000 -0.4999150000 -1.0952730000
C -2.7233620000 -0.1700000000 -0.5586520000
B -7.4319360000 1.0116210000 -0.0808170000
H -8.9303710000 1.8746200000 0.8164630000
H -6.0576730000 2.1019100000 -0.9051170000
H -5.1613400000 0.0778350000 3.0462080000
H -4.3114240000 -1.4882600000 2.9335900000
H -3.4122100000 -0.0074510000 3.4024150000
H -0.1477270000 -1.4580290000 -3.4358050000
H -0.4647650000 0.0936700000 -4.2603290000
H 0.5689250000 0.0599460000 -2.8039180000
H -0.0310910000 -2.3549070000 1.1872790000
H -5.5059830000 -3.8164760000 -1.8564340000
H -7.7241240000 -3.6729950000 -0.7301600000
H -8.5515100000 -1.4793790000 0.0867340000
H -4.1038460000 -1.7869210000 -2.0903760000
H -2.0343400000 -1.6607400000 2.4450080000
H 0.2999050000 -1.6672110000 -1.1608420000
```

(*Z*)-**3** bound

```
O -8.4641650000 1.1119220000 0.8742860000
O -6.6140190000 2.3279190000 0.2747760000
O -3.9713780000 0.2036220000 1.4618630000
O -1.5669090000 -0.2730560000 -2.5280890000
N -3.4828950000 0.9744570000 -1.1607000000
N -4.7090680000 0.9149450000 -1.3675920000
C -4.1748060000 -0.0263670000 2.8501190000
C -0.4254780000 -0.6696610000 -3.2797960000
C -7.4237460000 3.2287300000 1.0486520000
```

```
C -8.7441430000 2.4572080000 1.2989830000
C -0.7285020000 -1.4672750000 -0.5643860000
C -0.9240340000 -1.7685420000 0.7853800000
C -2.0002380000 -1.2394690000 1.4977320000
C -2.9074940000 -0.3877730000 0.8486860000
C -1.6324080000 -0.6127810000 -1.2075610000
C -5.0985900000 -1.4615020000 -1.8025760000
C -5.9162820000 -2.5895570000 -1.7284880000
C -7.1136670000 -2.5408710000 -1.0084820000
C -7.4954540000 -1.3493580000 -0.3880880000
C -6.7061150000 -0.1856230000 -0.4598280000
C -5.4792000000 -0.2748350000 -1.1579250000
C -2.7356060000 -0.0773190000 -0.5148260000
B -7.2395140000 1.1085520000 0.2292990000
H -5.0575880000 0.5557170000 3.1188170000
H -4.3630700000 -1.0877060000 3.0561450000
H -3.3174640000 0.3182200000 3.4421910000
H -0.3651660000 -1.7619570000 -3.3703030000
H -0.5580290000 -0.2314210000 -4.2699560000
H 0.4995050000 -0.2863690000 -2.8315050000
H -0.2255950000 -2.4302050000 1.2902340000
H -7.5693800000 4.1530740000 0.4817470000
H -6.8922470000 3.4676970000 1.9769010000
H -9.5766900000 2.8467060000 0.7023000000
H -9.0420030000 2.4458960000 2.3519900000
H -5.6181150000 -3.5034890000 -2.2355690000
H -7.7522990000 -3.4179130000 -0.9465060000
H -8.4344340000 -1.3052150000 0.1561590000
H -4.1803680000 -1.4845010000 -2.3800630000
H -2.1275230000 -1.4897210000 2.5435930000
H 0.1100070000 -1.8966780000 -1.0989840000
```

(*E*)-**5** unbound

```
O 1.2718100000 0.0362650000 -2.3682450000
O 0.8265380000 -1.0191130000 7.4987750000
O 1.3060960000 -0.7810440000 5.2017320000
O 1.4968560000 -0.4325140000 2.3435570000
N -0.8971430000 -0.5109600000 3.6017720000
N -1.4524690000 -0.3792500000 2.4748160000
C 2.9242120000 -0.4562840000 2.2735700000
C 0.5549360000 0.1665420000 -3.5938670000
C -1.1772260000 -0.7592420000 5.9841650000
C -1.7837180000 -0.5932060000 4.7135470000
C -3.1829110000 -0.5129400000 4.5822050000
C -3.9915560000 -0.5986530000 5.7105450000
C -3.4152590000 -0.7640890000 6.9781240000
C -2.0280650000 -0.8422520000 7.1028650000
C 1.3581310000 -0.1926610000 -0.0497730000
C 0.5716970000 -0.0627350000 -1.2065610000
C -0.8275940000 -0.0423450000 -1.1168850000
C -1.4063680000 -0.1536220000 0.1430830000
C -0.6586600000 -0.2863960000 1.3259550000
C 0.7705250000 -0.3050990000 1.2099240000
B 0.3870830000 -0.8537930000 6.2039820000
H 3.3119990000 0.4794440000 1.8535470000
H 3.2556230000 -0.5665720000 3.3059740000
H 3.2735140000 -1.3069850000 1.6761800000
H -2.4867210000 -0.1400830000 0.2517610000
H 0.8554590000 -0.6631210000 4.3351210000
H 1.7905650000 -1.0675900000 7.5395660000
H -0.0905920000 -0.7027660000 -3.7702120000
H -0.0478390000 1.0828250000 -3.6053910000
H 1.3142400000 0.2206680000 -4.3748570000
```

```
H -3.6122350000 -0.3833420000 3.5953360000
H -5.0722000000 -0.5356330000 5.6064700000
H -4.0470180000 -0.8305810000 7.8600120000
H -1.5805670000 -0.9703340000 8.0839870000
H 2.4336190000 -0.2027910000 -0.1752060000
H -1.4545550000 0.0579230000 -1.9936970000
```

(*E*)-**5** bound (most stable rotamer)

```
O 0.1221370000 12.6606530000 -0.3143930000
O 3.3403580000 3.6250170000 -0.6607050000
O 2.8760620000 5.8696090000 -0.6435740000
O -2.9606840000 8.9356780000 0.1746330000
N -0.9392610000 7.1909520000 -0.0811040000
N 0.0602980000 6.4300390000 -0.2107870000
C -0.9131130000 13.6287830000 -0.1968780000
C 4.6181250000 4.2753620000 -0.7434720000
C 4.2742840000 5.7651890000 -0.9679390000
C -4.0789480000 9.8013050000 0.3155530000
C 0.6541660000 9.0832170000 -0.3218040000
C 0.8874570000 10.4454950000 -0.3757540000
C -0.1936820000 11.3366470000 -0.2455180000
C -1.4961310000 10.8559230000 -0.0594850000
C -1.7255990000 9.4700680000 -0.0039630000
C -0.6437830000 8.5634330000 -0.1377660000
C -0.2265840000 5.0422100000 -0.1580210000
C 0.8742330000 4.1626580000 -0.3103900000
C 0.6145560000 2.7770860000 -0.2572660000
C -0.6727940000 2.2770300000 -0.0642530000
C -1.7463490000 3.1663750000 0.0833380000
C -1.5272550000 4.5386730000 0.0377410000
B 2.3607650000 4.5973950000 -0.5376170000
H -1.6560080000 13.5191170000 -0.9976730000
H -1.4114330000 13.5652080000 0.7791380000
H -0.4234060000 14.5993460000 -0.2887630000
H 1.4671220000 8.3714070000 -0.4219530000
H 5.1937360000 3.8370460000 -1.5645620000
H 5.1597290000 4.1071140000 0.1955910000
H 4.4140840000 6.0742700000 -2.0105940000
H 4.8431450000 6.4397260000 -0.3214360000
H -2.3436060000 5.2429870000 0.1513690000
H -4.2258560000 10.4190570000 -0.5804470000
H -4.9418010000 9.1466850000 0.4466160000
H -3.9779190000 10.4488990000 1.1962850000
H -2.3228030000 11.5439550000 0.0409490000
H 1.8846870000 10.8486530000 -0.5190740000
H -2.7531260000 2.7848260000 0.2357550000
H 1.4458710000 2.0877920000 -0.3708530000
H -0.8417710000 1.2037340000 -0.0281710000
```

(*E*)-**6** unbound

```
O 0.7036140000 0.9542870000 5.1037820000
O 0.6855200000 0.7880970000 7.4578200000
N -1.1582950000 -0.6022750000 3.8276320000
N -1.8614050000 -0.8426970000 2.8122880000
C 2.1385310000 -2.0454340000 1.2950460000
C -4.7908910000 0.6197880000 0.0635200000
C -1.0304120000 -0.6131590000 6.2436180000
C -1.6642230000 -1.0915580000 5.0701850000
C -2.7210350000 -2.0167310000 5.1344080000
C -3.1705780000 -2.4666210000 6.3717850000
C -2.5694090000 -1.9993500000 7.5483000000
```

C -1.5154670000 -1.0876000000 7.4765240000
C 0.3589840000 -0.1528810000 -0.1183180000
C -0.5790150000 0.4118970000 -0.9801820000
C -1.9138840000 0.5335870000 -0.5873500000
C -3.7693520000 0.2325410000 1.1386130000
C -2.3257740000 0.1061550000 0.6764580000
C -1.3456680000 -0.4189920000 1.5643350000
C 0.0114730000 -0.5814800000 1.1714230000
C 1.0585690000 -1.2541160000 2.0505840000
B 0.1684900000 0.4211200000 6.2390230000
H 0.2333840000 0.5851490000 4.3268060000
H 2.7997870000 -1.4002570000 0.7072980000
H 2.7685650000 -2.5827830000 2.0121020000
H 1.6957120000 -2.7826920000 0.6156240000
H -5.7970710000 0.6285540000 0.4957740000
H -4.6039060000 1.6195970000 -0.3442190000
H -4.7936740000 -0.0906860000 -0.7712830000
H 1.4107440000 1.4193950000 7.3610720000
H -3.1674850000 -2.3720090000 4.2126060000
H -3.9854240000 -3.1842860000 6.4227990000
H -2.9189170000 -2.3521770000 8.5147200000
H -1.0481420000 -0.7295390000 8.3885980000
H 1.3820660000 -0.2700730000 -0.4590370000
H -0.2726150000 0.7441900000 -1.9682900000
H -2.6348950000 0.9593300000 -1.2762780000
H -3.8158830000 0.9656680000 1.9553010000
H -4.0636890000 -0.7174440000 1.6001800000
H 1.5501320000 -0.5004190000 2.6792480000
H 0.5590190000 -1.9273980000 2.7533720000
O -2.9585220000 -2.7882630000 3.6474900000
O -4.9277770000 -1.6020410000 3.7156810000
N -1.3215780000 0.2255070000 3.8378330000
N -2.0840550000 -0.0699540000 2.8824740000
C -5.1833630000 -2.7390380000 2.8686470000
C -3.7888190000 -3.3571760000 2.6199510000
C 1.8257480000 -1.9263370000 1.6875190000
C -4.8337560000 1.2573240000 -0.1048880000
C -3.0407290000 -0.7990160000 5.3101350000
C -1.9181380000 0.0375430000 5.1138800000
C -1.3310090000 0.7402720000 6.1738110000
C -1.8871600000 0.6601750000 7.4512110000
C -3.0196910000 -0.1317330000 7.6634080000
C -3.5833130000 -0.8516670000 6.6014770000
C 0.1232800000 -0.3569430000 -0.1212200000
C -0.7414900000 0.1594890000 -1.0862510000
C -2.0210060000 0.5885740000 -0.7297100000
C -3.8295870000 0.9975700000 1.0247480000
C -2.4532350000 0.5109950000 0.5973360000
C -1.5478000000 0.0130340000 1.5726710000
C -0.2464060000 -0.4419370000 1.2285500000

(*E*)-**6** bound

C 0.7027610000 -1.0464170000 2.2539310000
B -3.6229760000 -1.6880800000 4.1561710000
H -5.6736590000 -2.4028090000 1.9503290000
H -5.8569030000 -3.4238040000 3.3984840000
H -3.3807490000 -3.0775530000 1.6411330000
H -3.7775890000 -4.4474570000 2.7121610000
H -3.7065860000 1.9198850000 1.6100450000
H -4.2510730000 0.2770070000 1.7347340000
H 1.1425490000 -0.2398360000 2.8516270000
H 0.1171040000 -1.6367360000 2.9674830000
H -0.4188470000 0.2193470000 -2.1226310000

```
H 1.4336180000 -2.7339660000 1.0585020000
H 2.5459760000 -1.3543450000 1.0923670000
H 2.3808310000 -2.3848630000 2.5126840000
H -4.5180090000 2.0734380000 -0.7645180000
H -4.9885450000 0.3654030000 -0.7241300000
H -5.8026490000 1.5391980000 0.3199060000
H -0.4578530000 1.3541280000 5.9727730000
H -1.4422660000 1.2120600000 8.2742700000
H -3.4592730000 -0.1986550000 8.6550610000
H -4.4545790000 -1.4747760000 6.7888400000
H 1.1026640000 -0.7060310000 -0.4283210000
H -2.6833000000 0.9825040000 -1.4929200000
```

(*Z*)-**6** unbound

```
O -7.1655830000 2.0332840000 -0.8147220000
O -9.0235890000 0.7851470000 -0.0691680000
N -3.7162850000 0.7164310000 -1.0558730000
N -4.9331400000 0.5430000000 -1.2835240000
C -3.8880050000 -0.2368890000 3.2518570000
C -0.3566830000 -0.4613160000 -3.4776000000
C -4.0703130000 -0.0901730000 1.7361100000
C -1.6598070000 -0.1620110000 -2.7288960000
C -0.7848400000 -1.5113590000 -0.7309890000
C -0.8904450000 -1.9218570000 0.5998940000
C -1.9459950000 -1.4693310000 1.3920240000
C -2.9396720000 -0.6281800000 0.8725520000
C -1.7384600000 -0.6574220000 -1.2946990000
C -5.0997530000 -1.9463840000 -1.4779890000
C -5.8955750000 -3.0893210000 -1.4157140000
C -7.2315730000 -2.9944870000 -1.0118860000
C -7.7784980000 -1.7455280000 -0.7095300000
C -7.0191980000 -0.5655290000 -0.7988420000
C -5.6505420000 -0.6953410000 -1.1501490000
C -2.8336920000 -0.2681880000 -0.4903620000
B -7.7367410000 0.8254970000 -0.5492700000
H -1.8391490000 0.9214840000 -2.7198050000
H -2.5008470000 -0.5806210000 -3.3014570000
H -4.2111850000 0.9722460000 1.5002960000
H -5.0095940000 -0.5801380000 1.4481930000
H -9.3949960000 1.6720040000 0.0274830000
H -6.2556400000 1.9034170000 -1.1549830000
H -4.7232930000 0.2432970000 3.7717900000
H -3.8702470000 -1.2861720000 3.5660490000
H -2.9621440000 0.2364390000 3.5970570000
H -0.1879370000 -1.5373100000 -3.5978860000
H -0.3935090000 -0.0216790000 -4.4792070000
H 0.5114770000 -0.0383080000 -2.9603250000
H -0.1368130000 -2.5788310000 1.0260250000
H -5.4698180000 -4.0532070000 -1.6807560000
H -7.8464710000 -3.8883530000 -0.9509000000
H -8.8209470000 -1.6682760000 -0.4165440000
H -4.0677210000 -2.0267300000 -1.7945480000
H -1.9922930000 -1.7703180000 2.4332750000
H 0.0554780000 -1.8506280000 -1.3279010000
```

(*Z*)-**6** bound

```
O -6.9406260000 1.6781840000 -0.3268860000
O -8.9405560000 0.6249520000 -0.7185880000
N -3.6169030000 0.4983340000 -1.4902400000
N -4.8113970000 0.2862780000 -1.7777750000
C -3.0299750000 -0.5241920000 0.7039920000
```

```
C -9.2864890000 1.9277920000 -0.2115100000
C -7.9461910000 2.6996220000 -0.1860660000
C -4.1042020000 0.3914830000 2.8723000000
C 0.0076290000 -0.8761750000 -3.3254470000
C -4.2521210000 0.0821500000 1.3753610000
C -1.3827760000 -0.5414140000 -2.7752730000
C -0.7030070000 -1.5595480000 -0.5248060000
C -0.9372950000 -1.7721190000 0.8362140000
C -2.0775860000 -1.2447960000 1.4400360000
C -1.6101270000 -0.8325400000 -1.3008920000
C -4.9579820000 -2.1821650000 -1.8179620000
C -5.7292260000 -3.3398430000 -1.7103840000
C -7.0530270000 -3.2634100000 -1.2683240000
C -7.6030510000 -2.0182640000 -0.9549980000
C -6.8586580000 -0.8296600000 -1.0676700000
C -5.5093890000 -0.9349880000 -1.4853840000
C -2.7945410000 -0.3649230000 -0.6810160000
B -7.5644910000 0.5174240000 -0.7137510000
```

(*E*)-**7** rotamer 1

```
F 1.2135790000 8.9596490000 1.3139750000
F -3.1737780000 9.0386390000 -0.5003450000
O 2.1629150000 4.6731470000 -0.2864440000
O 0.8931760000 6.0202980000 -1.8460440000
C 0.1016440000 9.6327210000 0.9057360000
C 0.1184450000 11.0156850000 1.0078990000
C -1.0081170000 11.7289920000 0.5906610000
C -2.1158700000 11.0462520000 0.0818550000
C -2.0741910000 9.6615400000 0.0015530000
C -0.9777610000 8.8746530000 0.4058930000
C -0.8758930000 7.4165260000 0.3539340000
C -1.7843430000 6.5268960000 -0.1023630000
C -1.5957440000 5.0659400000 -0.0982510000
C -2.7375240000 4.2827150000 0.1645520000
C -2.6564040000 2.8981260000 0.3021670000
C -1.4179790000 2.2634620000 0.1773280000
C -0.2844130000 3.0251590000 -0.1171660000
C -0.3431990000 4.4214370000 -0.2920630000
B 0.9699210000 5.1064290000 -0.8230410000
H 0.0586750000 7.0337570000 0.7519680000
H -2.7552730000 6.8719840000 -0.4415060000
H 2.9646590000 5.0320900000 -0.6851460000
H 1.7262020000 6.4095810000 -2.1366440000
```

(*E*)-**7** rotamer 2

```
F 1.1937670000 8.6768220000 1.3792800000
F -2.9235480000 9.1330900000 -0.9412290000
O -4.7289050000 6.0621960000 0.2770270000
O -5.4702870000 3.7948730000 -0.0749730000
C 0.2109490000 9.4430170000 0.8312750000
C 0.3535030000 10.8201810000 0.9130370000
C -0.6411730000 11.6279040000 0.3565710000
C -1.7463200000 11.0422500000 -0.2661710000
C -1.8355900000 9.6581430000 -0.3180860000
C -0.8755880000 8.7800770000 0.2229180000
C -0.9028350000 7.3169310000 0.1872520000
C -1.9087000000 6.5154590000 -0.2349760000
C -1.8279800000 5.0428700000 -0.2702630000
C -0.5713720000 4.4223210000 -0.4330120000
C -0.4387460000 3.0370070000 -0.4742550000
C -1.5726810000 2.2262350000 -0.3698720000
```

C -2.8249560000 2.8232190000 -0.2298490000
C -2.9921590000 4.2230190000 -0.1767660000
B -4.4651260000 4.7366240000 0.0160080000
H 0.0008830000 6.8598670000 0.5776390000
H -2.8459160000 6.9525960000 -0.5476420000
H -0.5558320000 12.7090600000 0.4072800000
H -5.6579840000 6.3049980000 0.3665040000
H -6.3665910000 4.1112800000 0.0842070000
H -2.5354760000 11.6370450000 -0.7134360000
H 1.2269050000 11.2361260000 1.4034010000
H -1.4826900000 1.1436470000 -0.4079570000
H -3.7072570000 2.1948630000 -0.1572470000
H 0.3121580000 5.0402680000 -0.5605510000
H 0.5448560000 2.5926040000 -0.6045510000

VI. Reversible binding of fluorophore

A stock solution (**A**) of **17** was prepared by dissolving 4.0 mg into 5 mL of 0.1 M PBS buffered at pH 7.5 in a 5 mL volumetric flask. Another stock solution (**B**) of **P1** was prepared by dissolving 44 mg into 440 uL of 0.1 M PBS buffered at pH 7.5. 306 uL of stock solution **A** and 10 uL of stock solution **B** (such that ratio of boronic acid to diol was 1:1) were added to a scintillation vial which was diluted to 3 mL with the PBS buffer. Three of these solutions were prepared. Solution one was placed in the dark for one hour, solution two was irradiated with red LEDs were one hour, and solution three was irradiated with red LEDs for one hour, followed by blue LEDs for 10 minutes. After, the 3 mL of each sample was loaded into a 15 mL Amicon ultra-15 centrifugal filter (MWCO= 3 kDa) and spin filtered for 20 minutes at 5000 RPM. The eluents were characterized by UV-Vis (Figure S24) and fluorescence (Figure 8b).

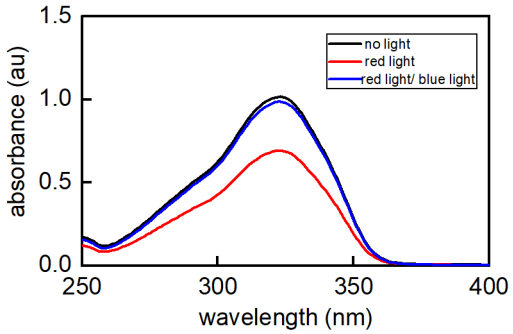

Figure S37. Results of reversible binding of fluorescence diol. Fluorescence spectrum of solution 1 eluents (no irradiation, black trace), solution 2 (60 min red light, red trace) and solution 3 (60 min red light, 10 min blue light, blue trace) in 0.1 M PBS pH 7.5.

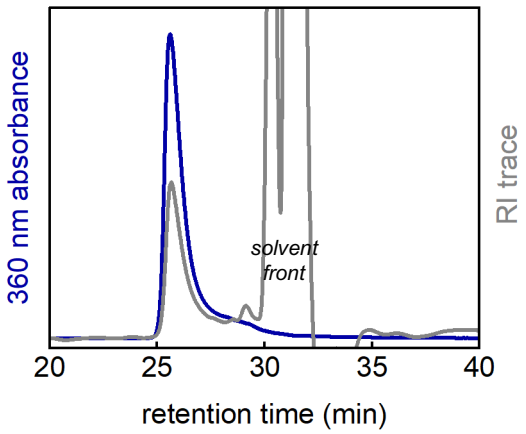

Figure S38. Normalized GPC traces of **P1** (1 mg/mL) in THF measured by 365 nm absorbance and RI trace.

VII. Hydrogel fabrication and rheological characterization

Gels were prepared by mixing 200 μL of **P1** (10 w/v%) with **P2** (10 w/v%) in either DMEM or 0.1 M PBS pH 7.5. Hydrogels prepared in PBS were too sticky and difficult to transfer from vials to the rheometer, as such were only characterized by the flow inversion method. Hydrogels in DMEM could easy be removed from the vial, and as such were characterized by photorheology. Mechanical characterization of the prepared hydrogels was performed using an Anton Paar MCR 302 Rheometer with a 25 mm, 5° cone-plate attachment. 10% strain was established to be within the linear viscoelastic regime for all time points tested (Figure SXX). Unless noted otherwise, oscillatory strain amplitude sweeps were conducted using a frequency of 25 rad/s and oscillatory frequencies were conducted using 10% strain. Gelation profiles were conducted with 10% strain and a frequency of 25 rad/s. Frequency sweeps were performed at 10% strain, with a frequency range of 100 to 0.1 rad/s. Data were collected at 25 °C.

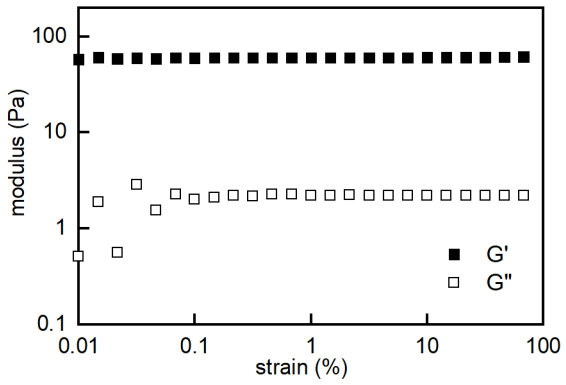

Figure S39. Amplitude sweep (25 rad/s) of hydrogel (1:1 **P1/P2**, 10 w/v% in DMEM) after three hours of irradiation with red light.

VIII. X-ray crystallographic data

(*E*)-**1**

Single crystals of (*E*)-**1** were grown by cooling a concentrated solution in acetonitrile.

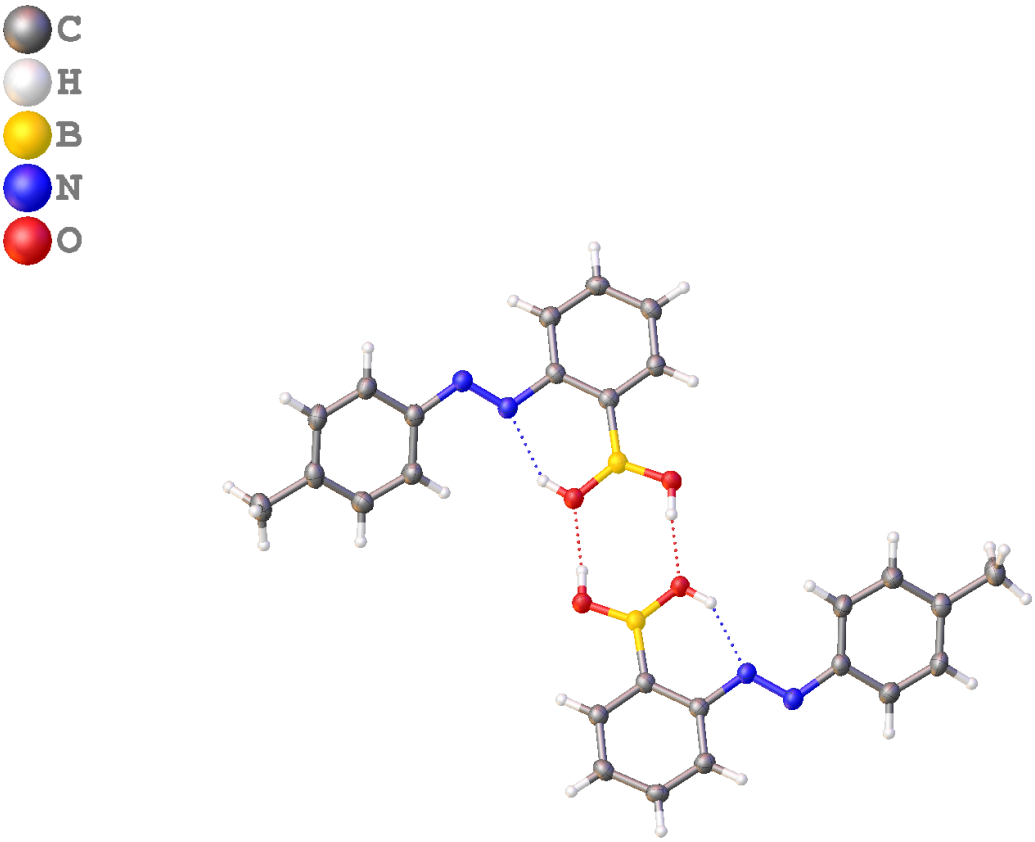

(*E*)-(2-(p-tolyldiazenyl)phenyl)boronic acid

Table 1 Crystal data and structure refinement for (*E*)-1.

Identification code	CCDC# 2022207
Empirical formula	$C_{26}H_{26}B_2N_4O_4$
Formula weight	480.13
Temperature/K	102(3)

Crystal system	monoclinic
Space group	$P2_1/c$
a/Å	10.7395(3)
b/Å	11.9528(2)
c/Å	19.6161(5)
α/°	90
β/°	101.882(2)
γ/°	90
Volume/Å^3	2464.11(10)
Z	4
ϱ_{calc}g/cm^3	1.294
μ/mm^{-1}	0.705
F(000)	1008.0
Crystal size/mm^3	0.14 × 0.07 × 0.02
Radiation	CuKα (λ = 1.54184)
2Θ range for data collection/°	8.414 to 157.658
Index ranges	-12 ≤ h ≤ 13, -14 ≤ k ≤ 14, -22 ≤ l ≤ 24
Reflections collected	20929
Independent reflections	5174 [R_{int} = 0.0384, R_{sigma} = 0.0331]
Data/restraints/parameters	5174/0/331
Goodness-of-fit on F^2	1.062
Final R indexes [I>=2σ (I)]	R_1 = 0.0462, wR_2 = 0.1175
Final R indexes [all data]	R_1 = 0.0569, wR_2 = 0.1235
Largest diff. peak/hole / e Å^{-3}	0.27/-0.21

Table 2 Fractional Atomic Coordinates (×10^4) and Equivalent Isotropic Displacement Parameters (Å^2×10^3) for cx1429xprep. U_{eq} is defined as 1/3 of of the trace of the orthogonalised U_{IJ} tensor.

Atom	*x*	*y*	*z*	U(eq)
O001	6233.4(10)	4991.6(8)	4579.8(5)	28.3(2)
O002	5912.1(10)	3015.5(9)	5262.4(5)	29.3(2)
O003	4132.4(10)	2798.6(8)	4338.4(5)	28.8(2)
O004	4512.1(10)	4715.0(9)	3634.7(5)	30.0(2)
N005	2625.4(11)	1032.7(10)	4453.0(6)	25.3(3)
N006	7854.3(12)	6650.2(10)	4400.2(6)	25.7(3)
N007	1584.0(12)	521.7(10)	4294.8(7)	28.1(3)
N008	8955.2(12)	7059.1(10)	4518.0(7)	28.3(3)
C009	5975.9(14)	6311.8(11)	3513.0(7)	24.7(3)
C00A	4505.4(14)	1360.7(11)	5345.2(7)	24.1(3)
C00B	7077.3(14)	6954.3(11)	3744.0(7)	24.5(3)
C00C	3416.9(14)	705.6(11)	5102.6(7)	24.0(3)

C00D	5300.8(14)	1040.9(12)	5972.6(8)	26.3(3)
C00E	9707.3(14)	6795.7(12)	5183.7(8)	27.5(3)
C00F	826.3(14)	801.2(12)	3634.6(8)	27.2(3)
C00G	5216.7(14)	6593.9(12)	2867.7(7)	26.8(3)
C00H	5524.6(15)	7478.3(12)	2474.8(8)	29.2(3)
C00I	7379.7(15)	7862.9(12)	3356.9(8)	27.3(3)
C00J	3947.1(15)	-514.9(12)	6090.3(8)	29.0(3)
C00K	5033.2(15)	114.7(12)	6343.9(8)	28.7(3)
C00L	11000.3(15)	7031.5(13)	5274.0(8)	31.2(3)
C00M	6602.5(15)	8117.4(12)	2724.1(8)	29.5(3)
C00N	3137.4(14)	-230.5(12)	5474.7(8)	27.7(3)
C00O	11345.4(15)	6384.8(12)	6465.1(8)	32.1(3)
C00P	-833.8(15)	1220.4(13)	2357.0(8)	31.3(3)
C00Q	-1267.5(15)	714.9(14)	2903.1(9)	33.2(3)
C00R	9226.5(15)	6368.3(13)	5740.2(8)	32.2(3)
C00S	1279.8(15)	1308.6(13)	3092.7(8)	32.0(3)
C00T	10044.8(16)	6173.3(13)	6371.5(9)	34.3(3)
C00U	11806.0(15)	6816.6(13)	5906.6(8)	32.3(3)
C00V	-447.6(15)	496.4(13)	3532.8(8)	31.9(3)
C00W	453.6(16)	1506.5(14)	2465.2(8)	35.0(4)
C00X	-1702.2(17)	1441.7(16)	1662.1(9)	39.7(4)
C00Y	12223.5(17)	6162.7(15)	7156.1(9)	40.6(4)
B1	5558.1(16)	5298.2(13)	3937.8(8)	25.1(3)
B2	4865.6(16)	2440.3(13)	4956.7(8)	24.6(3)

Table 3 Anisotropic Displacement Parameters ($Å^2×10^3$) for cx1429xprep. The Anisotropic displacement factor exponent takes the form: $-2\pi^2[h^2a^{*2}U_{11}+2hka^*b^*U_{12}+\ldots]$.

Atom	U_{11}	U_{22}	U_{33}	U_{23}	U_{13}	U_{12}
O001	29.1(6)	25.3(5)	28.2(5)	2.2(4)	0.7(4)	-4.4(4)
O002	31.1(6)	26.4(5)	27.8(5)	4.1(4)	0.1(4)	-5.4(4)
O003	31.3(6)	24.9(5)	27.2(5)	2.3(4)	-0.7(4)	-6.6(4)
O004	36.0(6)	26.2(5)	25.4(5)	2.2(4)	0.4(4)	-6.0(4)
N005	26.0(6)	23.0(6)	26.3(6)	-2.4(4)	3.8(5)	-2.3(5)
N006	26.4(6)	23.0(6)	26.8(6)	-1.6(5)	3.5(5)	-0.6(5)
N007	28.0(6)	26.8(6)	28.7(6)	-1.9(5)	3.7(5)	-3.3(5)
N008	28.4(7)	27.0(6)	28.6(6)	-1.3(5)	4.0(5)	-2.1(5)
C009	27.5(7)	20.9(6)	26.0(7)	-3.0(5)	6.3(6)	1.7(5)
C00A	27.0(7)	21.6(6)	23.5(7)	-3.0(5)	5.2(5)	0.5(5)
C00B	26.9(7)	23.5(6)	22.9(7)	-2.1(5)	4.8(5)	2.4(5)
C00C	26.0(7)	22.9(6)	23.4(7)	-2.5(5)	5.7(6)	0.9(5)
C00D	28.0(7)	25.0(7)	25.6(7)	-2.6(5)	4.9(6)	-0.8(5)
C00E	28.8(8)	24.3(7)	28.2(7)	-2.6(5)	2.8(6)	-0.7(6)
C00F	29.1(8)	24.6(7)	26.6(7)	-4.6(5)	2.6(6)	-2.8(6)

C00G	28.1(7)	25.9(7)	25.4(7)	-3.8(5)	3.2(6)	-0.8(6)
C00H	33.8(8)	28.8(7)	23.6(7)	-0.8(6)	2.7(6)	3.8(6)
C00I	29.1(7)	24.0(7)	29.3(7)	-2.1(5)	7.2(6)	-0.8(6)
C00J	36.7(8)	24.1(7)	27.4(7)	2.7(5)	9.3(6)	-1.6(6)
C00K	34.3(8)	29.0(7)	22.1(7)	0.6(5)	3.7(6)	2.1(6)
C00L	30.2(8)	31.5(8)	31.2(8)	-5.5(6)	5.1(6)	-5.8(6)
C00M	35.8(8)	24.7(7)	29.4(8)	3.2(6)	9.9(6)	0.6(6)
C00N	30.5(8)	24.9(7)	28.2(7)	-2.5(6)	7.1(6)	-3.5(6)
C00O	33.5(8)	25.5(7)	33.2(8)	-4.8(6)	-2.6(6)	2.4(6)
C00P	31.3(8)	30.7(8)	30.6(8)	-5.5(6)	3.0(6)	-0.2(6)
C00Q	24.4(7)	36.4(8)	36.9(8)	-3.8(6)	2.0(6)	-6.1(6)
C00R	27.3(8)	33.7(8)	33.9(8)	2.7(6)	2.7(6)	-1.9(6)
C00S	25.6(8)	38.1(8)	31.2(8)	-2.3(6)	3.1(6)	-7.5(6)
C00T	36.4(9)	34.1(8)	30.8(8)	4.9(6)	3.1(7)	-0.7(7)
C00U	26.0(8)	32.4(8)	36.2(8)	-7.6(6)	1.3(6)	-2.5(6)
C00V	31.0(8)	31.5(8)	32.7(8)	-0.5(6)	5.7(6)	-6.7(6)
C00W	33.7(8)	41.7(9)	28.6(8)	1.1(6)	4.0(6)	-5.5(7)
C00X	35.7(9)	46.6(10)	33.1(9)	-2.5(7)	-1.6(7)	-1.3(7)
C00Y	38.8(9)	40.3(9)	37.0(9)	-1.4(7)	-5.3(7)	4.0(7)
B1	26.8(8)	22.7(7)	25.3(8)	-3.4(6)	4.5(6)	0.9(6)
B2	25.9(8)	23.7(7)	23.9(8)	-3.5(6)	4.6(6)	-0.6(6)

Table 4 Bond Lengths for cx1429xprep.

Atom	Atom	Length/Å	Atom	Atom	Length/Å
O001	B1	1.3675(19)	C00E	C00L	1.392(2)
O002	B2	1.3483(19)	C00E	C00R	1.397(2)
O003	B2	1.3716(19)	C00F	C00S	1.396(2)
O004	B1	1.3514(19)	C00F	C00V	1.390(2)
N005	N007	1.2559(17)	C00G	C00H	1.388(2)
N005	C00C	1.4329(19)	C00H	C00M	1.389(2)
N006	N008	1.2561(17)	C00I	C00M	1.380(2)
N006	C00B	1.4294(19)	C00J	C00K	1.391(2)
N007	C00F	1.420(2)	C00J	C00N	1.378(2)
N008	C00E	1.422(2)	C00L	C00U	1.383(2)
C009	C00B	1.405(2)	C00O	C00T	1.394(2)
C009	C00G	1.399(2)	C00O	C00U	1.391(2)
C009	B1	1.587(2)	C00O	C00Y	1.507(2)
C00A	C00C	1.406(2)	C00P	C00Q	1.391(2)
C00A	C00D	1.399(2)	C00P	C00W	1.397(2)
C00A	B2	1.586(2)	C00P	C00X	1.508(2)
C00B	C00I	1.401(2)	C00Q	C00V	1.386(2)
C00C	C00N	1.402(2)	C00R	C00T	1.383(2)
C00D	C00K	1.387(2)	C00S	C00W	1.382(2)

Table 5 Bond Angles for cx1429xprep.

Atom	Atom	Atom	Angle/°	Atom	Atom	Atom	Angle/°
N007	N005	C00C	114.96(12)	C00M	C00I	C00B	119.58(14)
N008	N006	C00B	114.81(12)	C00N	C00J	C00K	120.76(13)
N005	N007	C00F	115.14(12)	C00D	C00K	C00J	119.53(14)
N006	N008	C00E	114.71(12)	C00U	C00L	C00E	120.00(15)
C00B	C009	B1	123.94(13)	C00I	C00M	C00H	120.10(14)
C00G	C009	C00B	117.09(13)	C00J	C00N	C00C	119.29(14)
C00G	C009	B1	118.97(13)	C00T	C00O	C00Y	120.74(16)
C00C	C00A	B2	123.94(13)	C00U	C00O	C00T	118.21(15)
C00D	C00A	C00C	117.39(13)	C00U	C00O	C00Y	121.04(15)
C00D	C00A	B2	118.66(13)	C00Q	C00P	C00W	117.85(15)
C009	C00B	N006	116.62(12)	C00Q	C00P	C00X	121.96(15)
C00I	C00B	N006	121.85(13)	C00W	C00P	C00X	120.18(15)
C00I	C00B	C009	121.51(13)	C00V	C00Q	C00P	121.06(15)
C00A	C00C	N005	116.66(12)	C00T	C00R	C00E	119.51(15)
C00N	C00C	N005	121.97(13)	C00W	C00S	C00F	119.49(14)
C00N	C00C	C00A	121.37(13)	C00R	C00T	C00O	121.48(15)
C00K	C00D	C00A	121.66(14)	C00L	C00U	C00O	121.16(15)
C00L	C00E	N008	115.80(13)	C00Q	C00V	C00F	120.31(15)
C00L	C00E	C00R	119.61(14)	C00S	C00W	C00P	121.82(15)
C00R	C00E	N008	124.54(14)	O001	B1	C009	122.32(13)
C00S	C00F	N007	124.92(14)	O004	B1	O001	120.14(13)
C00V	C00F	N007	115.58(13)	O004	B1	C009	117.53(13)
C00V	C00F	C00S	119.46(14)	O002	B2	O003	120.55(13)
C00H	C00G	C009	121.68(14)	O002	B2	C00A	117.68(13)
C00G	C00H	C00M	120.00(14)	O003	B2	C00A	121.76(13)

Table 6 Hydrogen Atom Coordinates (Å×10^4) and Isotropic Displacement Parameters (Å^2×10^3) for cx1429xprep.

Atom	*x*	*y*	*z*	U(eq)
H001	6880	5400	4689	42
H002	5965	3605	5036	44
H003	3539	2341	4205	43
H004	4408	4176	3892	45
H00D	6043	1469	6149	32
H00G	4471	6169	2694	32
H00H	4998	7647	2035	35
H00I	8115	8301	3529	33
H00J	3762	-1148	6345	35
H00K	5588	-88	6768	34
H00L	11329	7340	4901	37

H00M	6805	8731	2458	35
H00N	2397	-664	5304	33
H00Q	-2140	516	2843	40
H00R	8344	6213	5685	39
H00S	2150	1516	3155	38
H00T	9713	5889	6750	41
H00U	12690	6967	5961	39
H00V	-758	137	3896	38
H00W	769	1846	2097	42
H00E	-2543	1122	1660	60
H00F	-1346	1096	1291	60
H00O	-1782	2250	1583	60
H00A	11719	6019	7510	61
H00B	12769	6816	7292	61
H00C	12753	5509	7115	61

(*E*)-**2**

Single crystals of (*E*)-**2** were grown by cooling a concentrated solution in DCM.

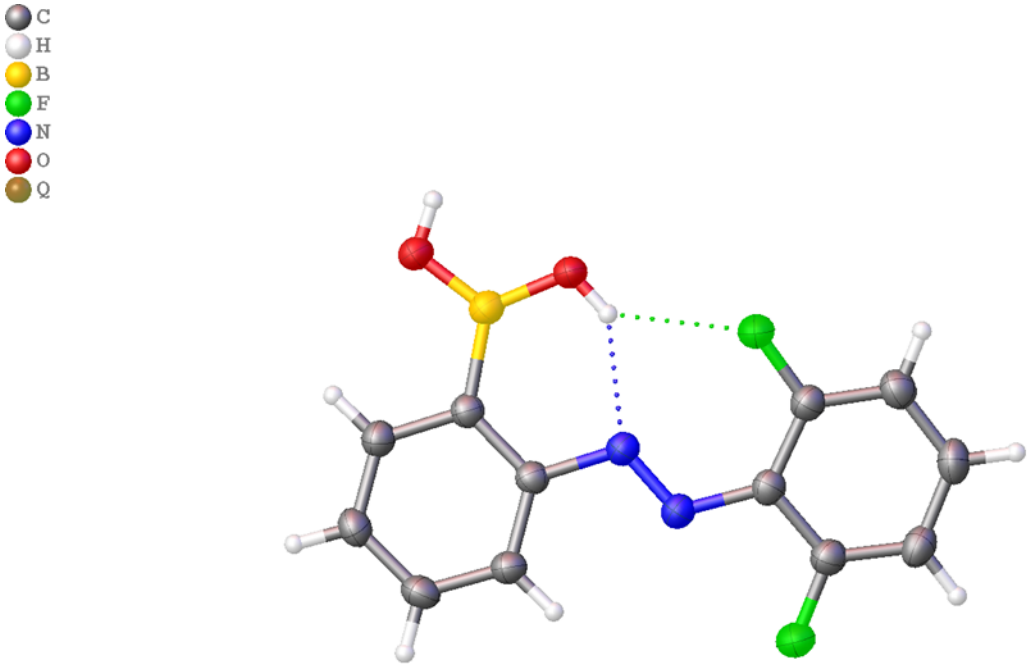

(*E*)-(2-((2,6-difluorophenyl)diazenyl)phenyl)boronic acid

Table 1 Crystal data and structure refinement for (*E*)-2.

Identification code	CCDC # 2020825
Empirical formula	$C_{12}H_9BF_2N_2O_2$
Formula weight	262.02
Temperature/K	200.00(10)
Crystal system	triclinic
Space group	P-1
a/Å	3.81460(10)
b/Å	11.3358(2)
c/Å	14.5651(3)
α/°	112.536(2)
β/°	93.972(2)
γ/°	92.375(2)
Volume/Å^3	578.74(2)

Z	2
ρ_{calc}g/cm^3	1.504
μ/mm^{-1}	1.063
F(000)	268.0
Crystal size/mm^3	0.342 × 0.096 × 0.031
Radiation	CuKα (λ = 1.54184)
2Θ range for data collection/°	6.598 to 152.982
Index ranges	-4 ≤ h ≤ 4, -14 ≤ k ≤ 14, -18 ≤ l ≤ 18
Reflections collected	17174
Independent reflections	2389 [R_{int} = 0.0454, R_{sigma} = 0.0241]
Data/restraints/parameters	2389/0/174
Goodness-of-fit on F^2	1.088
Final R indexes [I>=2σ (I)]	R_1 = 0.0355, wR_2 = 0.1035
Final R indexes [all data]	R_1 = 0.0382, wR_2 = 0.1066
Largest diff. peak/hole / e Å^{-3}	0.30/-0.20

Table 2 Fractional Atomic Coordinates (×10^4) and Equivalent Isotropic Displacement Parameters (Å^2×10^3) for cx1948. U_{eq} is defined as 1/3 of of the trace of the orthogonalised U_{IJ} tensor.

Atom	*x*	*y*	*z*	U(eq)
F18	6269(2)	2483.5(7)	6190.5(5)	47.1(2)
F19	2662(2)	5826.2(7)	9001.0(5)	47.4(2)
O17	7265(3)	10269.1(8)	8971.4(6)	43.5(2)
O16	5085(3)	8407.9(8)	9152.3(6)	41.5(2)
N8	5851(3)	6172.1(9)	7523.4(7)	31.1(2)
N7	5770(3)	4982.2(9)	7060.4(7)	33.4(2)
C9	7120(3)	6890.3(10)	6978.1(8)	28.9(2)
C14	7543(3)	8225.8(10)	7490.2(8)	29.8(2)
C1	4608(3)	4216.8(10)	7565.9(8)	31.5(3)
C2	4937(3)	2900.1(11)	7083.3(9)	35.3(3)
C6	3203(3)	4583.3(11)	8492.3(9)	34.1(3)
C10	7905(3)	6302.7(11)	5985.1(8)	33.9(3)
C13	8839(3)	8932.8(11)	6962.4(9)	34.3(3)
C12	9618(3)	8357.8(12)	5982.1(9)	37.2(3)
C3	4026(3)	2016.8(11)	7475.5(10)	39.7(3)
C11	9139(3)	7034.2(12)	5490.6(9)	37.3(3)
C5	2297(3)	3726.7(12)	8911.4(9)	38.7(3)
C4	2717(3)	2437.0(12)	8400.1(10)	40.8(3)
B15	6598(4)	8985.7(12)	8594.0(10)	33.4(3)

Table 3 Anisotropic Displacement Parameters ($Å^2×10^3$) for cx1948. The Anisotropic displacement factor exponent takes the form: $-2π^2[h^2a^{*2}U_{11}+2hka^*b^*U_{12}+…]$.

Atom	U_{11}	U_{22}	U_{33}	U_{23}	U_{13}	U_{12}
F18	64.6(5)	32.3(4)	41.8(4)	8.9(3)	20.1(4)	3.8(3)
F19	70.8(5)	30.8(4)	40.0(4)	10.0(3)	23.5(4)	3.5(3)
O17	62.8(6)	27.5(4)	36.5(5)	6.6(3)	18.2(4)	-2.8(4)
O16	61.9(6)	26.7(4)	32.4(4)	6.0(3)	17.5(4)	-3.1(4)
N8	34.2(5)	27.1(4)	30.2(5)	8.9(4)	5.6(4)	-0.6(4)
N7	38.6(5)	27.5(5)	32.2(5)	9.5(4)	6.2(4)	-1.0(4)
C9	27.3(5)	29.3(5)	29.0(5)	10.0(4)	4.8(4)	0.6(4)
C14	28.4(5)	29.1(5)	30.8(5)	10.3(4)	4.7(4)	0.2(4)
C1	31.2(6)	29.2(5)	32.8(6)	11.2(4)	2.0(4)	-2.3(4)
C2	35.9(6)	31.8(6)	35.3(6)	10.0(5)	5.4(5)	-1.4(4)
C6	35.8(6)	30.0(5)	33.9(6)	10.0(4)	3.8(5)	-1.3(4)
C10	37.9(6)	30.0(5)	30.7(5)	7.9(4)	7.0(4)	1.5(4)
C13	35.9(6)	29.5(5)	36.7(6)	11.5(5)	7.2(5)	-1.3(4)
C12	38.2(6)	38.7(6)	39.3(6)	19.2(5)	10.3(5)	0.0(5)
C3	39.3(7)	28.7(6)	50.5(7)	15.1(5)	4.9(5)	-1.4(5)
C11	40.9(7)	40.4(6)	29.7(5)	11.4(5)	10.6(5)	3.3(5)
C5	39.4(6)	40.5(6)	37.8(6)	16.7(5)	6.7(5)	-2.3(5)
C4	39.0(6)	38.4(6)	51.1(7)	24.5(6)	5.1(5)	-4.5(5)
B15	36.7(7)	28.3(6)	32.5(6)	8.6(5)	6.2(5)	0.0(5)

Table 4 Bond Lengths for cx1948.

Atom	Atom	Length/Å	Atom	Atom	Length/Å
F18	C2	1.3466(14)	C14	B15	1.5815(16)
F19	C6	1.3497(13)	C1	C2	1.4004(16)
O17	B15	1.3492(15)	C1	C6	1.4034(16)
O16	B15	1.3658(15)	C2	C3	1.3736(17)
N8	N7	1.2536(13)	C6	C5	1.3750(16)
N8	C9	1.4298(13)	C10	C11	1.3786(16)
N7	C1	1.4121(14)	C13	C12	1.3834(16)
C9	C14	1.4043(15)	C12	C11	1.3903(17)
C9	C10	1.4011(15)	C3	C4	1.3823(19)
C14	C13	1.4033(15)	C5	C4	1.3853(18)

Table 5 Bond Angles for cx1948.

Atom	Atom	Atom	Angle/°	Atom	Atom	Atom	Angle/°
N7	N8	C9	113.99(9)	F19	C6	C1	119.43(10)
N8	N7	C1	116.83(9)	F19	C6	C5	117.61(10)
C14	C9	N8	116.45(9)	C5	C6	C1	122.96(11)
C10	C9	N8	122.22(10)	C11	C10	C9	120.18(10)
C10	C9	C14	121.32(10)	C12	C13	C14	122.28(10)
C9	C14	B15	125.30(10)	C13	C12	C11	119.81(10)
C13	C14	C9	116.63(10)	C2	C3	C4	118.86(11)
C13	C14	B15	118.05(10)	C10	C11	C12	119.76(10)
C2	C1	N7	115.73(10)	C6	C5	C4	119.41(11)
C2	C1	C6	114.82(10)	C3	C4	C5	120.19(11)
C6	C1	N7	129.45(10)	O17	B15	O16	119.91(10)
F18	C2	C1	117.87(10)	O17	B15	C14	116.90(10)
F18	C2	C3	118.38(10)	O16	B15	C14	123.17(10)
C3	C2	C1	123.74(11)				

Table 6 Hydrogen Bonds for cx1948.

D	H	A	d(D-H)/Å	d(H-A)/Å	d(D-A)/Å	D-H-A/°
O17	H17	O16[1]	0.84	1.97	2.7982(11)	169.3
O16	H16	F19	0.84	2.27	2.9531(11)	138.9
O16	H16	N8	0.84	2.05	2.7724(12)	144.1

[1]1-X,2-Y,2-Z

Table 7 Torsion Angles for cx1948.

A	B	C	D	Angle/°	A	B	C	D	Angle/°
F18	C2	C3	C4	178.80(11)	C9	C10	C11	C12	0.30(19)
F19	C6	C5	C4	178.18(11)	C14	C9	C10	C11	0.38(18)
N8	N7	C1	C2	-172.67(10)	C14	C13	C12	C11	-0.35(19)
N8	N7	C1	C6	6.46(18)	C1	C2	C3	C4	-0.2(2)
N8	C9	C14	C13	179.08(9)	C1	C6	C5	C4	-1.10(19)
N8	C9	C14	B15	-2.43(17)	C2	C1	C6	F19	-177.65(10)
N8	C9	C10	C11	-179.69(10)	C2	C1	C6	C5	1.62(18)
N7	N8	C9	C14	-174.93(10)	C2	C3	C4	C5	0.8(2)
N7	N8	C9	C10	5.14(16)	C6	C1	C2	F18	-179.98(10)
N7	C1	C2	F18	-0.72(16)	C6	C1	C2	C3	-0.96(18)
N7	C1	C2	C3	178.30(11)	C6	C5	C4	C3	-0.2(2)
N7	C1	C6	F19	3.22(19)	C10	C9	C14	C13	-0.99(16)
N7	C1	C6	C5	-177.52(11)	C10	C9	C14	B15	177.51(11)

C9	N8	N7	C1	178.75(9)	
C9	C14	C13	C12	0.98(17)	
C9	C14	B15	O17	178.46(11)	
C9	C14	B15	O16	-3.32(19)	
C13	C14	B15	O17	-3.07(17)	
C13	C14	B15	O16	175.15(11)	
C13	C12	C11	C10	-0.31(19)	
B15	C14	C13	C12	-177.63(11)	

Table 8 Hydrogen Atom Coordinates (Å×10^4) and Isotropic Displacement Parameters (Å^2×10^3) for cx1948.

Atom	*x*	*y*	*z*	U(eq)
H17	6621.28	10582	9551.21	65
H16	4921.82	7610.25	8836.64	62
H10	7585.68	5397.8	5651.68	41
H13	9191.99	9837.77	7289.76	41
H12	10479.26	8865.9	5645.74	45
H3	4291.04	1132.21	7117.49	48
H11	9659.72	6635.36	4816.29	45
H5	1391.12	4016.68	9545.98	46
H4	2103.61	1839.6	8685.6	49

(*E*)-**3**

Single crystals of (*E*)-**3** were grown by slow evaporation of a solution of ACN.

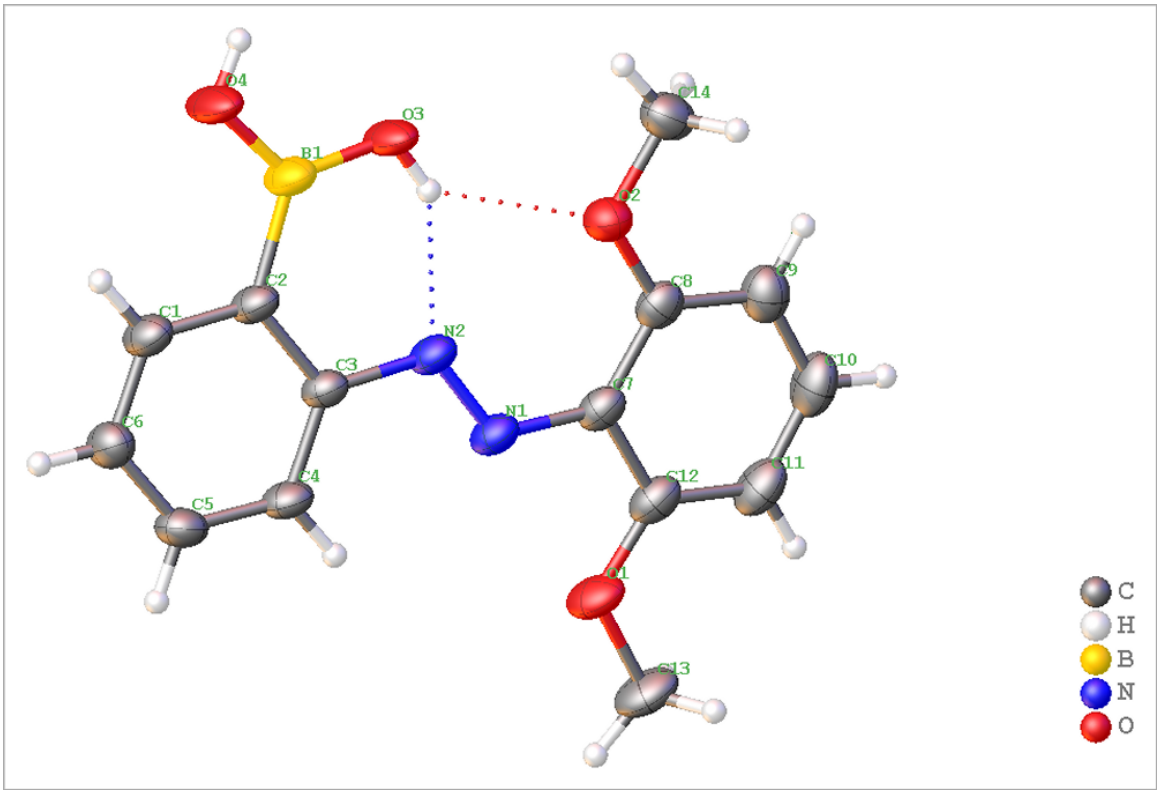

(*E*)-(2-((2,6-dimethoxyphenyl)diazenyl)phenyl)boronic acid

Table 1 Crystal data and structure refinement for (*E*)-3

Identification code	CCDC #2008419
Empirical formula	$C_{14}H_{15}BN_2O_4$
Formula weight	286.09
Temperature/K	200.01(10)
Crystal system	monoclinic
Space group	$P2_1/n$
a/Å	17.8347(3)
b/Å	4.10813(10)
c/Å	19.0734(4)
α/°	90
β/°	101.795(2)
γ/°	90
Volume/Å^3	1367.95(5)
Z	4

ϱ_{calc}g/cm^3	1.389
μ/mm^{-1}	0.840
F(000)	600.0
Crystal size/mm^3	0.228 × 0.104 × 0.048
Radiation	CuKα (λ = 1.54184)
2Θ range for data collection/°	6.184 to 154.312
Index ranges	-17 ≤ h ≤ 21, -4 ≤ k ≤ 5, -24 ≤ l ≤ 24
Reflections collected	8314
Independent reflections	2755 [R_{int} = 0.0349, R_{sigma} = 0.0361]
Data/restraints/parameters	2755/0/194
Goodness-of-fit on F^2	1.060
Final R indexes [I>=2σ (I)]	R_1 = 0.0419, wR_2 = 0.1185
Final R indexes [all data]	R_1 = 0.0471, wR_2 = 0.1227
Largest diff. peak/hole / e Å^{-3}	0.18/-0.21

Table 2 Fractional Atomic Coordinates (×10^4) and Equivalent Isotropic Displacement Parameters (Å^2×10^3) for cx1670. U_{eq} is defined as 1/3 of of the trace of the 62rthogonalized U_{IJ} tensor.

Atom	*x*	*y*	*z*	U(eq)
N2	2422.0(6)	1268(3)	9953.9(6)	32.3(3)
N1	3136.7(6)	1030(3)	10151.5(6)	32.8(3)
O2	2264.0(5)	-2697(3)	11002.0(5)	38.0(3)
O1	4584.0(5)	1789(3)	10622.5(5)	44.1(3)
O3	957.8(5)	19(3)	10055.4(5)	46.5(3)
O4	24.4(5)	1800(4)	9076.7(6)	57.6(4)
C2	1384.9(6)	3012(4)	9010.7(6)	32.6(3)
C3	2181.2(6)	2865(3)	9281.2(6)	29.2(3)
C4	2694.5(7)	4297(4)	8910.7(7)	34.6(3)
C7	3428.6(7)	-420(3)	10818.3(7)	32.2(3)
C5	2429.3(7)	5873(4)	8272.9(7)	37.2(3)
C8	3026.3(7)	-2225(4)	11255.5(7)	34.1(3)
C12	4229.5(7)	42(4)	11063.8(7)	37.0(3)
C9	3408.5(9)	-3453(4)	11909.7(8)	43.3(4)
C6	1645.1(8)	6030(4)	7991.8(7)	38.4(3)
C1	1138.1(7)	4610(4)	8359.0(7)	37.9(3)
C11	4599.7(8)	-1186(4)	11719.8(8)	44.2(4)
B1	768.6(8)	1518(5)	9407.0(8)	39.3(4)
C10	4188.0(9)	-2907(4)	12136.2(8)	48.4(4)
C13	5392.2(7)	2254(5)	10829.7(9)	49.1(4)

C14	1853.1(9)	-4674(4)	11412.8(8)	44.0(4)

Table 3 Anisotropic Displacement Parameters ($Å^2×10^3$) for cx1670. The Anisotropic displacement factor exponent takes the form: $-2\pi^2[h^2a^{*2}U_{11}+2hka^*b^*U_{12}+\ldots]$.

Atom	U_{11}	U_{22}	U_{33}	U_{23}	U_{13}	U_{12}
N2	20.0(5)	45.4(7)	30.6(5)	-1.6(5)	3.3(4)	0.7(4)
N1	20.8(5)	44.3(7)	32.1(5)	-3.5(5)	2.7(4)	0.2(4)
O2	30.1(5)	45.7(6)	38.5(5)	4.6(4)	7.6(4)	-1.6(4)
O1	20.8(4)	66.9(7)	42.6(5)	-2.5(5)	1.5(4)	-3.0(4)
O3	19.0(4)	81.6(8)	39.1(5)	14.6(5)	6.0(4)	-3.3(5)
O4	19.7(5)	106.6(11)	46.1(6)	26.6(6)	5.4(4)	-2.3(5)
C2	20.5(6)	47.6(8)	29.6(6)	-2.2(6)	4.7(4)	0.2(5)
C3	21.4(5)	38.3(7)	28.1(6)	-3.6(5)	5.2(4)	-0.8(5)
C4	21.0(5)	46.1(8)	37.1(7)	-2.3(6)	7.1(5)	-3.7(5)
C7	24.9(6)	40.0(7)	30.5(6)	-6.0(5)	2.8(5)	3.5(5)
C5	30.4(6)	46.1(8)	37.7(7)	0.8(6)	12.9(5)	-5.0(6)
C8	31.3(6)	37.3(7)	33.0(6)	-5.7(5)	4.7(5)	4.5(5)
C12	26.9(6)	44.8(8)	37.4(7)	-8.9(6)	2.2(5)	4.2(5)
C9	48.5(8)	44.6(8)	34.7(7)	0.4(6)	3.9(6)	4.9(6)
C6	34.0(7)	50.0(8)	30.9(6)	4.4(6)	6.0(5)	1.4(6)
C1	24.0(6)	55.5(9)	33.3(6)	2.4(6)	3.9(5)	1.2(6)
C11	32.1(7)	54.6(9)	40.5(7)	-8.3(7)	-5.5(6)	6.9(6)
B1	21.3(6)	61.2(10)	35.3(7)	3.9(7)	5.4(5)	-1.4(7)
C10	48.4(8)	55.2(10)	35.0(7)	-1.3(7)	-7.2(6)	12.1(7)
C13	21.9(6)	66.8(11)	55.6(9)	-12.2(8)	0.6(6)	-2.4(6)
C14	45.2(8)	43.9(8)	46.5(8)	3.6(7)	17.6(6)	-2.4(6)

Table 4 Bond Lengths for cx1670.

Atom	Atom	Length/Å	Atom	Atom	Length/Å
N2	N1	1.2569(14)	C2	B1	1.580(2)
N2	C3	1.4270(17)	C3	C4	1.3957(18)
N1	C7	1.4046(17)	C4	C5	1.3738(19)
O2	C8	1.3605(15)	C7	C8	1.416(2)
O2	C14	1.4303(17)	C7	C12	1.4221(17)
O1	C12	1.3565(19)	C5	C6	1.3932(18)
O1	C13	1.4275(15)	C8	C9	1.3886(19)
O3	B1	1.3608(19)	C12	C11	1.385(2)
O4	B1	1.3528(17)	C9	C10	1.387(2)
C2	C3	1.4096(15)	C6	C1	1.381(2)

C2	C1	1.3950(19)	C11	C10	1.381(2)

Table 5 Bond Angles for cx1670.

Atom	Atom	Atom	Angle/°	Atom	Atom	Atom	Angle/°
N1	N2	C3	113.93(10)	O2	C8	C7	117.07(11)
N2	N1	C7	118.03(11)	O2	C8	C9	122.61(13)
C8	O2	C14	118.22(11)	C9	C8	C7	120.31(12)
C12	O1	C13	118.11(11)	O1	C12	C7	115.50(12)
C3	C2	B1	123.76(12)	O1	C12	C11	123.83(12)
C1	C2	C3	117.20(11)	C11	C12	C7	120.66(14)
C1	C2	B1	119.04(11)	C10	C9	C8	119.85(15)
C2	C3	N2	116.38(11)	C1	C6	C5	119.68(12)
C4	C3	N2	122.76(11)	C6	C1	C2	122.04(12)
C4	C3	C2	120.84(12)	C10	C11	C12	119.65(13)
C5	C4	C3	120.28(11)	O3	B1	C2	122.89(11)
N1	C7	C8	128.08(11)	O4	B1	O3	119.96(12)
N1	C7	C12	113.76(12)	O4	B1	C2	117.15(13)
C8	C7	C12	118.16(12)	C11	C10	C9	121.36(13)
C4	C5	C6	119.96(12)				

Table 6 Hydrogen Bonds for cx1670.

D	H	A	d(D-H)/Å	d(H-A)/Å	d(D-A)/Å	D-H-A/°
O3	H3	N2	0.82	1.99	2.7067(13)	145.7
O3	H3	O2	0.82	2.22	2.8657(14)	136.3
O4	H4	O3[1]	0.82	1.93	2.7483(14)	171.9

[1]-X,-Y,2-Z

Table 7 Hydrogen Atom Coordinates (Å×10^4) and Isotropic Displacement Parameters (Å^2×10^3) for cx1670.

Atom	*x*	*y*	*z*	U(eq)
H3	1425	-32	10185	70
H4	-248	1078	9338	86
H4A	3218	4185	9096	41
H5	2773	6834	8029	45
H9	3142	-4639	12195	52
H6	1464	7085	7559	46
H1	616	4722	8166	45

H11	5123	-854	11879	53
H10	4439	-3716	12577	58
H13A	5568	3518	10472	74
H13B	5644	176	10877	74
H13C	5508	3380	11280	74
H14A	1331	-4889	11162	66
H14B	1867	-3673	11870	66
H14C	2086	-6788	11482	66

IX. NMR data

SI-**1**

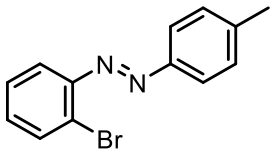

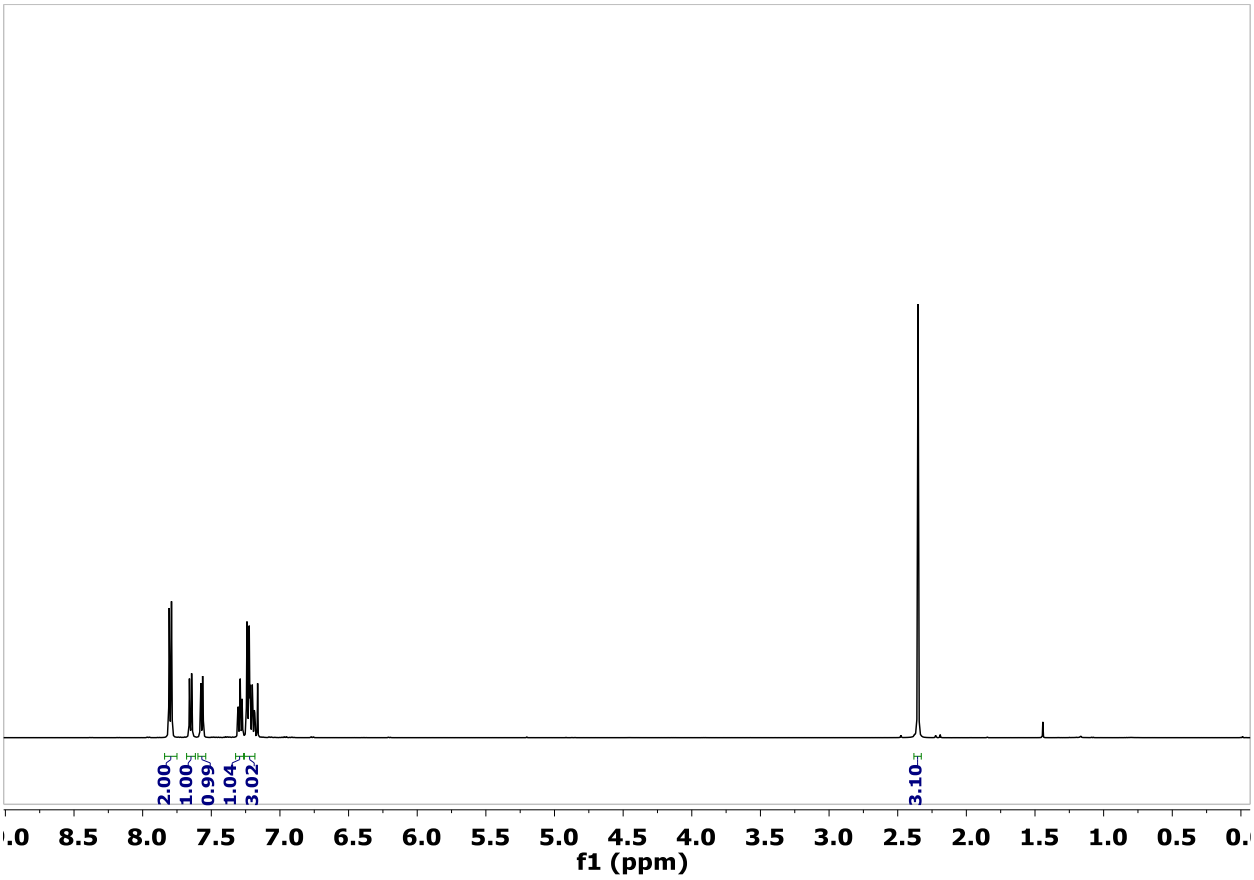

^{1}H NMR, $CDCl_3$

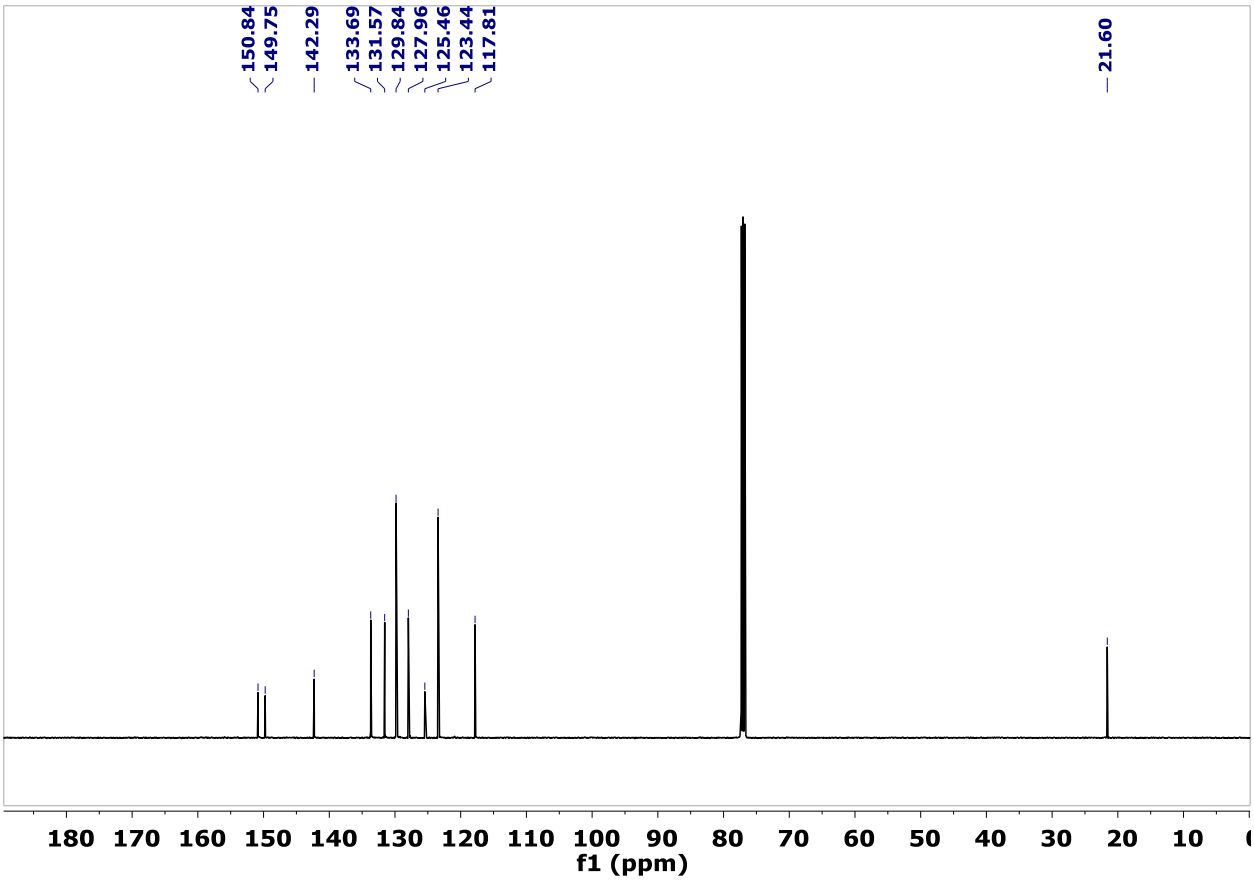

^{13}C NMR, $CDCl_3$

1

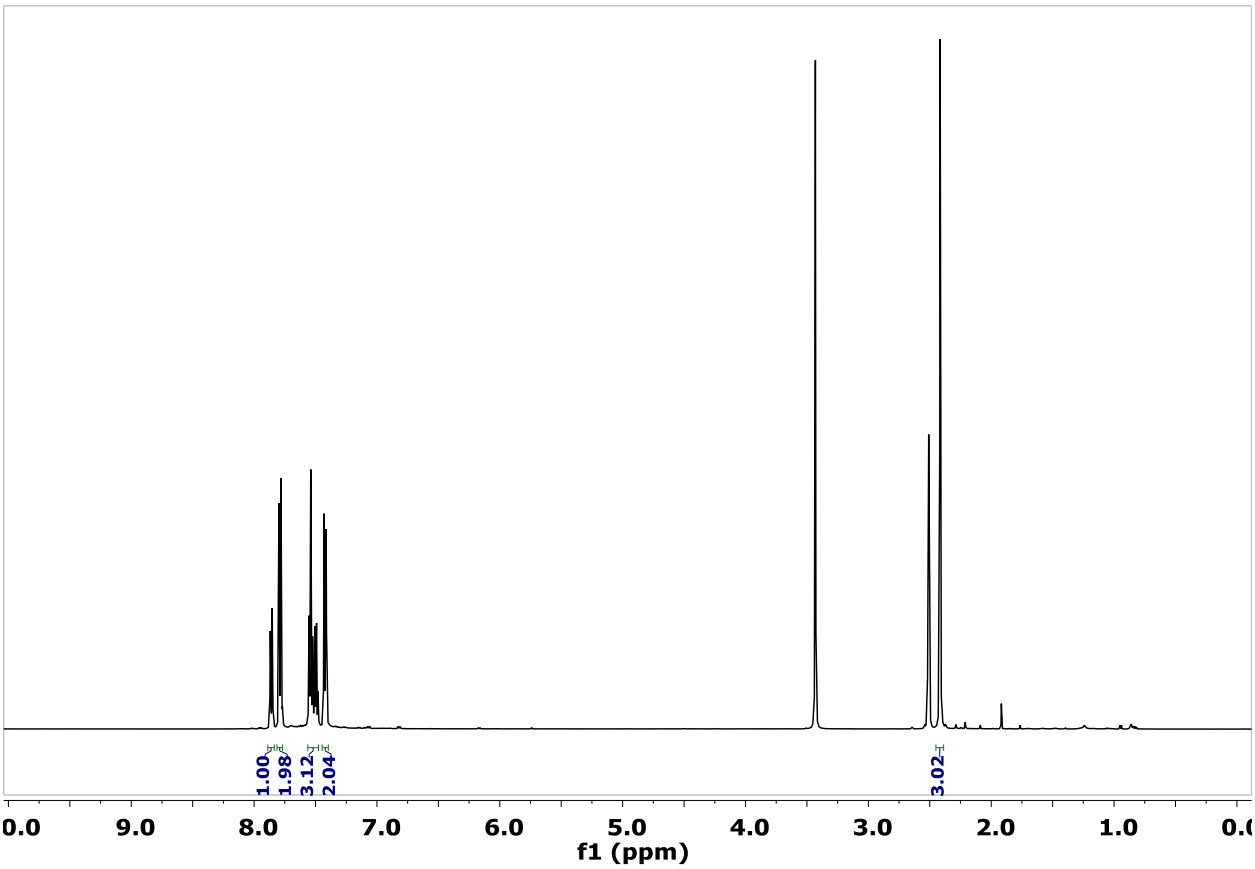

^{1}H NMR, DMSO-d_6

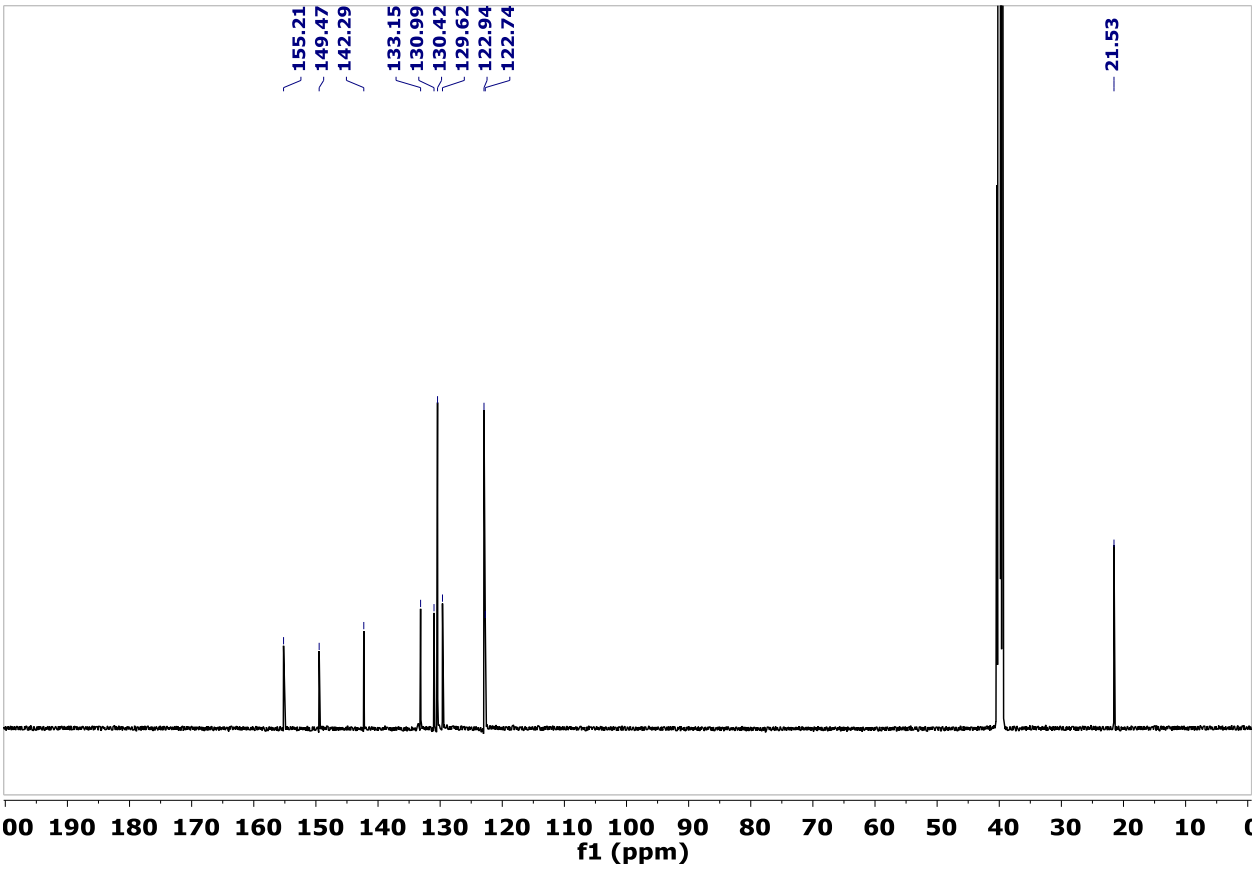

^{13}C NMR, DMSO-d_6

2

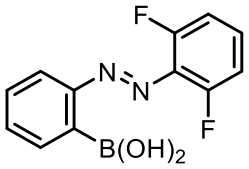

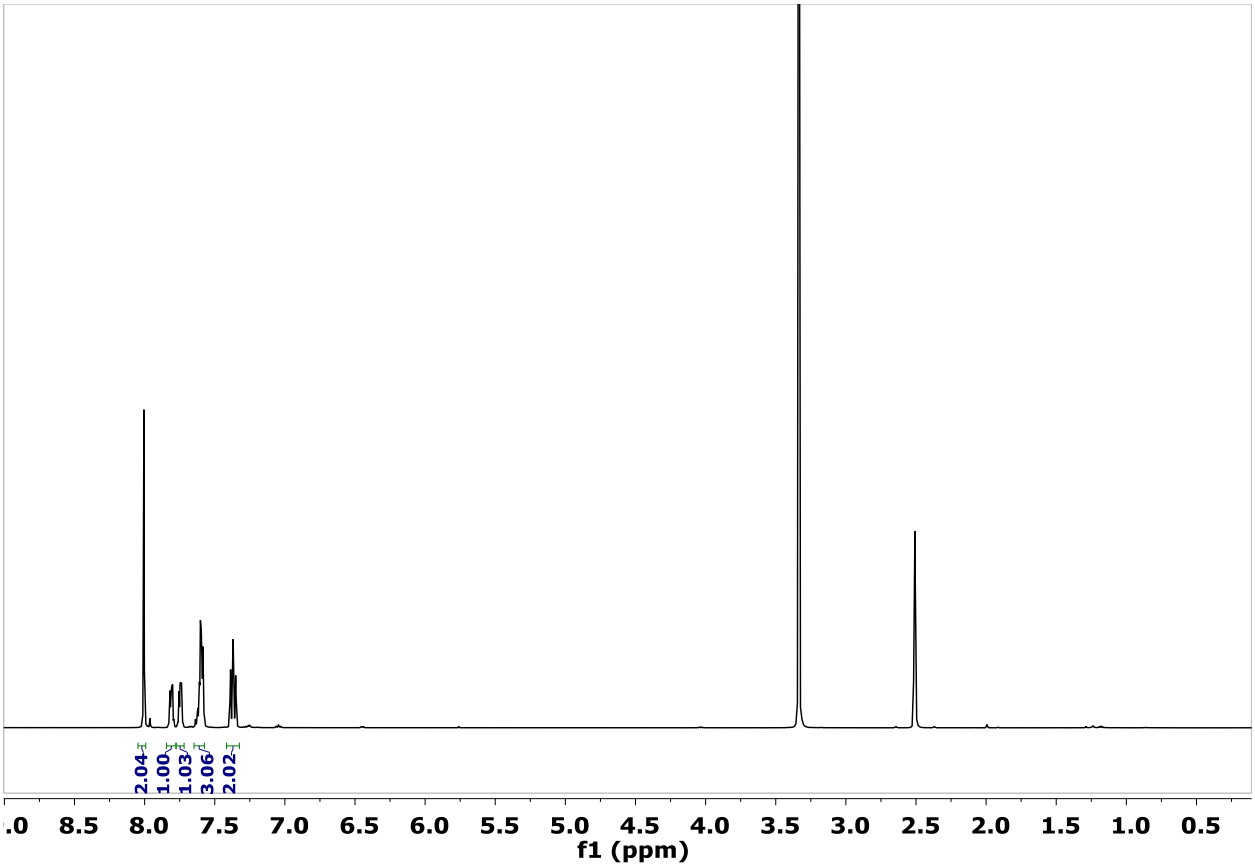

^{1}H NMR, DMSO-d_6

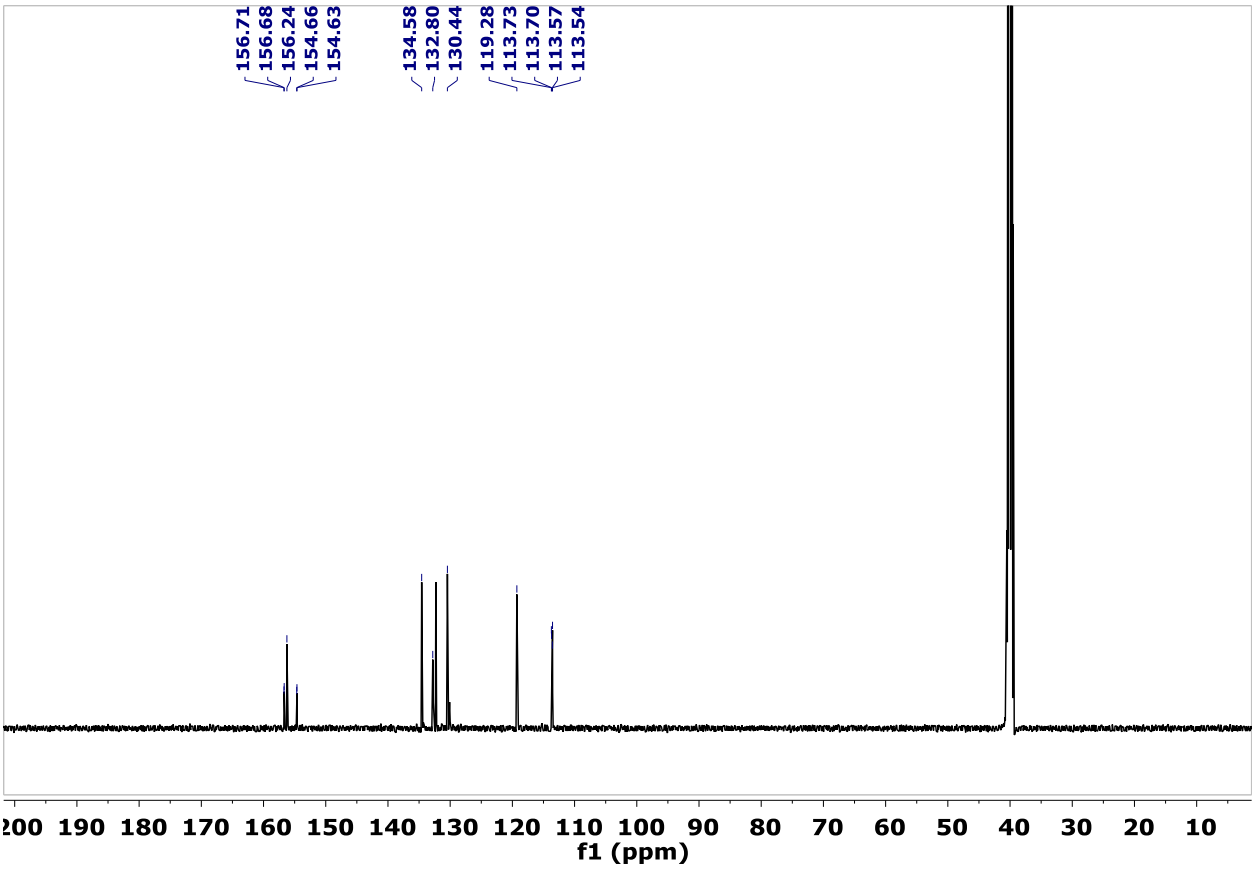

^{13}C NMR, DMSO-d_6

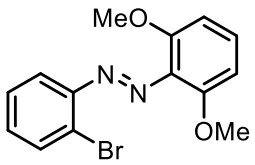

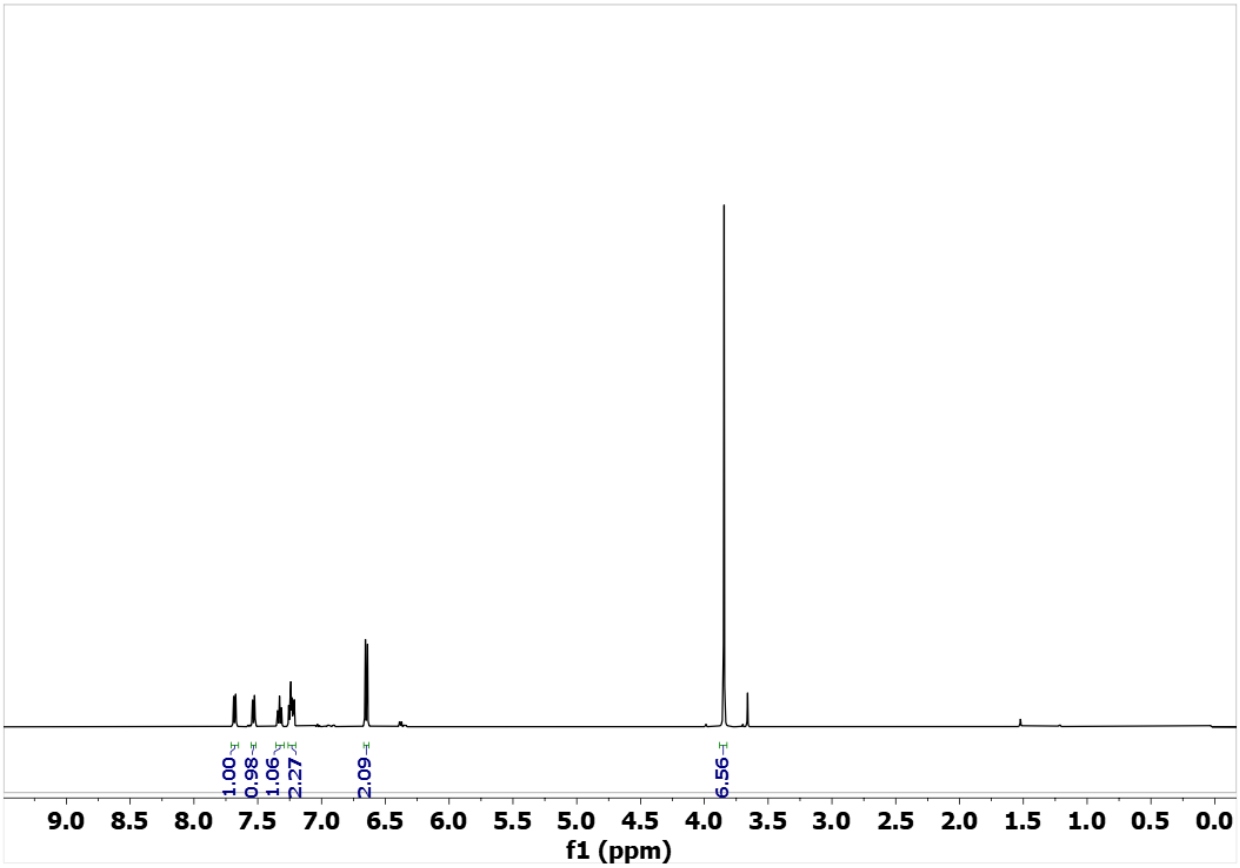

^{1}H NMR, DMSO-d_6

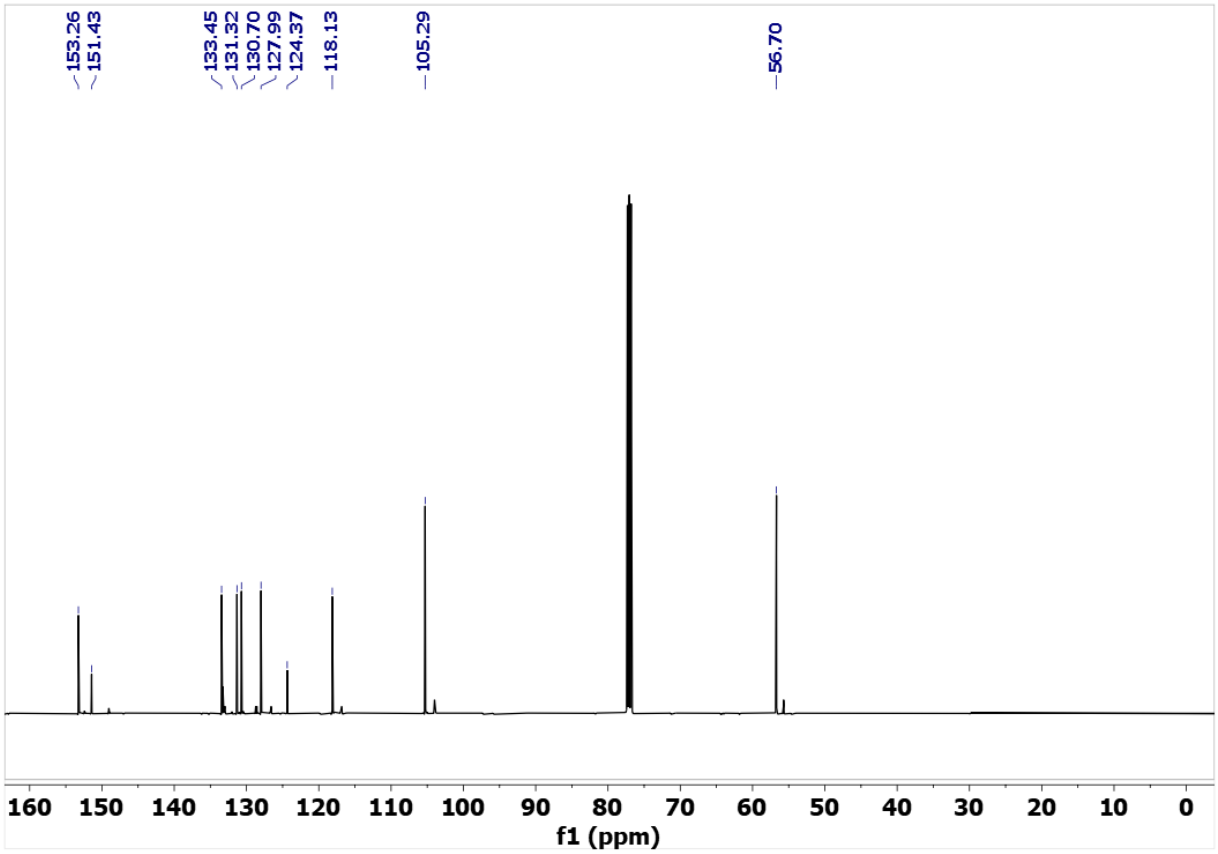

^{13}C NMR, DMSO-d_6

3

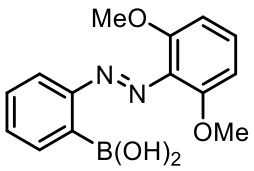

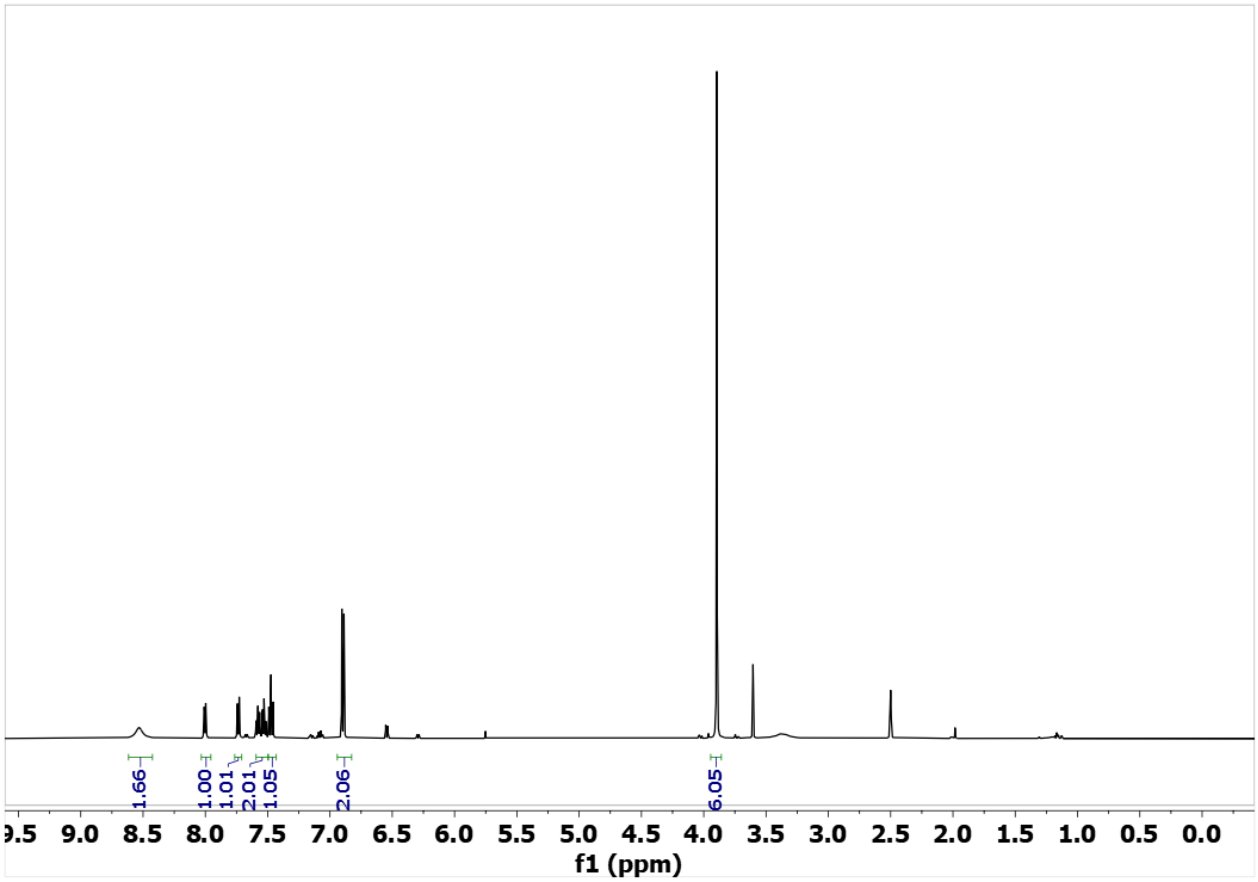

^{1}H NMR, DMSO-d_6

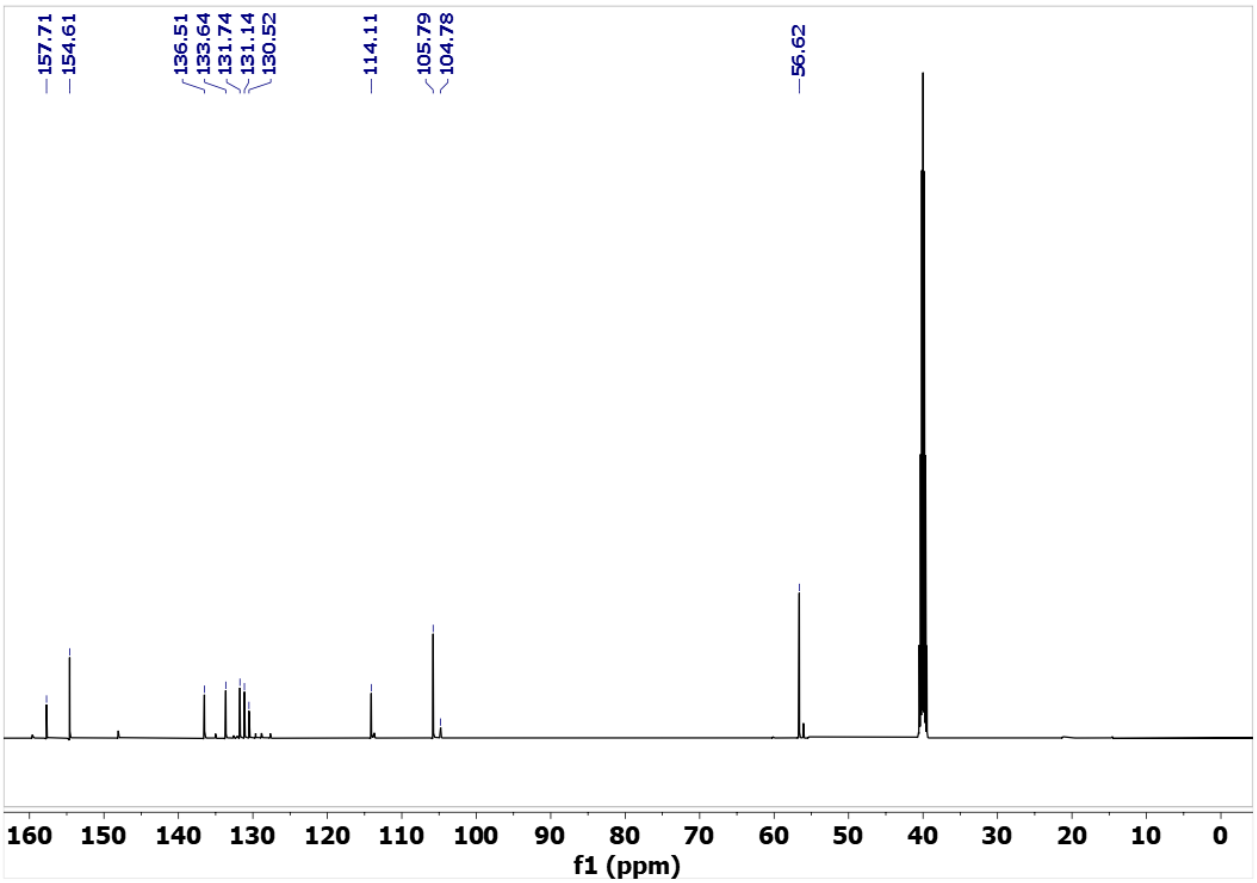

^{13}C NMR, DMSO-d_6

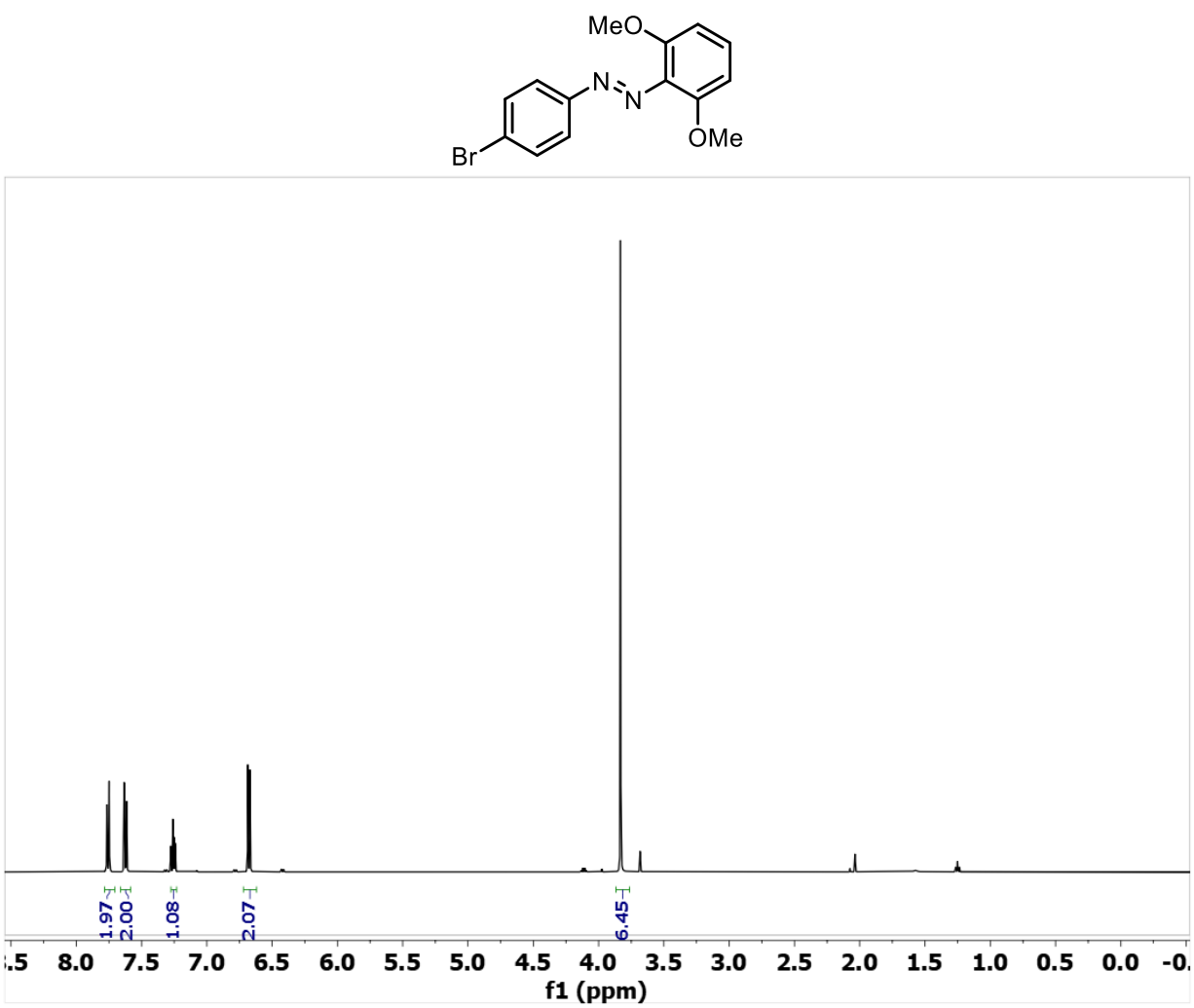

^{1}H NMR, DMSO-d_6

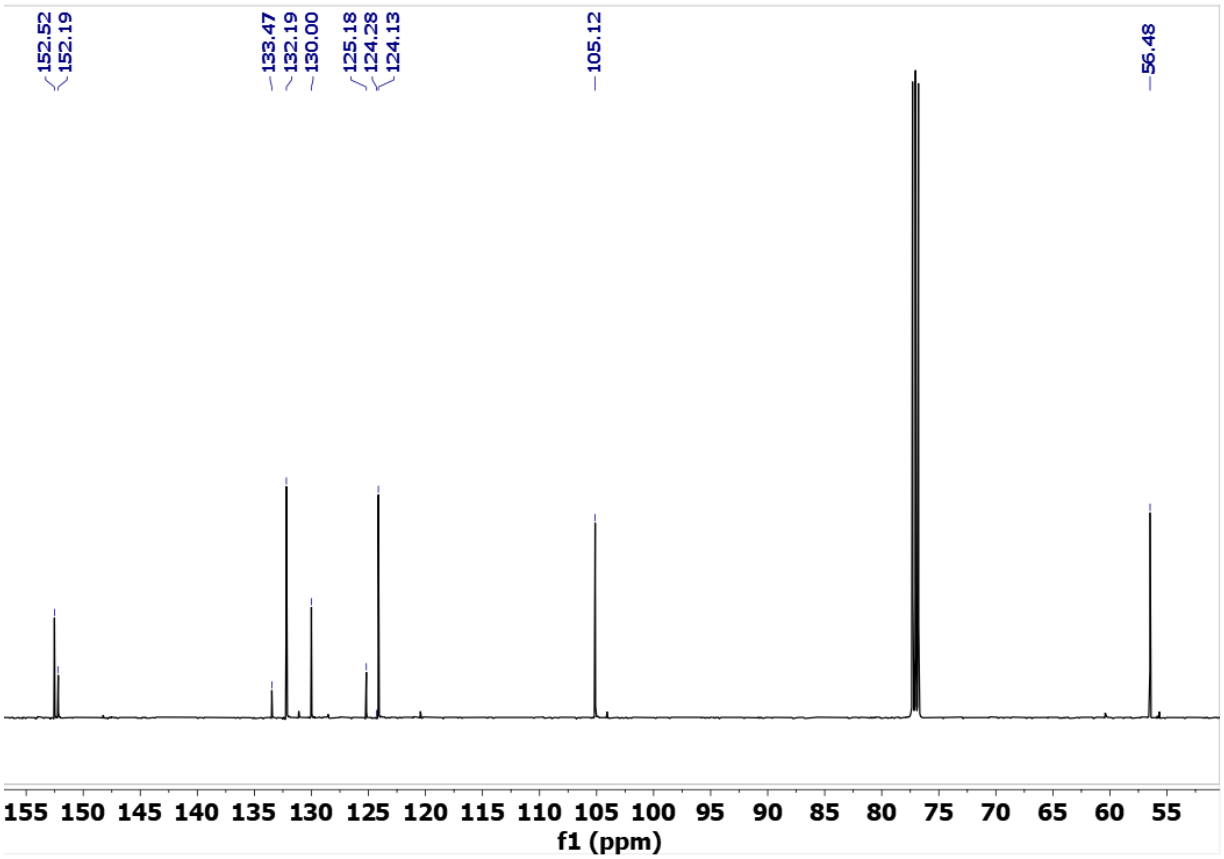

^{13}C NMR, DMSO-d_6

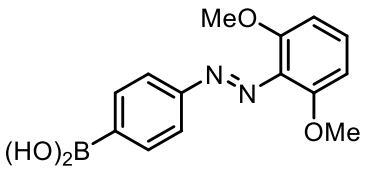

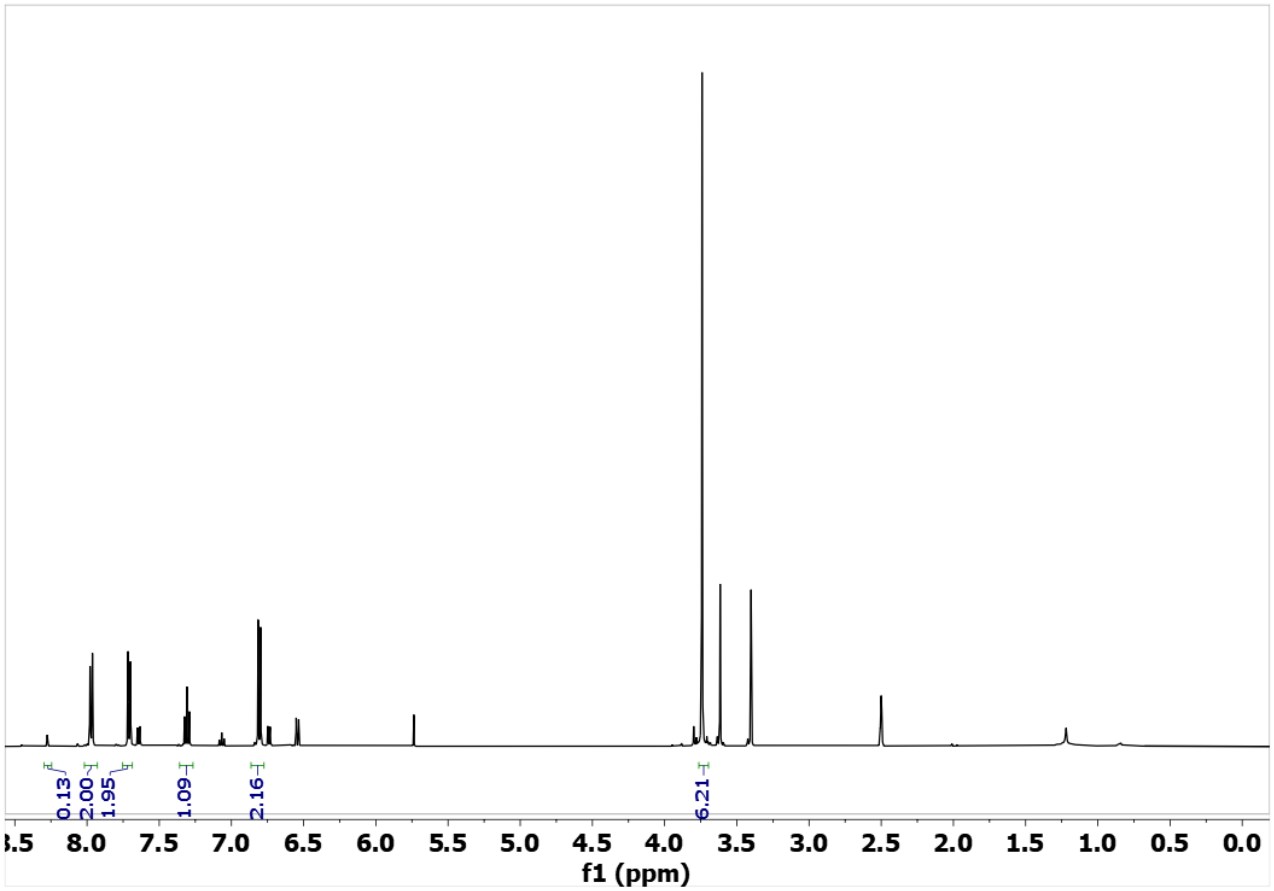

^{1}H NMR, DMSO-d_6

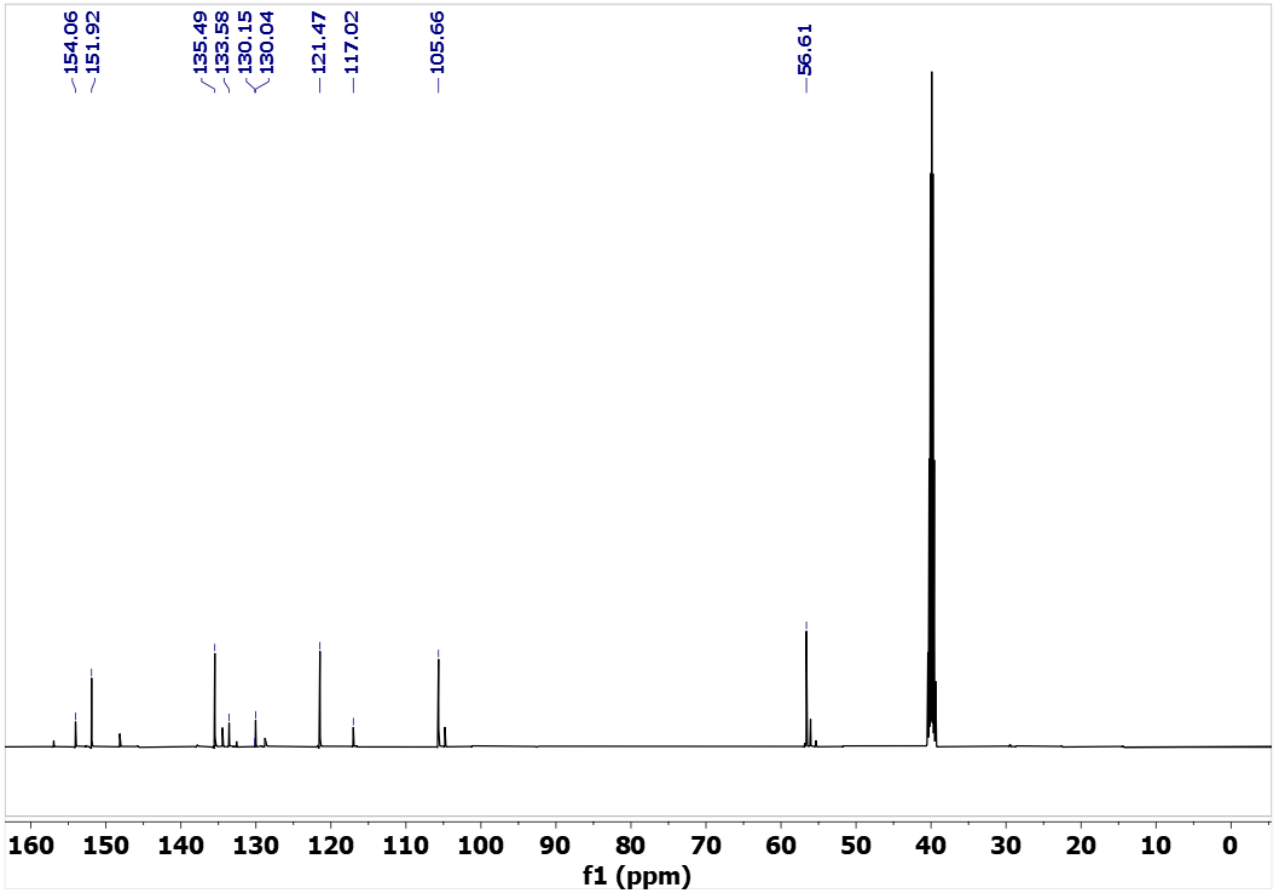

^{13}C NMR, DMSO-d_6

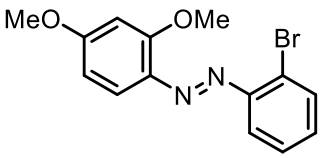

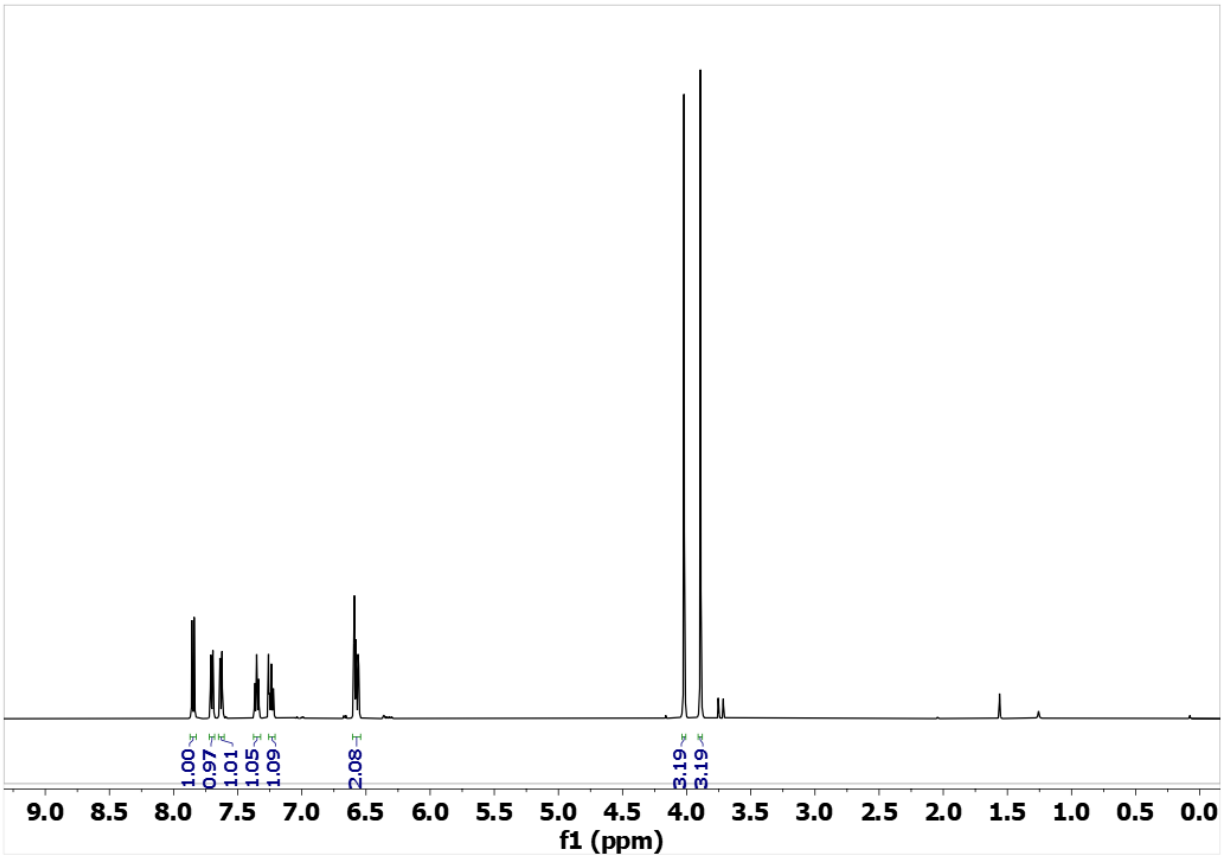

^{1}H NMR, DMSO-d_6

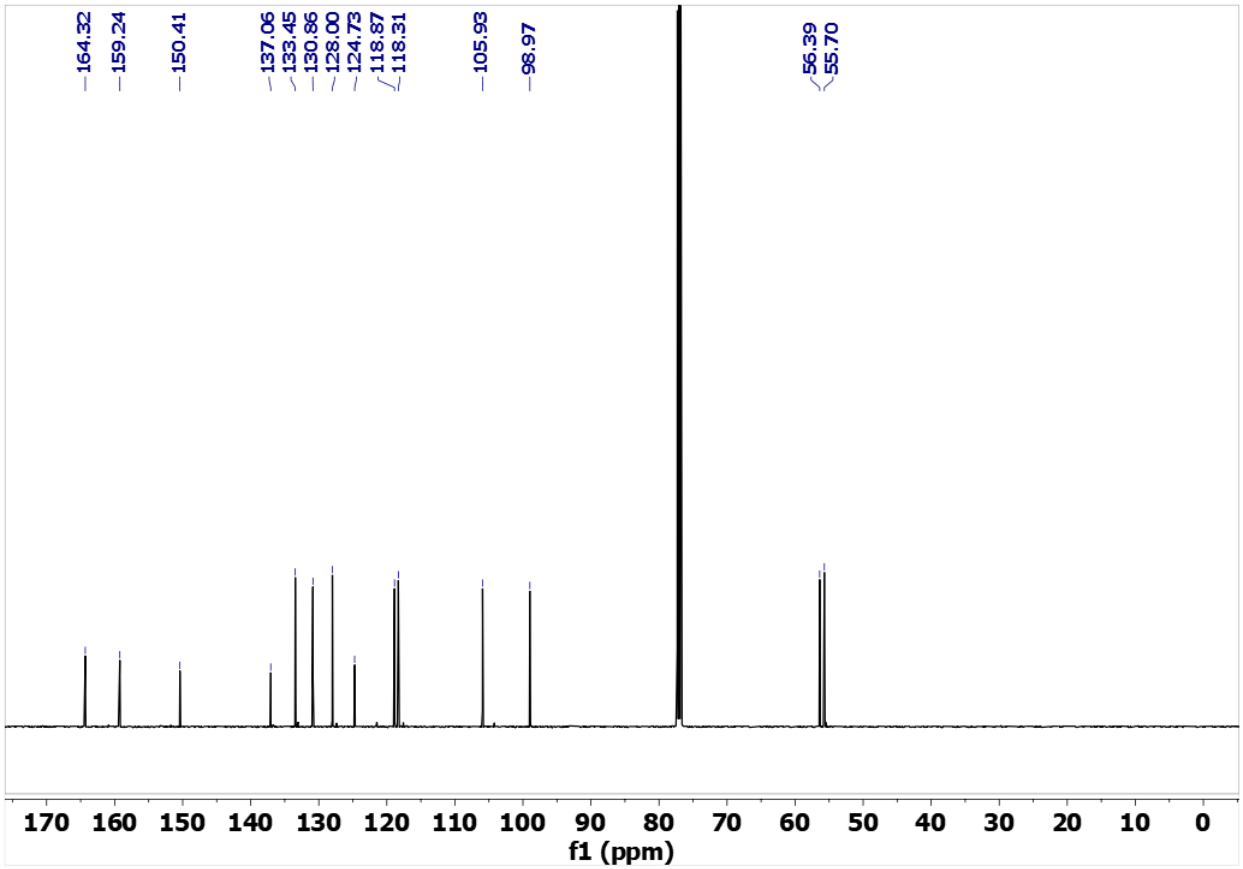

^{13}C NMR, DMSO-d_6

5

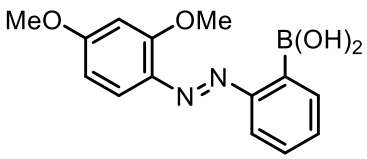

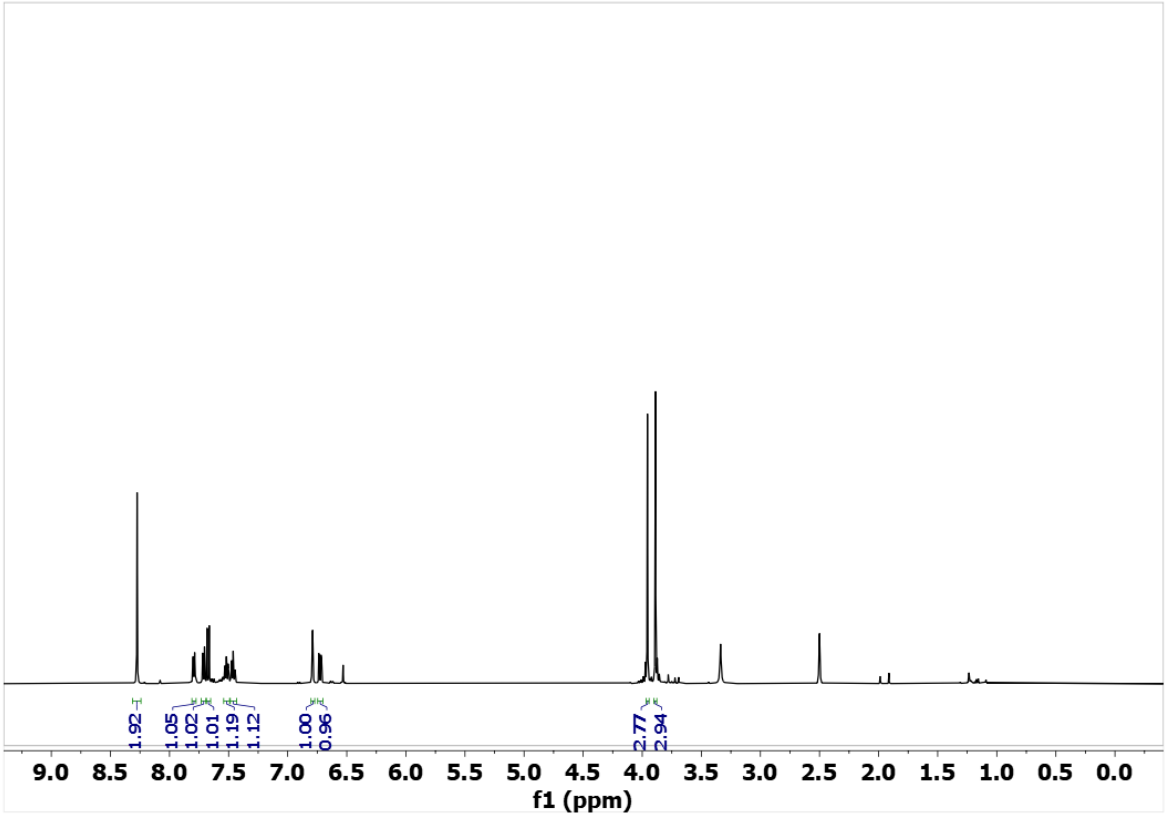

^{1}H NMR, DMSO-d_6

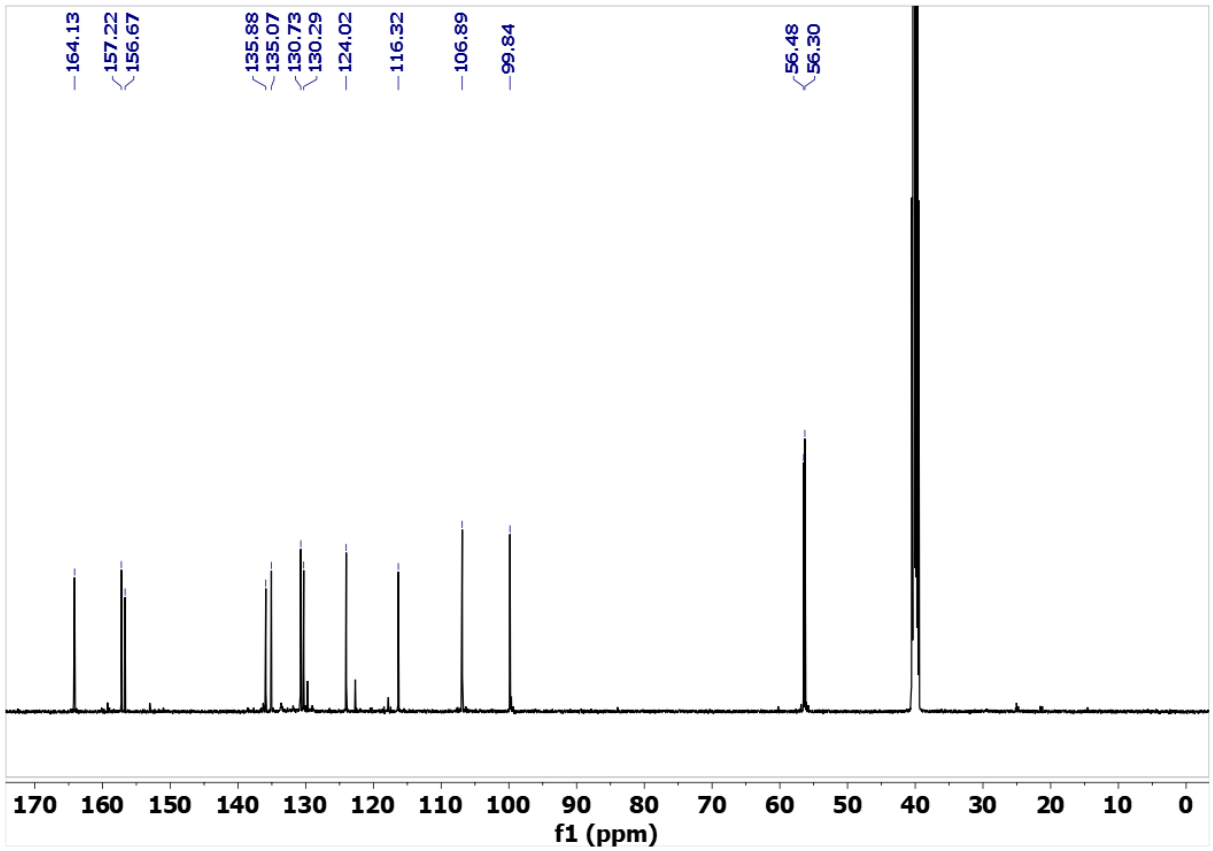

^{13}C NMR, DMSO-d_6

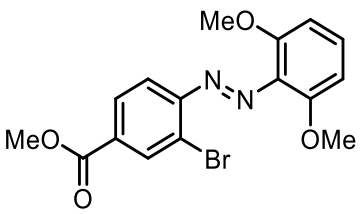
MeO
N
N
MeO
OMe
Br
O

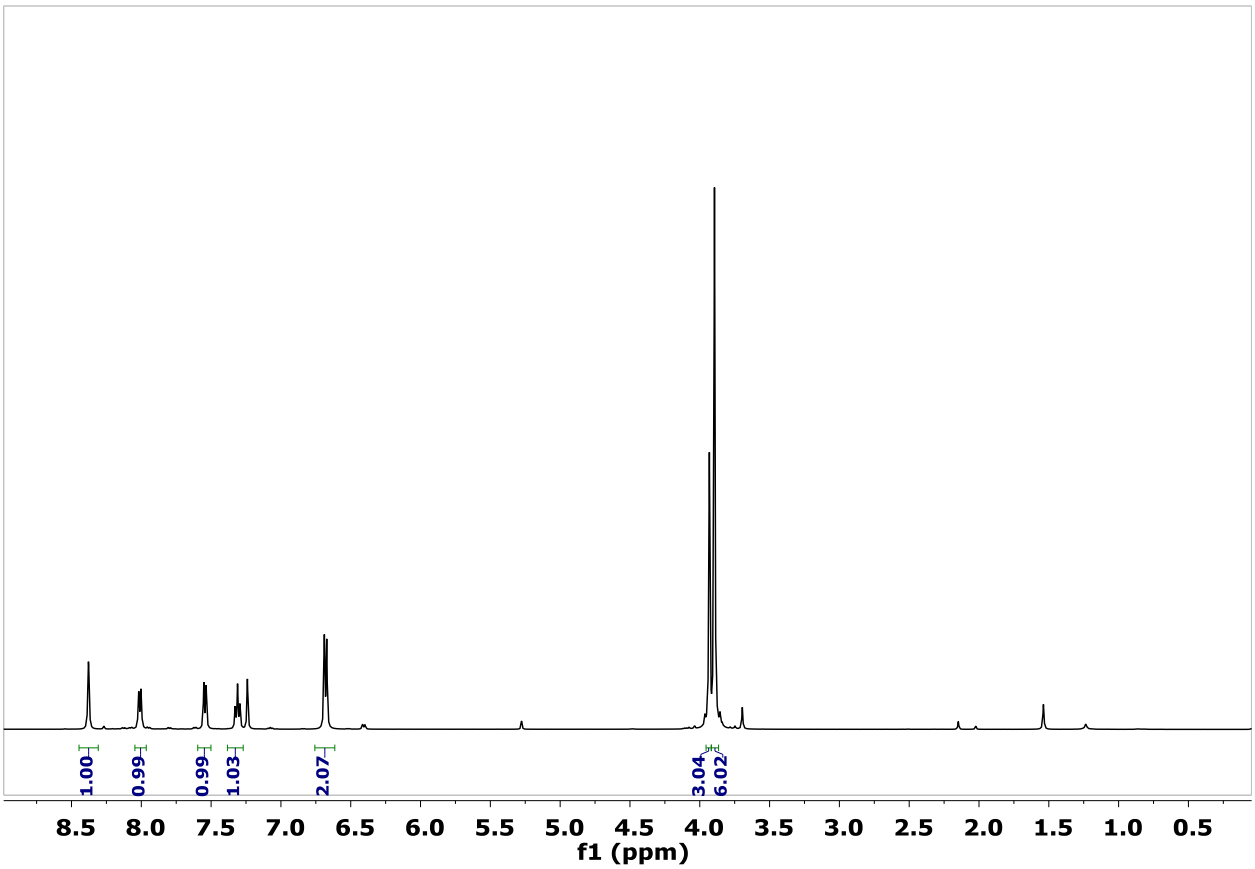
1.00
0.99
0.99
1.03
2.07
3.04
6.02
8.5 8.0 7.5 7.0 6.5 6.0 5.5 5.0 4.5 4.0 3.5 3.0 2.5 2.0 1.5 1.0 0.5
f1 (ppm)

^{1}H NMR, $CDCl_3$

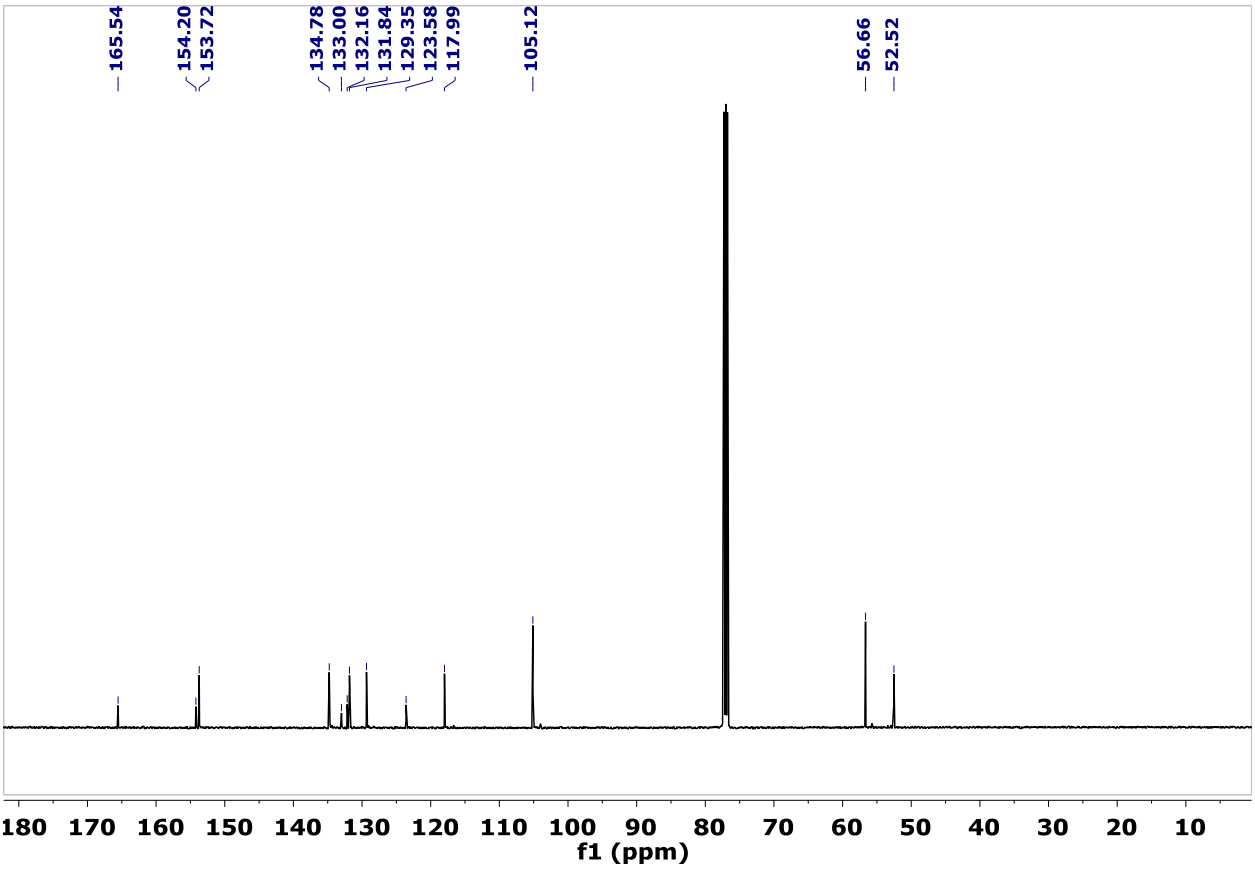

^{13}C NMR, $CDCl_3$

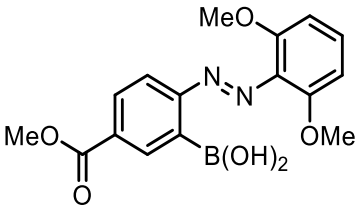

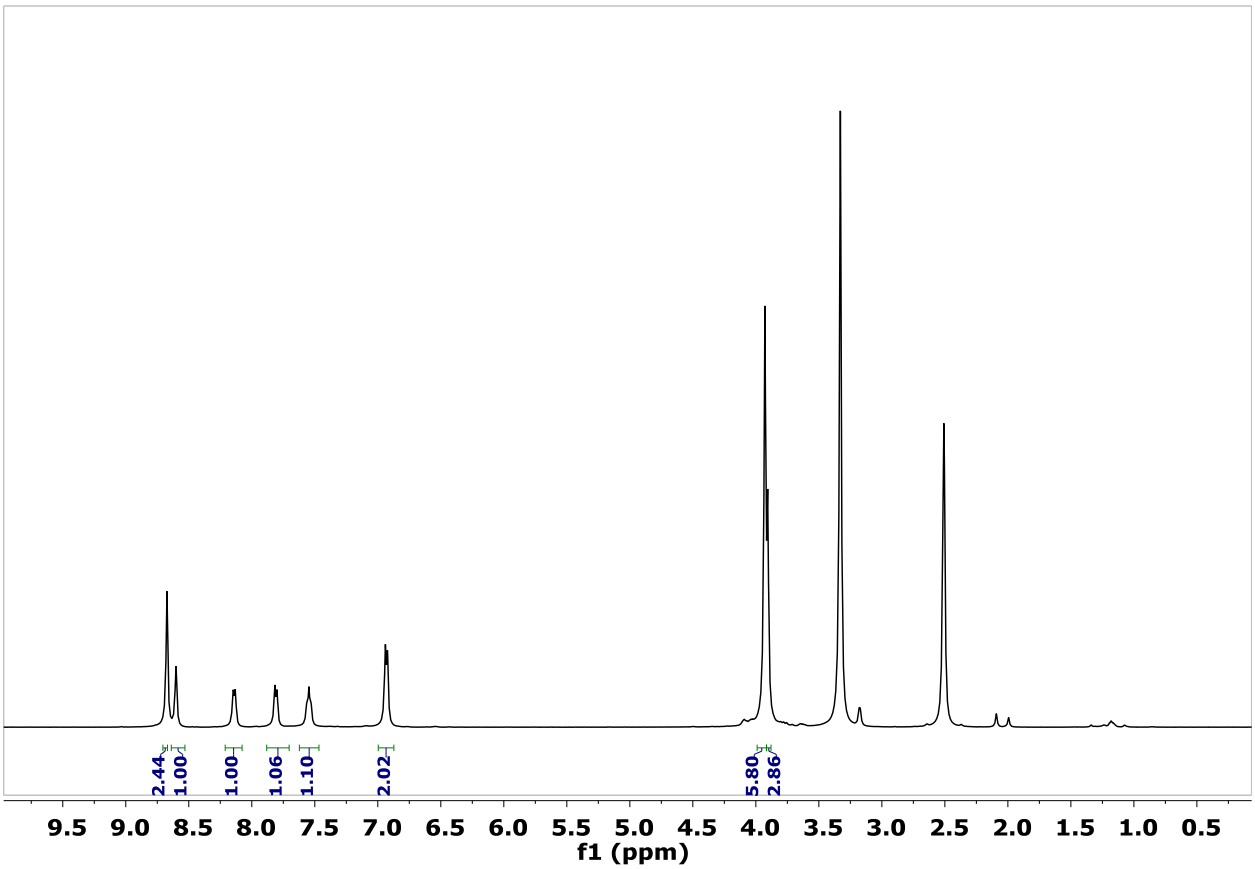

^{1}H NMR, DMSO-*d*$_6$

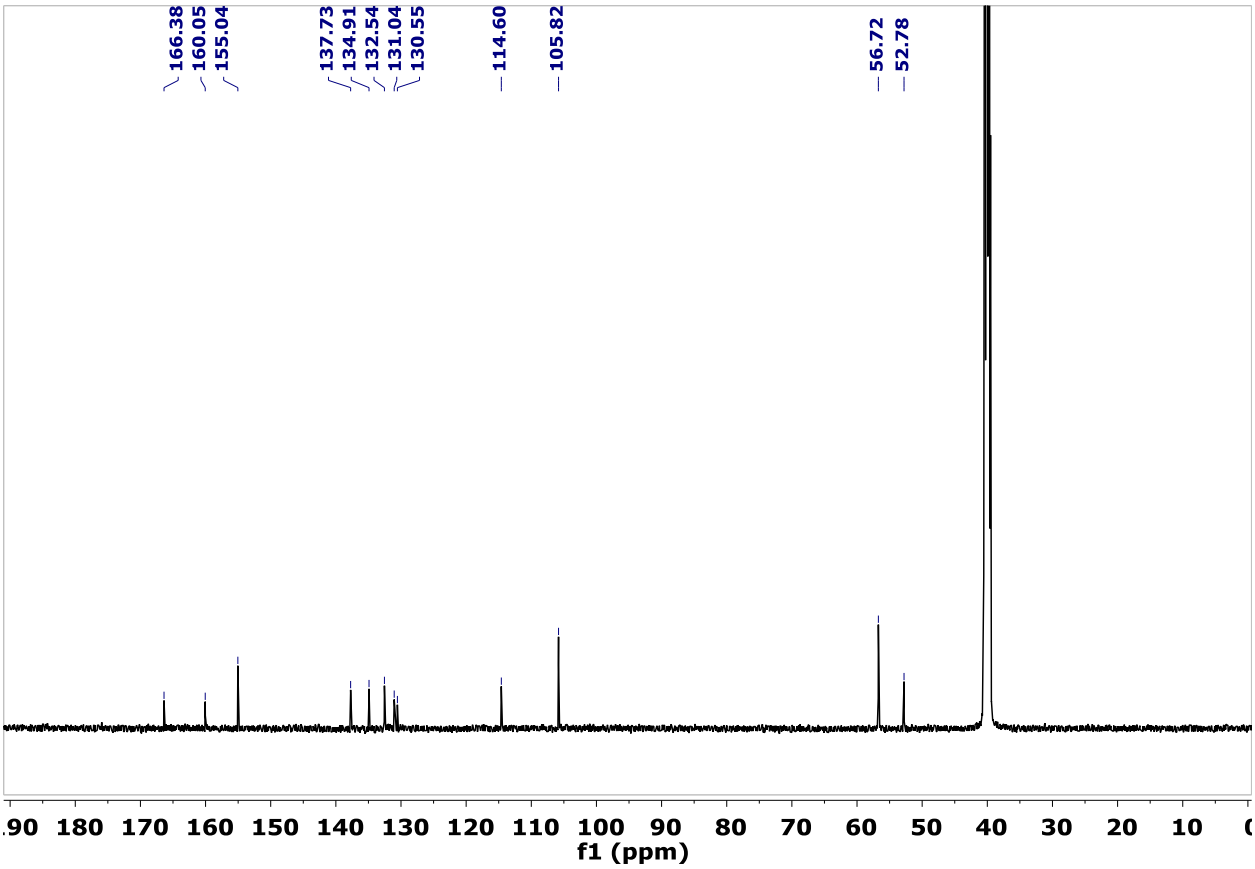

^{13}C NMR, DMSO-d_6

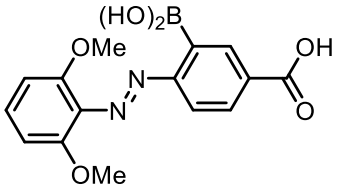

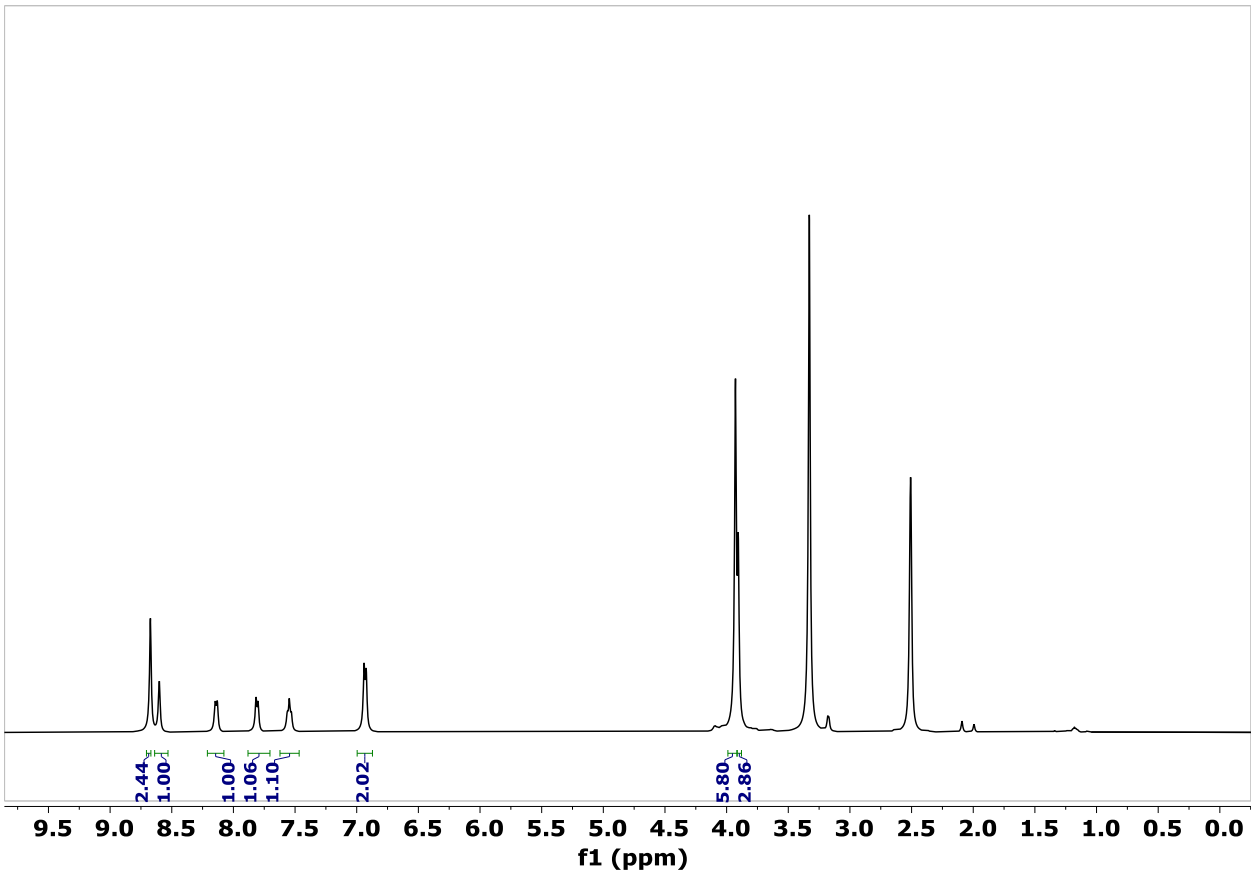

^{1}H NMR, DMSO-d_6

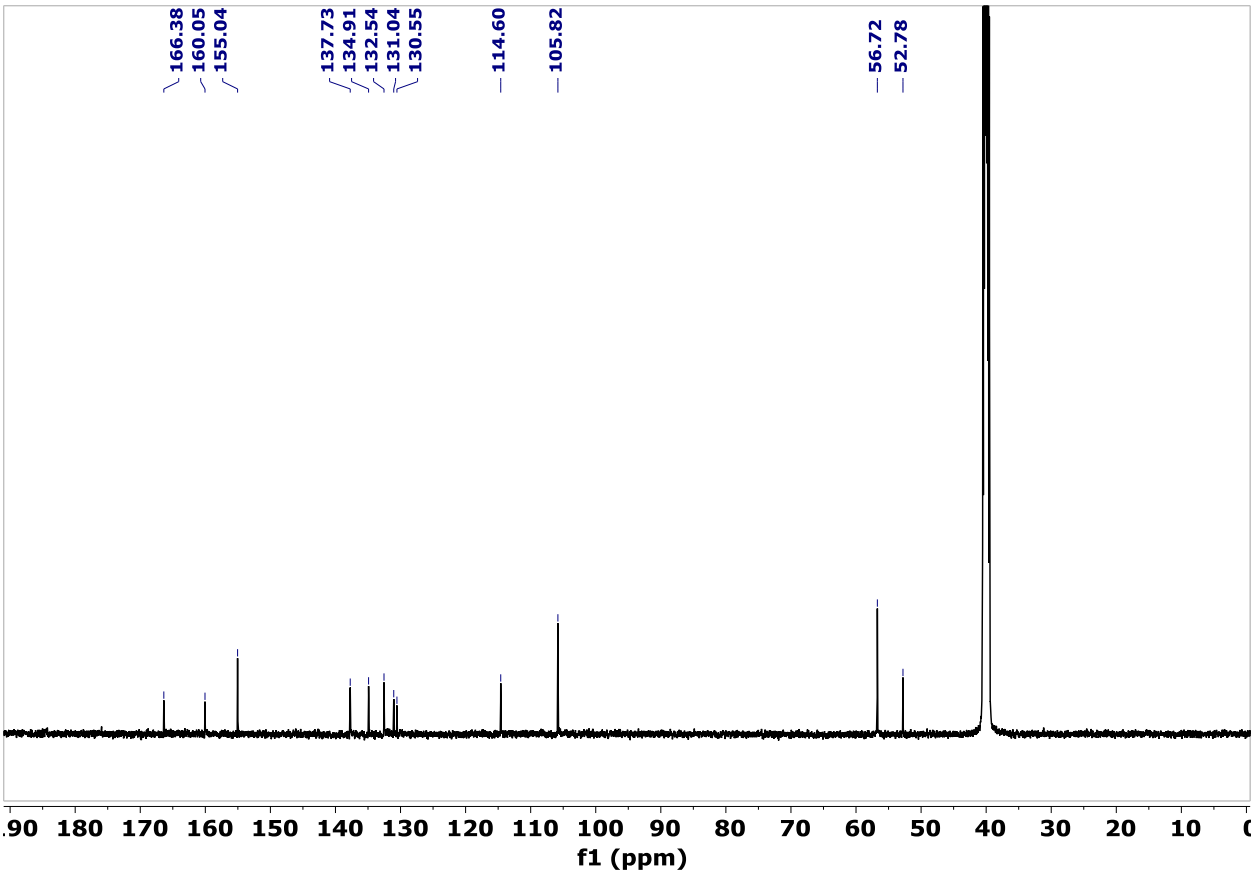

^{13}C NMR, DMSO-d_6

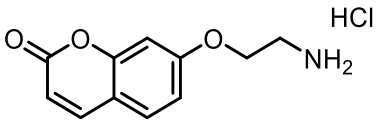

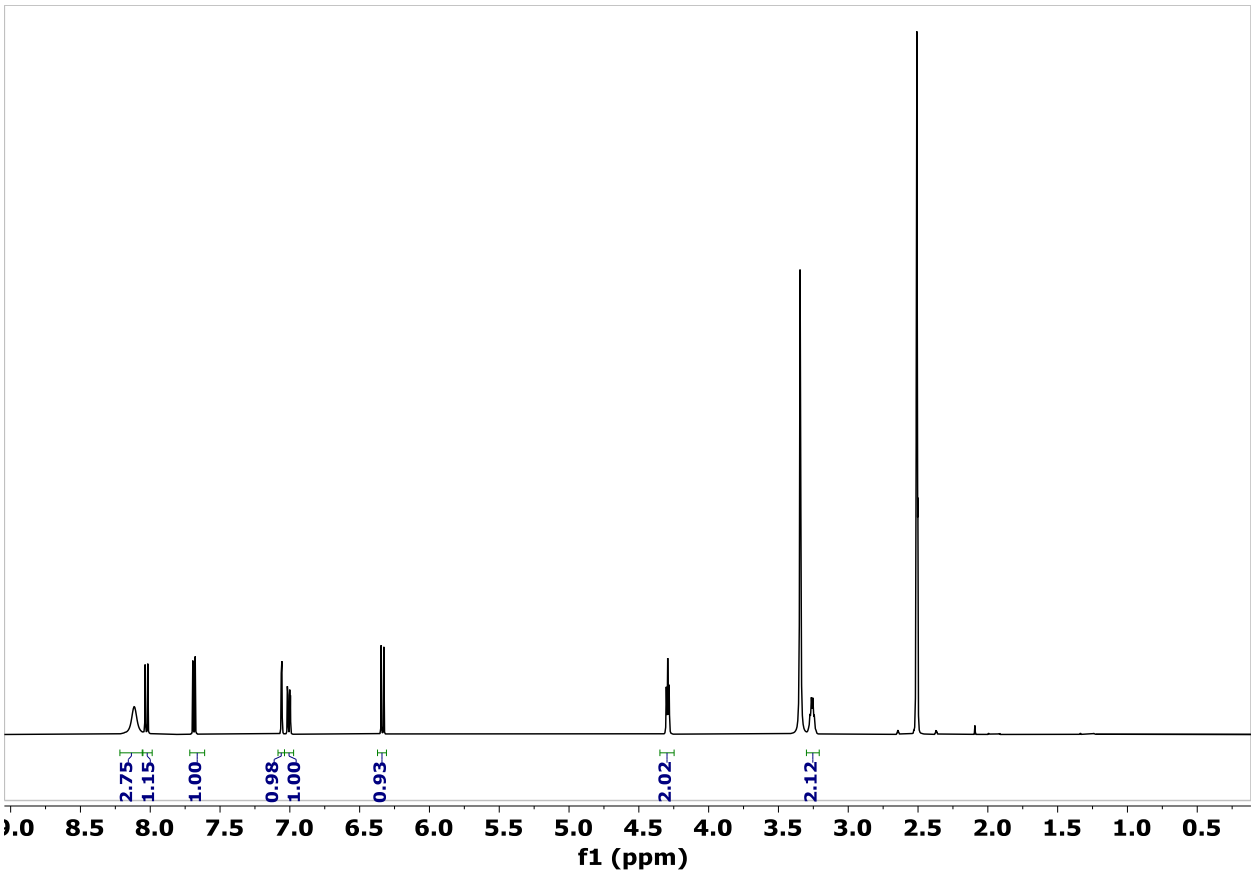

1H NMR, DMSO-d_6

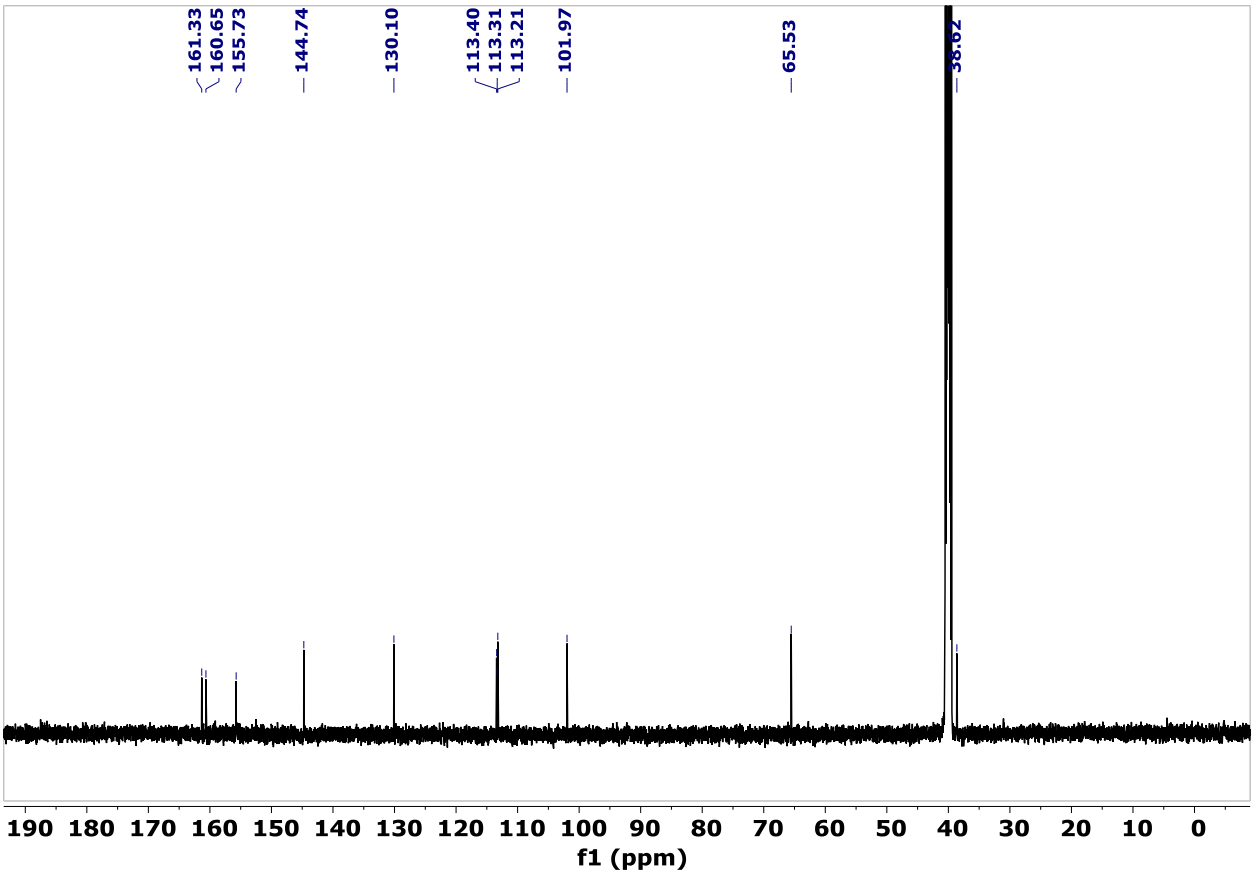

^{13}C NMR, DMSO-d_6

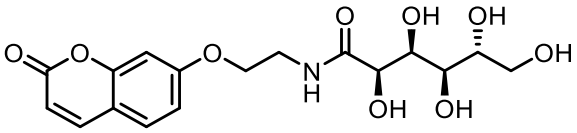

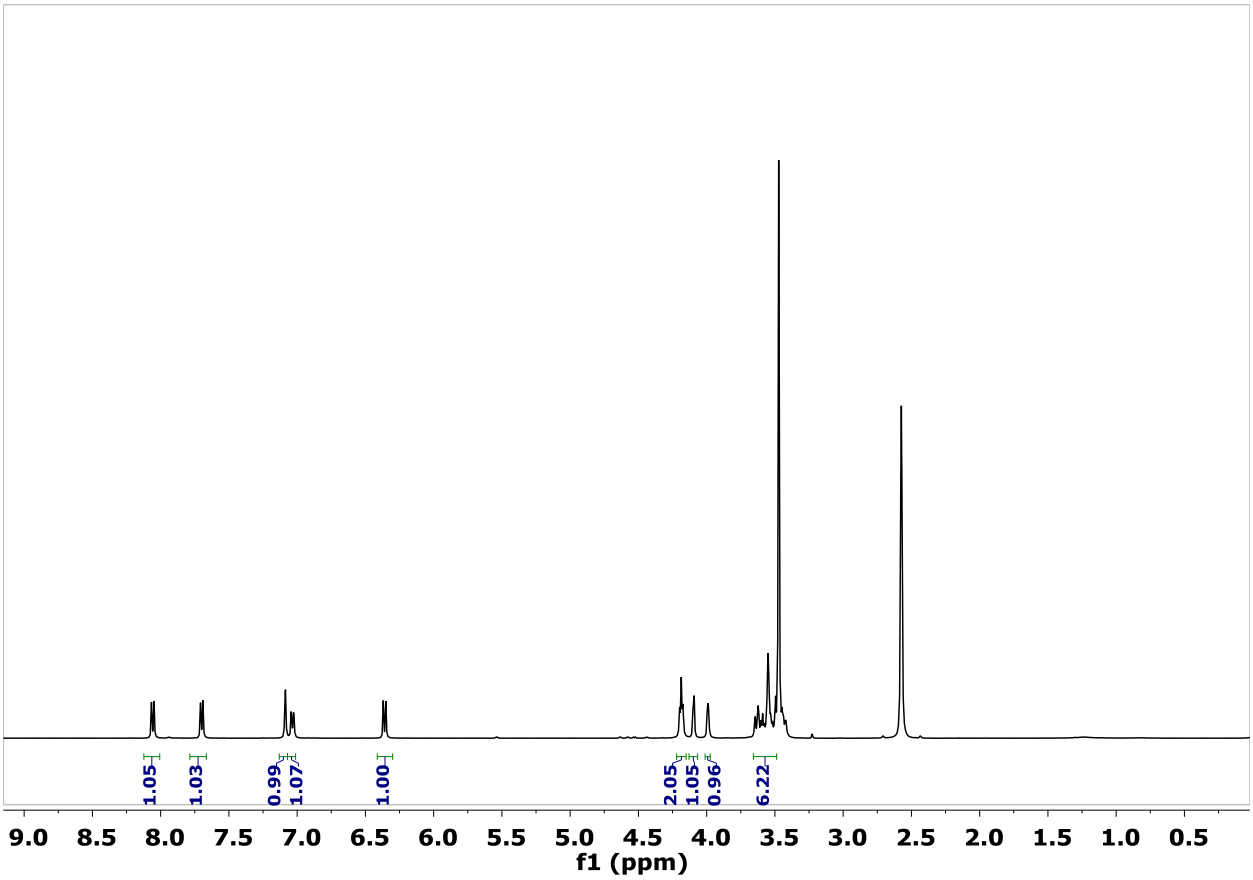

^{1}H NMR, DMSO-d_6

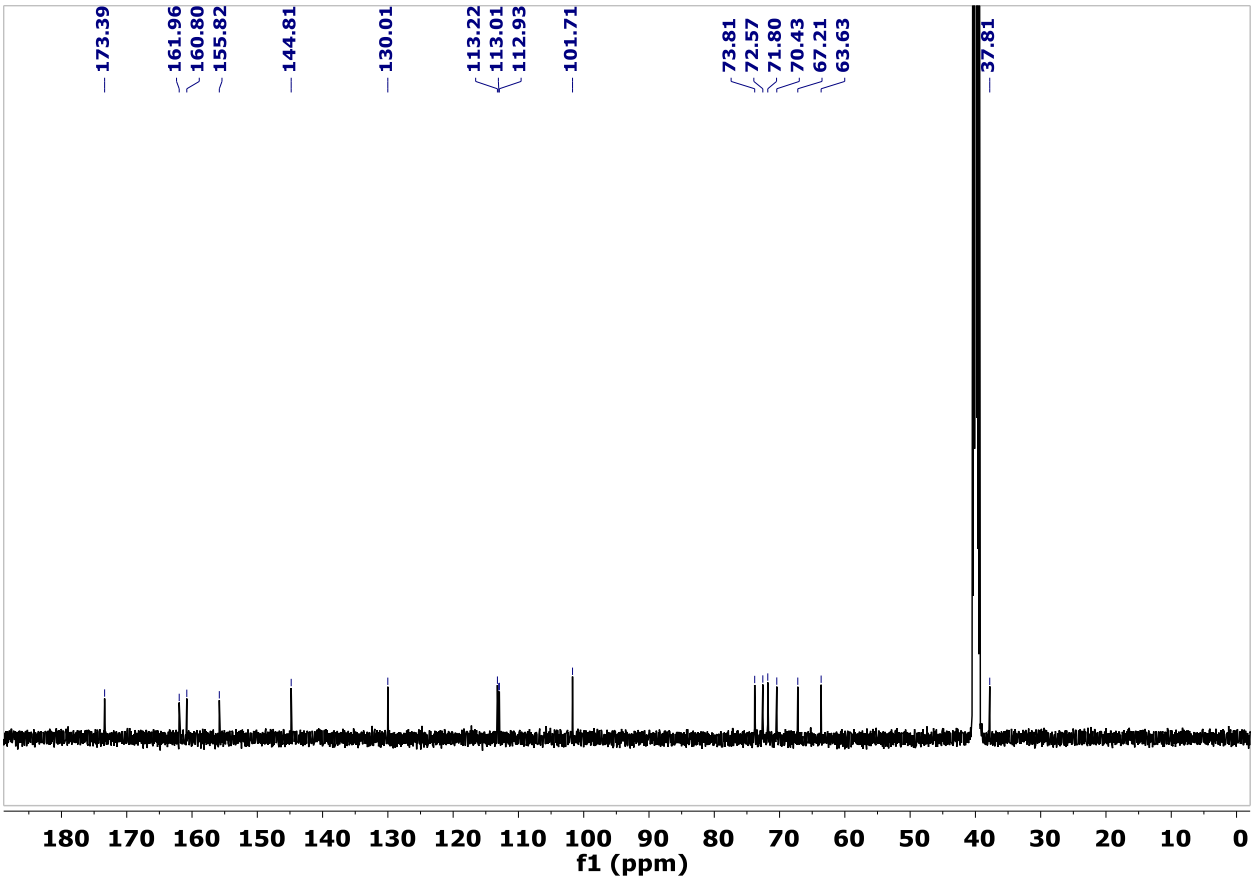

^{13}C NMR, DMSO-d_6

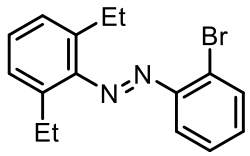

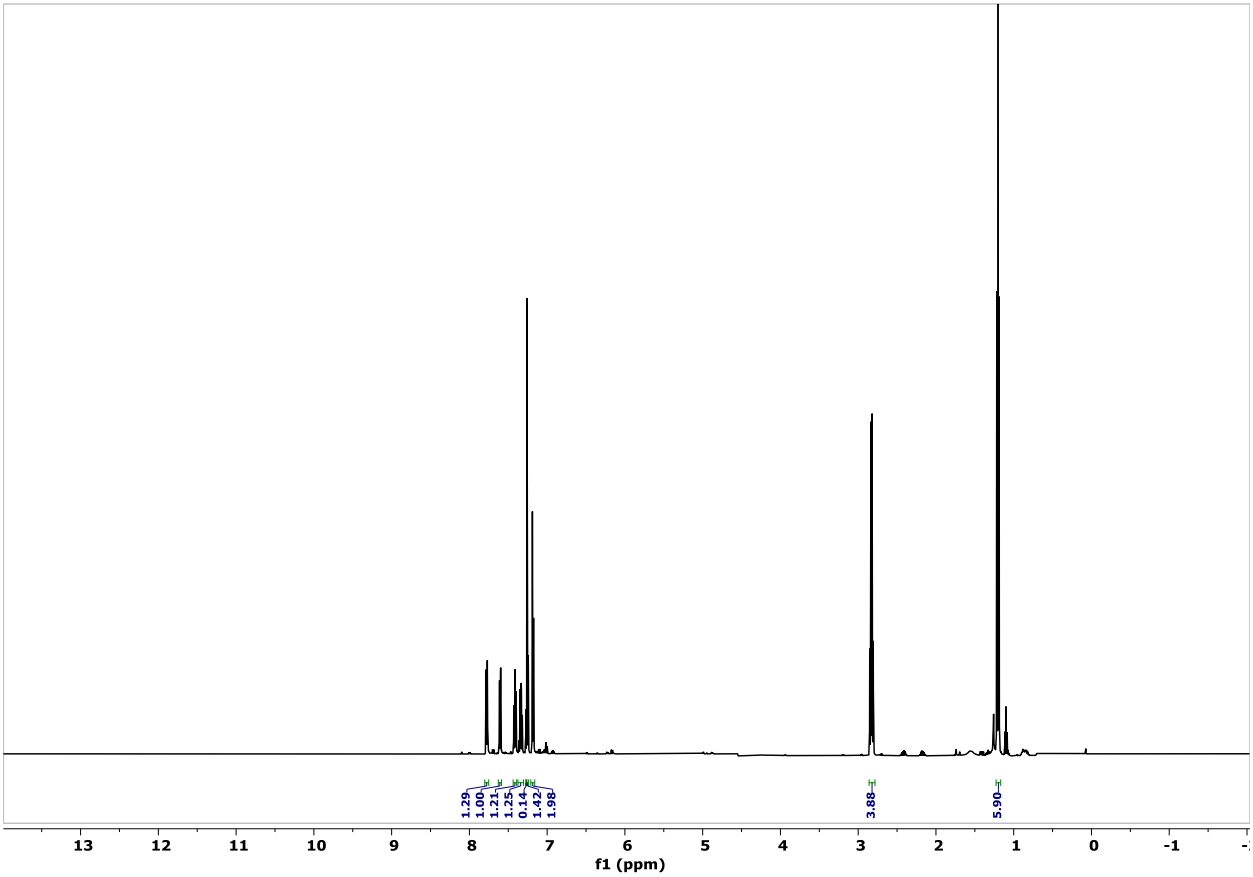

^{1}H NMR, $CDCl_3$ (crude)

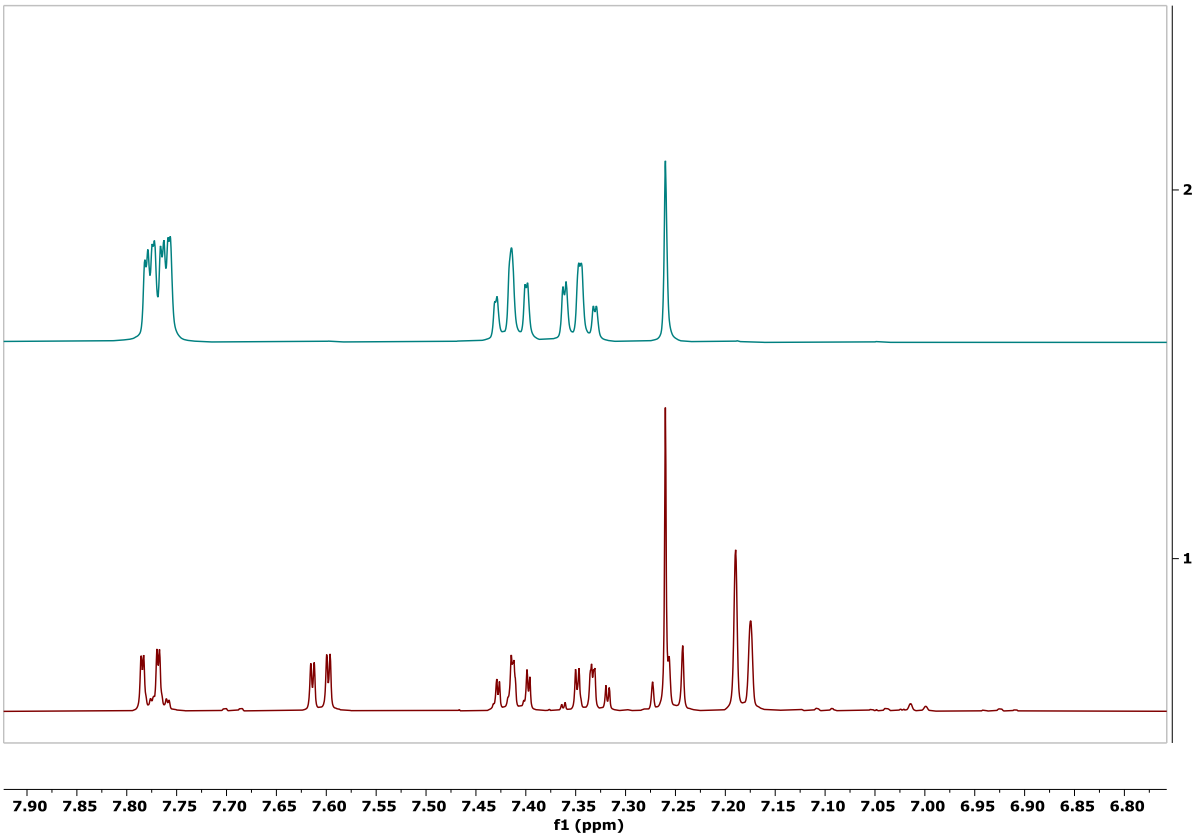

^{1}H NMR, $CDCl_3$ (crude) overlayed with unknown impurity which was mostly removed through crystallization in cool hexane.

(*E*)-**6**

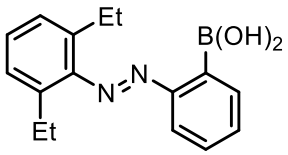

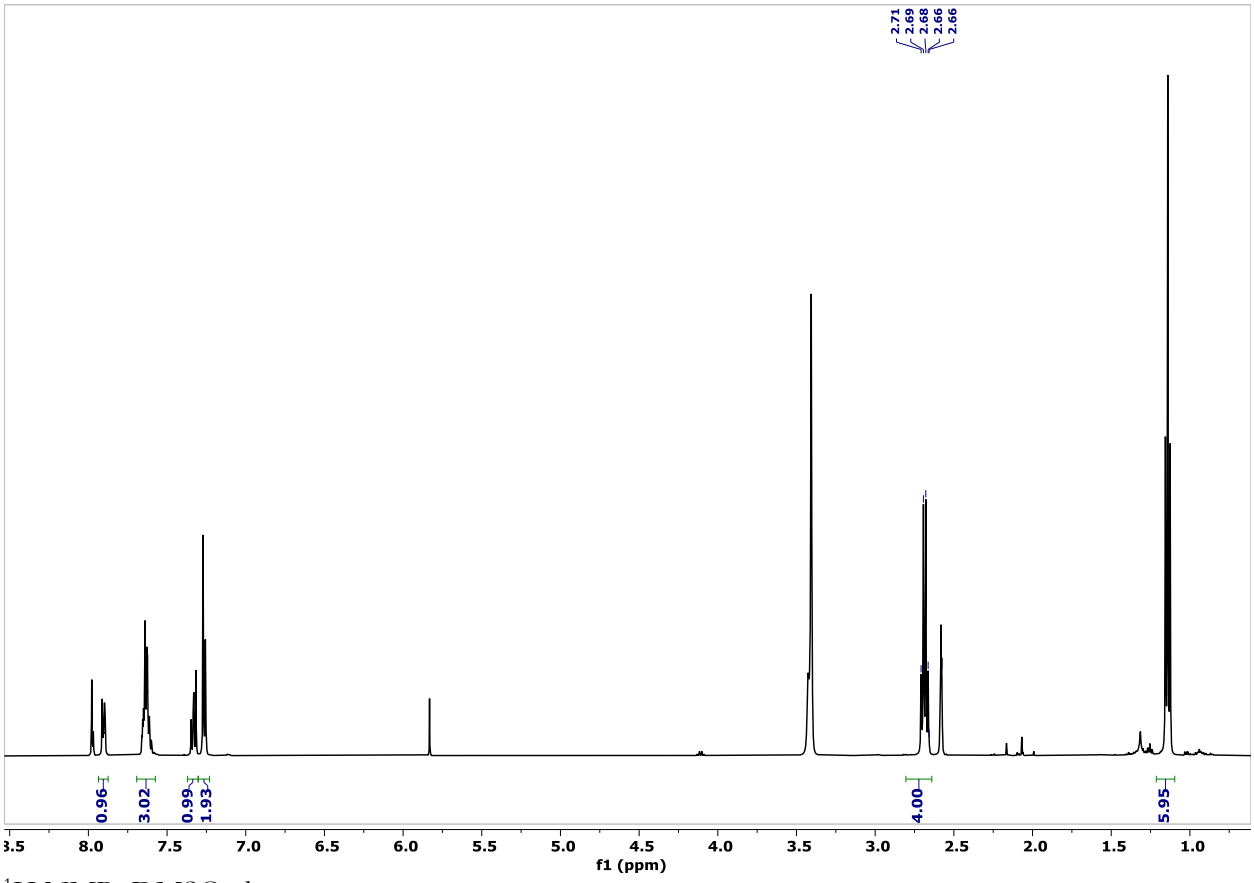

^{1}H NMR, DMSO-d_6

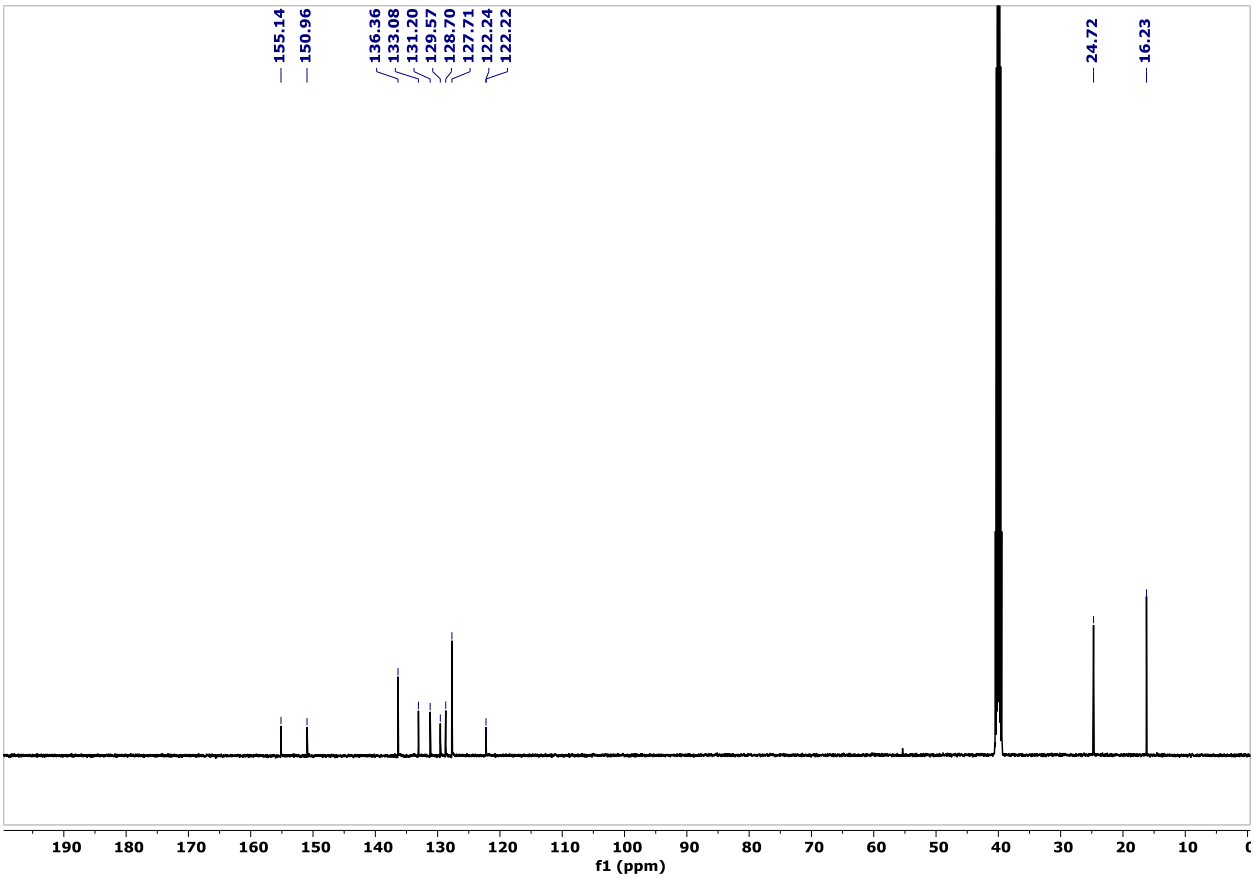

^{13}C NMR, DMSO-d_6

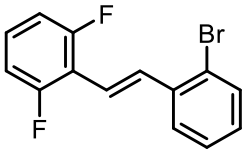

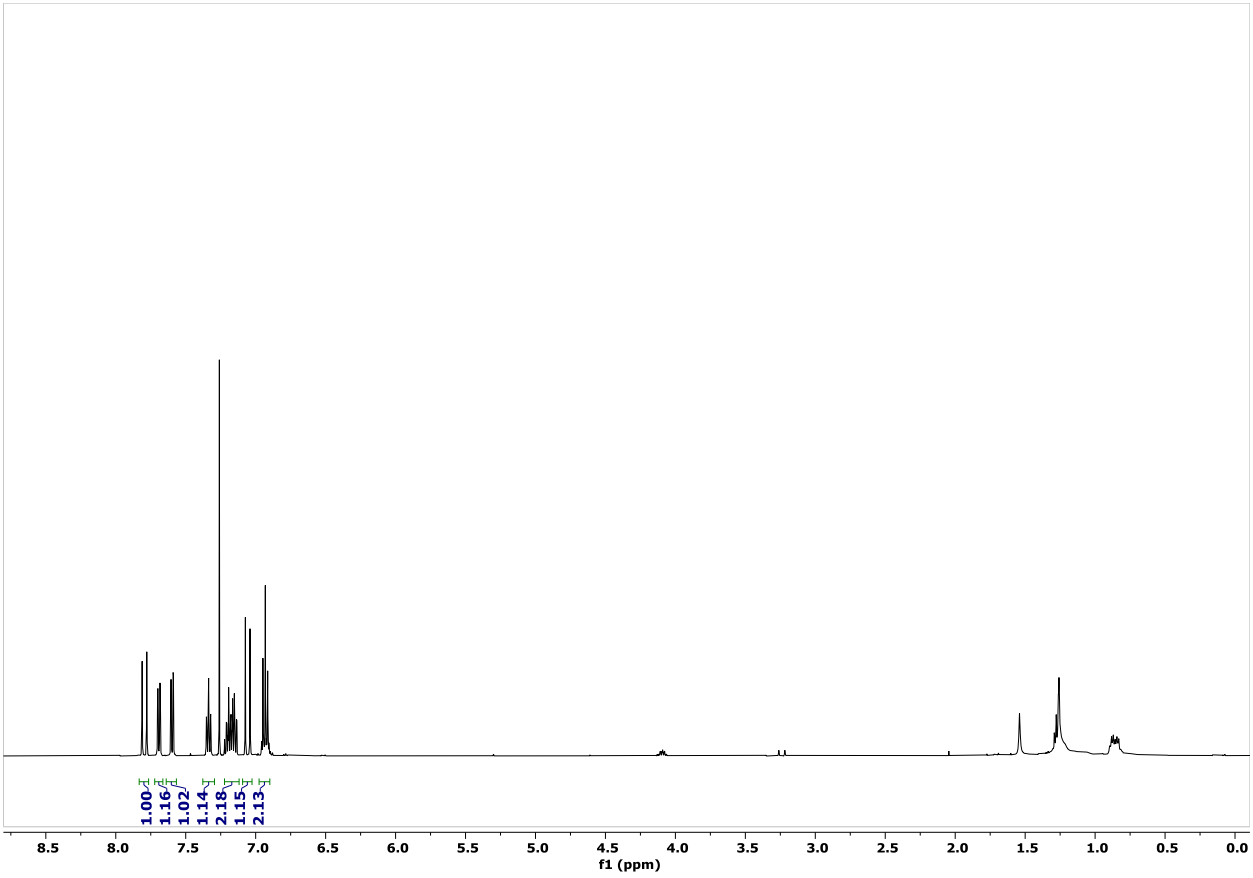

^{1}H NMR, $CDCl_3$ (crude)

(*E*)-**7**

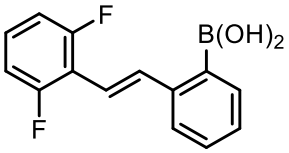

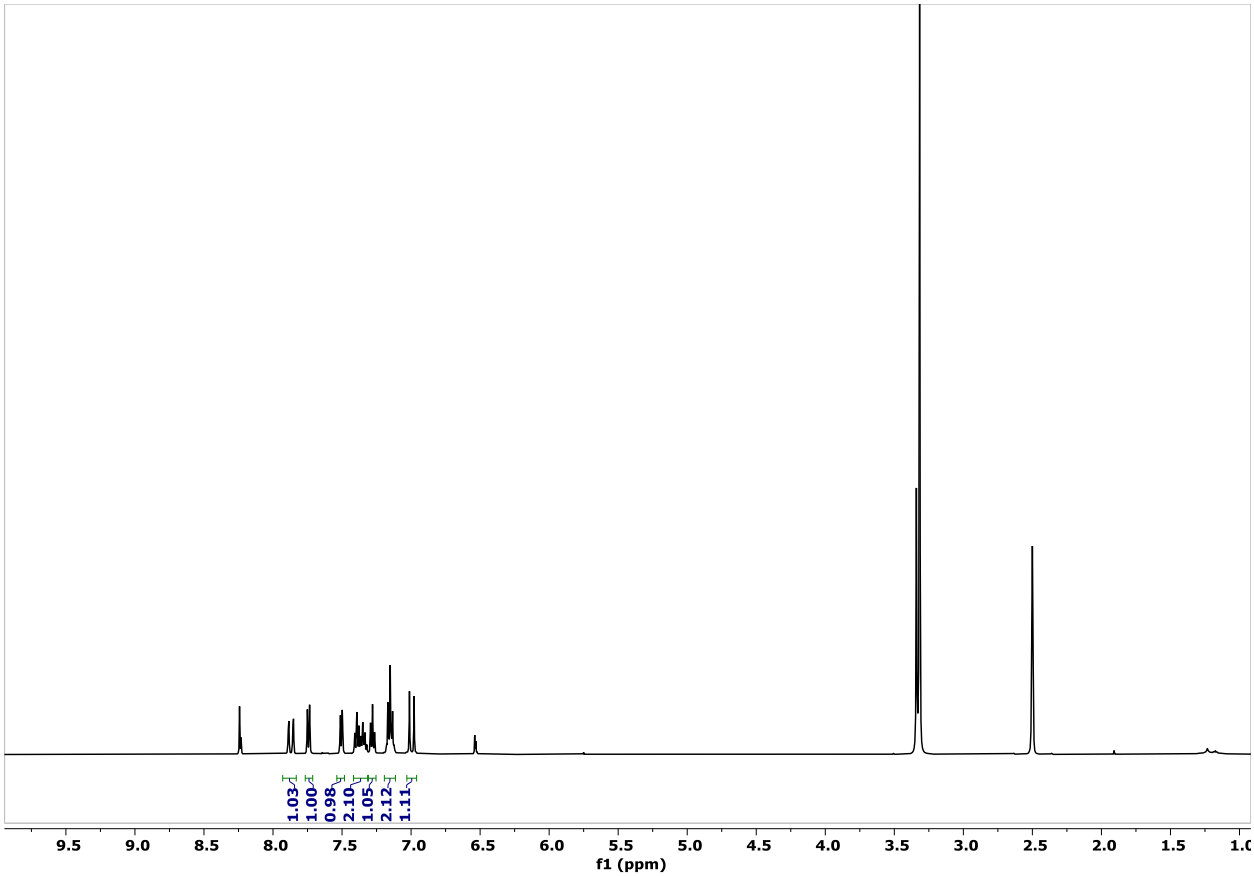

^{1}H NMR, DMSO-d_6

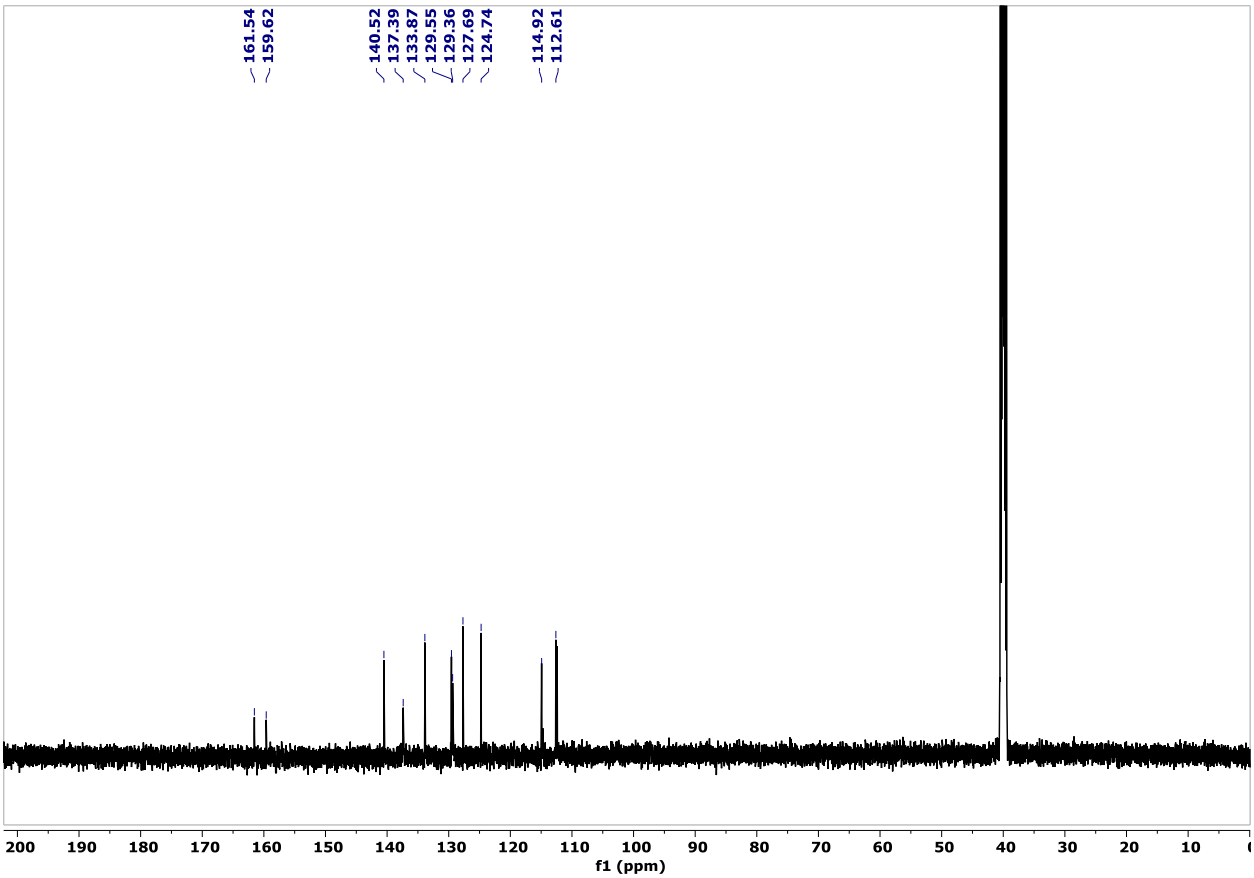

^{13}C NMR, DMSO-d_6

P1

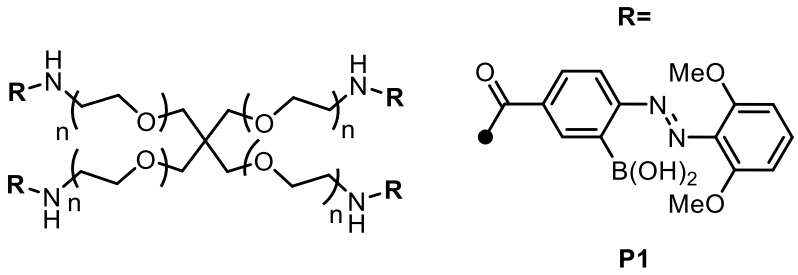

P1

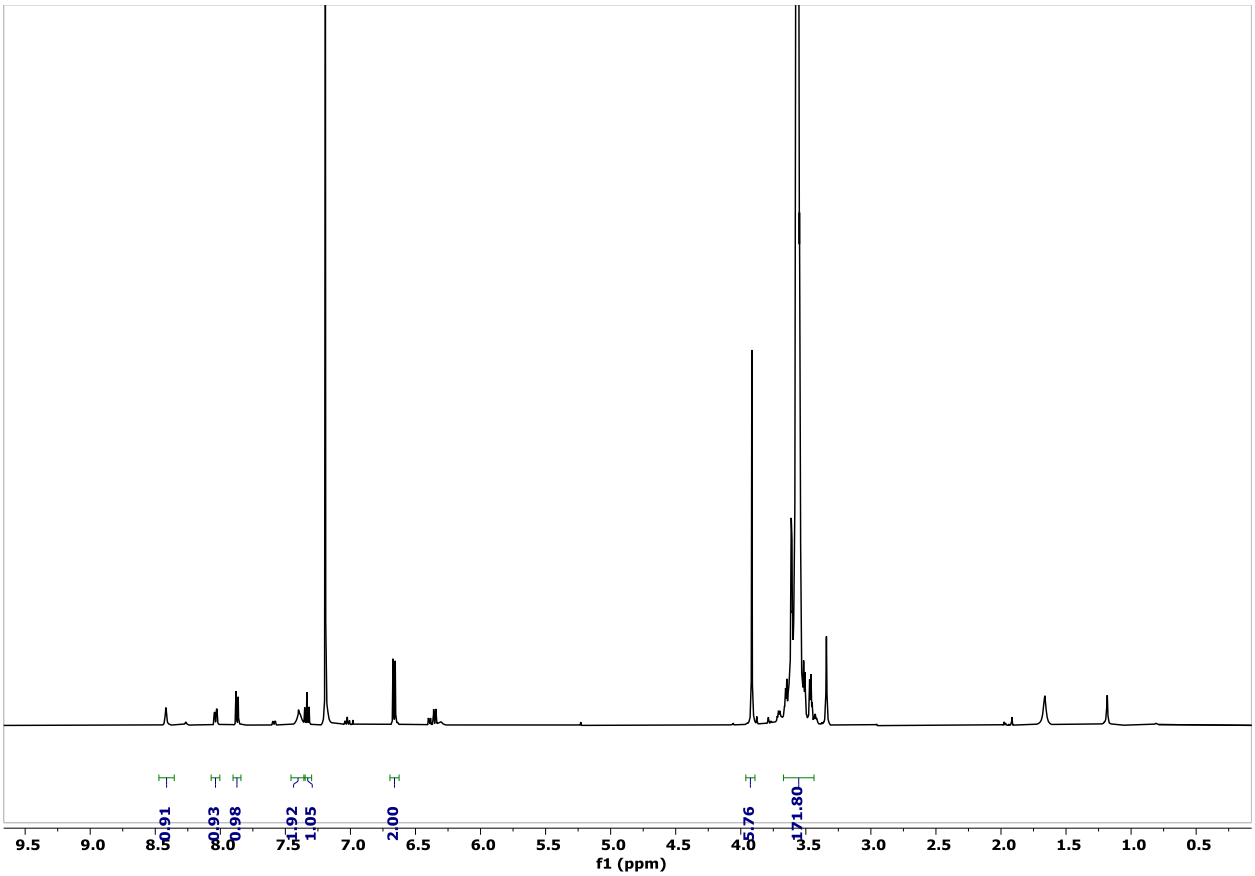

^{1}H NMR, $CDCl_3$ -smaller peaks represent the *Z* isomer. The functionality of PEG-NH_2 was determined to be ≥ 80 % by end group analysis.

X. References

1. Priewisch, B.; Rück-Braun, K., *J. Org. Chem.* **2005**, 70, 2350
2. Yesilyurt, V.; Ayoob, A. M.; Appel, E. A.; Borenstein, J. T.; Langer, R.; Anderson, D. G., Mixed Reversible Covalent Crosslink Kinetics Enable Precise, Hierarchical Mechanical Tuning of Hydrogel Networks. *Adv. Mater.* **2017,** *29*.
3. Neese, F., 2018. Software update: the ORCA program system, version 4.0. Wiley Interdisciplinary Reviews: Computational Molecular Science, 8(1), p.e1327.